2007-08-29

Lateral Resistance of Piles at the Crest of Slopes in Sand

Artak Davit Mirzoyan
Brigham Young University - Provo

LATERAL RESISTANCE OF PILES AT THE CREST

OF SLOPES IN SAND

by

Artak D. Mirzoyan

A thesis submitted to the faculty of

Brigham Young University

in partial fulfillment of the requirements for the degree of

Master of Science

Department of Civil and Environmental Engineering

Brigham Young University

December 2007

BRIGHAM YOUNG UNIVERSITY

GRADUATE COMMITTEE APPROVAL

of a thesis submitted by

Artak D. Mirzoyan

This thesis has been read by each member of the following graduate committee and by majority vote has been found to be satisfactory.

Date	Kyle M. Rollins, Chair

Date	Fernando S. Fonseca

Date	Paul W. Richards

BRIGHAM YOUNG UNIVERSITY

As chair of the candidate's graduate committee, I have read the thesis of Artak D. Mirzoyan in its final form and have found that (1) its format, citations, and bibliographical style are consistent and acceptable and fulfill university and department style requirements; (2) its illustrative materials including figures, tables, and charts are in place; and (3) the final manuscript is satisfactory to the graduate committee and is ready for submission to the university library.

_____
Date

_____
Kyle M. Rollins
Chair, Graduate Committee

Accepted for the Department

_____
 E. James Nelson
Graduate Coordinator

Accepted for the College

_____
Alan R. Parkinson
Dean, Ira A. Fulton College of Engineering and Technology

ABSTRACT

LATERAL RESISTANCE OF PILES AT THE CREST

OF SLOPES IN SAND

Artak D. Mirzoyan

Department of Civil and Environmental Engineering

Master of Science

Pile foundations near the crest of a slope are often required to resist lateral loads. This is particularly important for piles at the abutments of bridges. However, limited full-scale test data are available to indicate how the lateral resistance of a pile would be affected when it is located near the crest of a slope. To investigate the effect of a slope on lateral pile resistance, three full scale lateral load tests were conducted on an instrumented steel pipe pile. For the first test, the pile was laterally loaded in horizontal ground. For the second test the pile was at the crest of a 30 degree slope and in the third test the pile was placed three diameters behind the crest of the 30 degree slope. The soil around the pile consisted of clean sand compacted to about 95% of the modified Proctor maximum unit weight for all three tests. Laboratory and in-situ direct shear tests indicated that the friction angle of the sand was approximately 39 degrees. The pile was

instrumented with strain gages at approximately 1.5 ft intervals along its length so that the bending moment versus depth profile could be determined. Pile head load, deflection, and rotation were also measured. Based on the results, the presence of the slope decreased the ultimate lateral resistance of the pile-soil system by approximately 25% and 10% for tests two and three, respectively. The presence of the slope also resulted in an increase in the maximum bending moment of approximately 40% and 30% for tests two and three, respectively. Analyses using LPILE matched the lateral resistance for the pile in horizontal ground, but significantly overestimated the decrease in resistance due to the sloping ground. A mathematical model was developed to predict the ultimate strength of a pile located some distance from the crest of a cohesionless sloping profile. Parametric test results using the model were within 2.6 % of the measured results of tests two and three.

ACKNOWLEDGMENTS

I would like to thank all those who have helped me with this research. I would first like to thank Dr. Rollins, my graduate advisor, for approaching me and offering me this opportunity to conduct this research under his supervision. This research experience has truly taught me a great deal about the discipline of geotechnical engineering. It has given me invaluable experience in conducting research and communicating it in an effective manner. It has taught me how to deal with challenges and problems that arise in the conducting and analyzing of the research. I am grateful for Dr. Rollins' continual assistance and advice in the issues relating to this research. I would like to thank Dave Anderson for the time he put forth in setting up and performing the field tests involved in the research. I am also thankful for his assistants, Sam and Rodney, who also helped in the setup and testing.

I wish to express my gratitude to the department for providing the funding and the facilities for conducting these tests. I express my gratitude to the Salt Lake City Airport for providing the test site and for their cooperation in providing necessary utilities. I am also very grateful for Dr. Richards and Dr Fonseca, my graduate committee members, for their support and their advice and for evaluating this thesis.

I am extremely grateful for my family for their unwaning support, love, and patience.

TABLE OF CONTENTS

x

LIST OF TABLES

LIST OF FIGURES

CHAPTER 1 - INTRODUCTION

Deep foundations are a form of foundation used to bypass weak layers of soil and bear on a dense stratum or develop sufficient skin friction around the shaft to support the structure above. Deep pile foundations are also used in locations where the use of shallow foundations would lead to unacceptably low factors of safety against shear failure or excessive settlement. The latter is the primary reason pile foundations are used in the construction of bridges and it is the use of pile foundations for bridges that has motivated this research study. In addition to resisting vertical structural loads, the foundation must also withstand the lateral loads, which may be caused by wind, wave action, earthquakes, or, in the case of bridges, traffic. The lateral loads placed on the piles are largely transferred to the soil surrounding the pile within a depth equal to 5 to 10 pile diameters (Reese and van Impe 2001). Therefore, the lateral resistance of a pile foundation is dependent on both the structural properties of the pile and the properties of the surrounding soil. The resistance of the soil is primarily dependent on the properties of the soil and the geometry of the soil (i.e. the slope of the soil in the direction of the load). Because the primary purpose of a bridge is to provide clearance over the underlying road, river, or gorge, bridges and their foundations are naturally at a higher elevation than the surrounding terrain. As such, it is most often the case that bridge

foundations are placed on or near a slope that connects the different elevations. A typical bridge abutment with its foundation in sloping soil is illustrated in Figure 1.1.
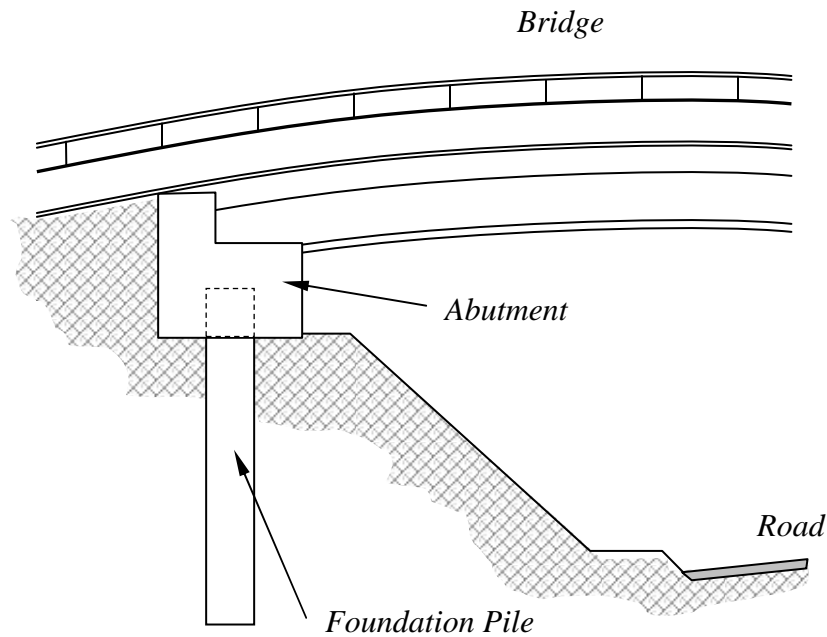
Figure 1.1 Typical Bridge and Foundation.

The slope reduces the lateral resistance of the soil, and therefore, of the foundation in the direction of the slope. While weak soil adjacent to a pile can be replaced to increase the lateral pile resistance, not much can be done regarding the undesirable effects of the soil slope except to move the pile further away from the crest. Therefore, it is crucial to know the extent to which the lateral strength of a foundation is reduced by the presence of a slope and how this reduction in strength varies with horizontal distance from the edge of the slope.

1.1 INTRODUCTION OF THEORY

The strength of single piles in a horizontal soil profile is most commonly determined by modeling the soil and pile relationship with *p-y* curves. The *p-y curve* method models the pile as a beam and the soil resistance around the pile is modeled using a series of non-linear springs along the length of the pile, know as p-y curves. The lateral soil resistance per unit pile length is defined as *p* and the lateral soil deflection is defined as *y*. An illustration of this model is presented in Figure 1.2.
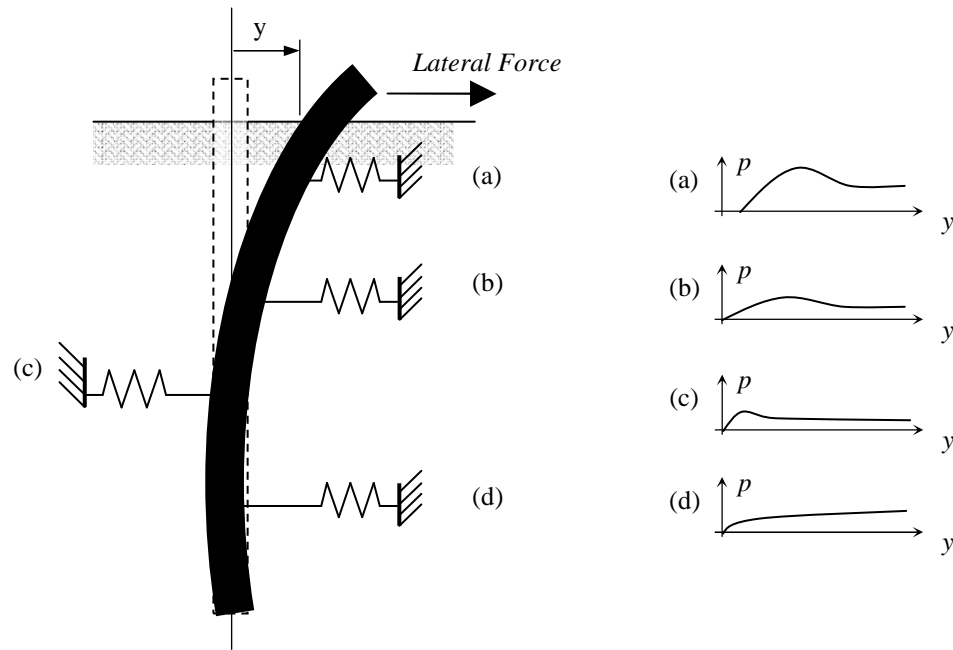
Figure 1.2 Illustration of p-y Curve Model.

The method, which was introduced in early 1950's, has evolved and, with the advent of computers, has become a practical means for design (Reese et al., 2000). Although research on the method is continuing, it has been and is being used with a certain degree of confidence in design and analysis of piles in horizontal and sloped soil

profiles. However, limited full-scale test data are available in the literature to indicate how the lateral resistance of a pile would be affected when it is located near the edge of a slope. Although methods are available to predict the lateral resistance of a pile within a slope, current computer models have no adjustment procedures available for predicting the lateral resistance when a pile is located behind the crest of slope .

The purpose of this research is to quantify the effects of slope and pile distance from the crest of the slope on the lateral strength of a pile foundation. A mathematical model is developed to account for the reduction in p-y curve stiffness near a slope and reduction factors are determined relative to the resistance in a horizontal profile. Ideally, the improved model will represent the measured strength of the foundation piles.

1.2 OBJECTIVES

To fulfill the purpose of this research, the following objectives must be met:

- Determine the effect of pile distance from slope crest on resistance of laterally loaded foundation piles.

- Evaluate available computer models for lateral pile behavior which account for slope effects.

- Obtain load resistance factors to account for different slope geometries and soil profiles.

- Develop a mathematical relationship between pile distance from slope crest and resistance of laterally loaded foundation piles.

- Compare and contrast the results from field tests with existing data from scaled model and numerical model studies.

1.3   PROJECT SCOPE

To investigate the effect of a slope on lateral pile resistance, three full scale lateral load tests were conducted on an instrumented steel pipe pile. The testing was conducted at a site at the Salt Lake International Airport. The pile used for the testing was a hollow steel pipe pile with an outside diameter of 12.75 inches and a wall thickness of 0.375 inch. The pile was driven 44 feet into the soil profile.

For the first test, the pile was laterally loaded in horizontal ground to provide a baseline for comparison with subsequent tests. For the second test, the pile was at the crest of a 30 degree slope and in the third test the pile was placed three diameters behind the crest of the 30 degree slope. The soil around the pile consisted of clean sand (concrete sand) and was compacted to 95% of the modified Proctor maximum unit weight for all three tests. This slope and backfill density are typical of slopes at Utah bridge abutments. Laboratory and in-situ direct shear tests indicated that the friction angle of the sand was approximately 39 degrees. To ensure consistency in the soil profile being tested, the soil in the affected zone was excavated and re-compacted to the original density after each test.

Load was applied using a hydraulic jack fitted with a pin connection. A load cell was placed between the hydraulic jack and the pile to measure the magnitude of the applied load, while pile head deflection and rotation were obtained with an independent reference frame. The pile was instrumented along its length with strain gages at regular intervals so that the bending moment versus depth profile could be determined. All field data were collected with an electronic data acquisition system.

The field data were then imported into a spreadsheet and used to generate plots showing (1) load vs. deflection, (2) load vs. rotation, (3) bending moment vs. depth, and (4) load vs. maximum bending moment. These plots were developed for each test and were used in evaluating the effect of the slope and pile offset distance on these curves. These relationships then were used to quantify the effects of placing piles in or near slopes.

The full-scale test results were also compared with results from small-scale tests and predictions form various analytical method. In addition, the results obtained from the field tests were compared to results from the lateral pile analysis program LPILE Plus v 4.0 (Reese et al., 2000) to evaluate the accuracy of the model for both horizontal and slope conditions. Finally, a mathematical model was developed to compute the ultimate soil resistance as a function of both soil slope and pile distance from the slope crest.

CHAPTER 2 - LITERATURE REVIEW

2.1   INTRODUCTION

Because of the great variety of uses of piles in geotechnical applications, piles have been the subject of many research projects spanning several decades. Theories on piles under lateral loading have been developed by various means, including, full-scale field testing, model testing, and numerical analysis. Of the types of methods mentioned, the most significant have been full-scale tests; however, because of the higher cost, full scale tests are far less common than numerical analysis and small-scale model testing. Model tests and numerical methods do, however, yield useful results and are most valuable in analyzing the effects of multiple variables, which would otherwise be too costly to obtain with full-scale tests.   This literature review presents work that has been performed with full-scale piles and scale-model piles, as well as numerical methods.

The evolution of research on piles in horizontal soil profiles is fundamental in understanding the research associated with piles in sloping soils. However, since the focus of the research presented in this thesis is piles in sloping soils, that is where the main emphasis of the literature review is placed and only a brief overview of research on piles in horizontal soil profiles is presented.

Research conducted on piles, both in horizontal and sloping soil profiles, falls under the general categories of full-scale tests, model tests, and numerical modeling. Each category has its advantages and disadvantages which are a deciding factor in choosing one method of research over another. When combined, results from the various methods add a piece to the puzzle. Hopefully, with the addition of more research using these different methods a consistent picture will emerge which will give the engineering community a better understanding of soil-pile interaction.

Full-scale pile tests are tests conducted on piles that have dimensions that are comparable to the dimensions of piles used under normal conditions in construction. In addition, the material properties of the piles themselves and the properties of the soil in which the piles are tested are in congruence with properties that are present with piles in construction. Because of the similarities of the conditions and materials used during full-scale tests and actual construction, full scale pile tests yield results that are considered most accurate. Unfortunately, full-scale tests are also the most expensive to perform and this disadvantage significantly limits their use. In addition, multiple tests with variable parameters are relatively difficult to conduct.

Model tests are often performed in laboratories on small scale models of the pile and soil geometry. Model pile dimensions often differ from those of full-scale piles by an order of magnitude or more. Often the scale model is placed within a centrifuge to simulate better the soil pressure acting on the piles. Although less accurate than full-scale pile tests, model tests have an advantage that makes them a preferred choice in research. That advantage is the ease with which variables involved in the pile-soil

interaction can be changed and the tests repeated, allowing the researcher to determine the effects of individual variables.

Numerical models are mathematical equations that have been derived to simulate the soil and pile interaction. The equations are usually incorporated into computer software, which allow the user to input the soil and pile parameters for analysis. With today's powerful computers, analysis with numerical models takes a short amount of time and the researcher is able to conduct multiple analyses in a fraction of the time required to conduct a model or full-scale test. Numerical models, however, are based on general and idealistic assumptions which often are not representative of real conditions. For example, the behavior at the interface between the pile and the surrounding soil has proven difficult to simulate. Nevertheless, numerical models offer the least expensive means of researching the soil-pile interaction.

The majority of this chapter is a compilation of summaries of research that has been conducted on piles in sloping soil profiles subject to lateral loads. As an introduction to the theory behind piles subject to lateral loading in sloping soils, a brief summary of research and the development of theory on piles in horizontal soil profiles is first considered. Research on piles in horizontal soil profile has served as the stepping stone for research on piles in sloping soil profiles and is therefore an integral part of this review. The research included in this review is organized from least to most recent and a summary is provided at the end of the chapter.

2.2   RESEARCH AND THEORY ON HORIZONTAL SOIL PROFILES

Because of the long history of the use of piles to resist lateral loads, it is difficult to determine when and by whom the very first research was conducted to develop a theory of the pile and soil interaction. It is, however, fair to state that the beginnings of modern research on piles under lateral loads were laid by Hetenyi (1946), who introduced a method of calculating lateral load resistance of the soil by treating it as a Winkler spring. Hetenyi's solution considered only one layer of soil with the "soil spring" derived from the subgrade modulus which was constant throughout the length of the pile.

Reese and Matlock (1956) improved existing methods by suggesting a theory for laterally loaded piles that assumed a subgrade modulus that was proportional to the depth of the soil layer. Still, the theory allowed only one layer of soil to be considered. Both Hetenyi (1946) and Reese & Matlock (1956) considered the subgrade modulus to be elastic. A substantial improvement in the subgrade reaction theory was brought about by the introduction of the nonlinear p-y method (McClelland and Focht 1958; Matlock 1970; Reese and Welch 1975), which has become the most widely used method for calculating pile response in soils under lateral loads. The p-y approach assigns a nonlinear spring/soil subgrade modulus to each layer in the profile. The subgrade moduli that are applied have been developed over the years by calibrating analytical results with full scale field tests and allow the method to reasonably simulate common field conditions. As Ashour and Norris (2000) discussed, however, the nonlinear p-y method is limited in that the p-y curve for a particular soil developed for computations incorporates the effects of the pile properties from the field test used to develop the curve. Therefore, the p-y curves cannot be considered truly unique to a soil but rather to a soil and pile combination. In addition,

10

the p-y approach does not take into account the interaction between the soil layers and represents the p-y curves as independent of each other, which, as Ashour and Norris (2000) show, is an incorrect assumption for both sands and clays.

As an alternative to the subgrade reaction theories, Poulos and Davis (1980) used the elastic continuum theory to provide solutions for deflections and rotations of piles under lateral loads. In Poulos' and Davis' approach the pile is modeled as an infinitely long strip with a width and flexural stiffness equal to the full scale pile. The soil is modeled as an ideal, homogeneous, isotropic, semi-infinite material. Initially, the theory assumed a constant soil modulus of elasticity, E_s, but later Poulos (1975) and Randolph (1981) improved the model, allowing for a linearly increasing E_s with depth. The main shortcoming of the theory is its flawed assumption of the ideal conditions of the soil. The method is, however, a theoretically reasonable approach for determining pile response in soil for working loads (Prakash and Sharma 1990). A common application of the elastic continuum method is its use in Finite Element (FE) analyses for modeling the behavior of piles loaded laterally (Randolph 1981). In the analyses, the soil is often modeled as having elasto-plastic properties with no tension capacity. P-Y curves determined from field tests may be used to model the soil elements in the analysis (Reese and van Impe 2001). In addition, the FE approach allows for a friction plane along the pile-soil interface. By conducting model tests on a 3 by 3 group of piles and comparing the results with results obtained from FE analyses, Wakai (1999) concluded that the FE method can be used to accurately simulate experimental results. The FE method falls short, however, in that is fails to account for soil layering, collapse of soil behind the pile during the separation of the pile from the soil, and change in soil characteristics due to

11

the type of loading (Reese and van Impe 2001). In addition, the method requires complex software to perform the analysis, which can be rather expensive.

Although over the years many more methods for determining pile behavior under lateral loads have been presented, such as the Characteristic Load Method (Duncan et al., 1994) and the Stress Wedge Model (Ashour et al., 1998), the three previously mentioned methods remain the most accepted and used methods in the industry. The non-linear p-y method is the most commonly used; however, Finite Element Analysis is fast gaining acceptance. The methods used in this research to provide a comparison with field results has been the non-linear p-y method presented by Reese et al. (2000) and a newly developed analytical method based on the formation of a failure wedge.

2.3   RESEARCH CONDUCTED ON SLOPED SOIL PROFILES.

Although research has been conducted to determine the effects of a slope on lateral pile behavior, neither the amount nor the rigor is comparable to that for piles in horizontal profiles. A vast majority of the research on piles in sloping soil profiles has been conducted on either small-scale models or with the use of numerical models such as Finite Element analysis. The results and observations from these tests, however, have been a valuable asset in the process of the research presented in this thesis and are reviewed in this chapter in some detail.

2.3.1   Research Conducted Prior to 1980

One of the first studies undertaken to examine the effects of a slope on the lateral strength of a long flexible pile in soil was by Poulos (1976), who conducted small scale

laboratory tests on brass piles in clay and later derived a mathematical solution based on the elastic continuum theory. In addition to the effect of slope, Poulos studied the effects of pile placement relative to the crest of the slope. Figure 2.1 shows a schematic elevation drawing of the pile-soil geometry.
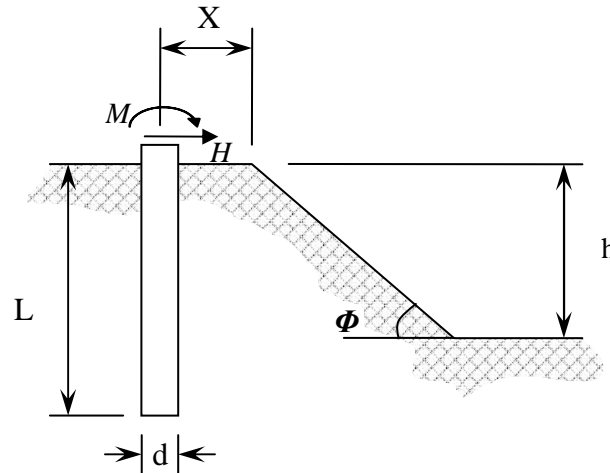
Figure 2.1 Pile-Soil Geometry and Corresponding Symbols Used by Poulos.

In this analytical approach, Poulos assumed the soil to behave as an elastic homogenous material with a constant modulus of elasticity, which led to a slight overestimation of the ultimate lateral strength. The analytical approach and laboratory tests agreed, however, that the effect of slope on the strength of the pile-soil system could be neglected for piles located beyond 5 pile diameters (5D) from the crest of the slope. The derived equations and the laboratory tests were conducted on a vertical cut rather than a slope and, therefore, the analytical solution and field results are of little use in relation to a soil profile with a 30° angle slope–the subject of this thesis. In addition, due to the vertical cut, no analysis exists for a pile located at the slope crest. Poulos does,

13

however, provide a correction factor in terms of an equivalent distance, Xe, (for the case

of X/d ratio of 1) to account for slope angles other than 90° as shown in Figure 2.2, where

Ke (a misprint of K_R) is the pile flexibility with Ke = 10^{-5} signifying long flexible piles.

With this correction factor, deflection factors, C_{pF}, to account for the slope effect on pile

behavior, can be obtained from Figure 2.3, which suggests that a pile located three pile

diameters (3D) from the crest of a 30° angle slope would experience approximately 1.45

times the lateral deflection of a pile in a horizontal profile.

 A deflection factor of 1.45 suggests that the resistance ratio, Ψ, of the pile 3D

from the crest to the lateral resistance of a pile in horizontal ground would be about 0.69.

Such a value is based on the assumption that the lateral load and deflection relationship is

linear – an assumption, which Poulos makes in his derivations.
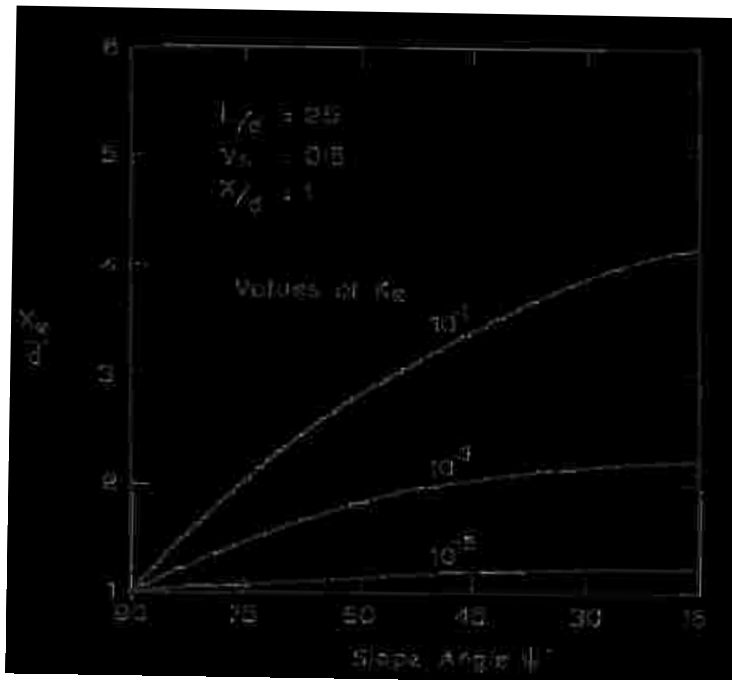
Figure 2.2 Equivalent Distances for Non-Vertical Slopes (Poulos, 1976).
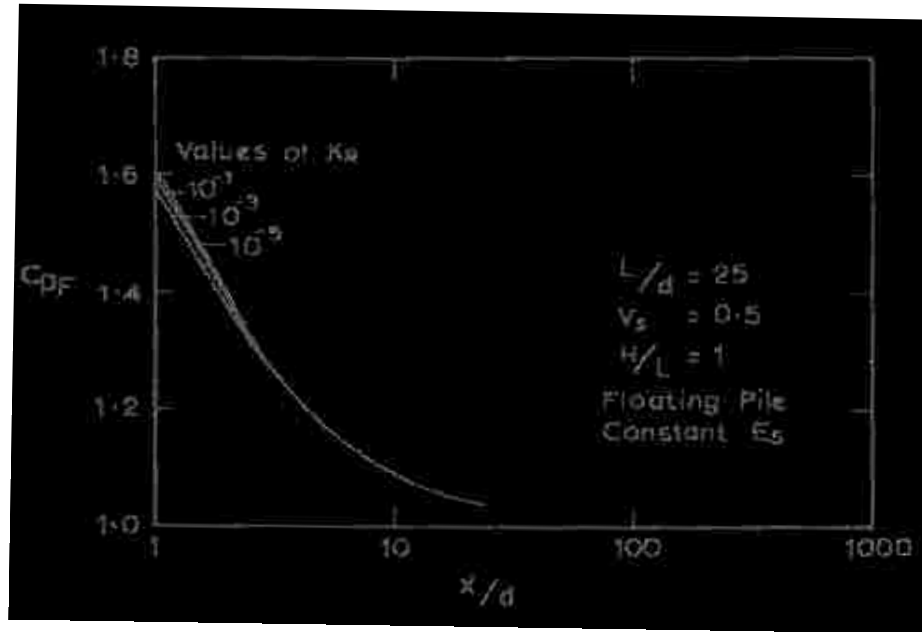
Figure 2.3 Deflection Correction Factors for Slope Effect (Poulos, 1976).

2.3.2   Research Conducted Between 1981 - 1990

Gabr and Borden (1990) conducted research on piers constructed on slopes to analyze the effect of slope on the lateral resistance of the piers. Based on their research, Gabr and Borden present an analytical model, primarily based on the stress wedge approach developed by Reese (1962), for computing the ultimate p value for p-y curves in sand. In addition, Gabr and Borden conducted large scale pier tests to validate the analytical method. In the model, the resistance of the soil to the movement of the pile is provided by a failure wedge forming in front of the pier as illustrated in Figure 2.4. The total pile head resistance, P_u, is obtained by summing the resisting forces that develop along the faces of the failure wedge, namely, planes DEA, FEAB, and CFB. The complex analytical model takes into account the geometry of the soil and pier, as well as

the properties of the soil such as friction angle, φ, and cohesion, c; however, the model does not account for the presence of multiple soil layers.
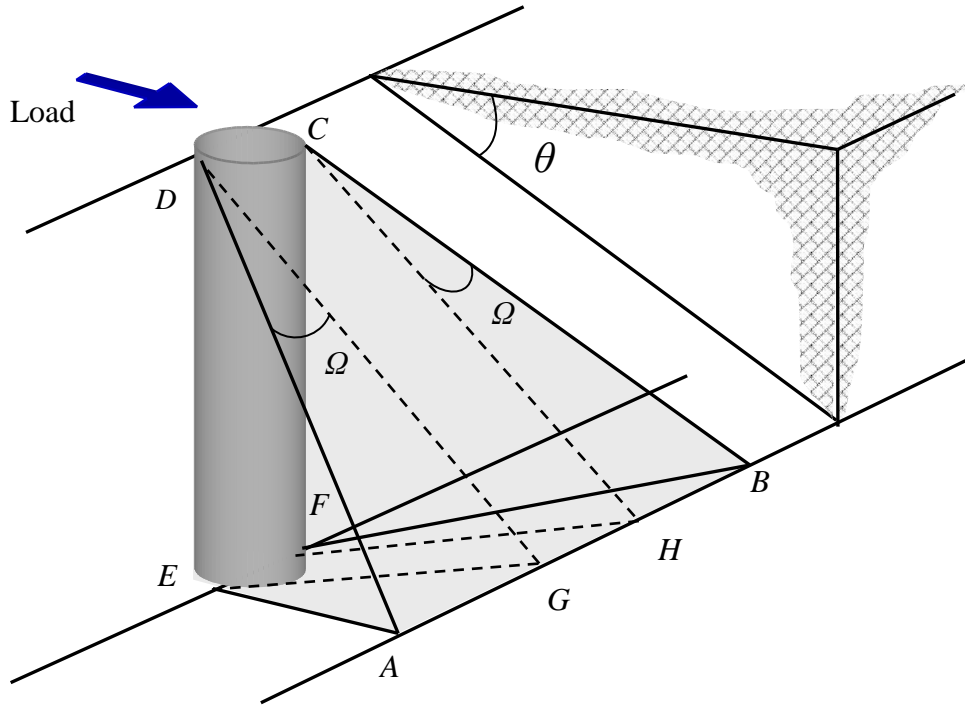
Figure 2.4 Illustration of the Failure Wedge Method.

The analytical model treats the pier as a frictionless rigid pier and assumes the failure angle, Ω, to be φ/2. Such an assumption was based on experimental work by Bowman (1958), who suggested that the measure of angle Ω ranged from φ/3 to φ/2 for loose sands and was approximately equal to φ for dense sands. In addition, the model assumes that the planes along which the wedge fails are flat, which was based on the work of Reese (1962). The ultimate pile head force, P_u, is then given by Equation 2-1.

16

$$P_u = \gamma H \, [\, H \, (S_{1\phi} + 3K_o \, S_{3\phi}) + b \, S_{2\phi} - K_a \, b\,]$$

$$+ \, c \, [\, H \, (S_{1c} + S_{3c}) + b \, S_{2c} - 2b \, K_a^{0.5}\,] \tag{2-1}$$

where H, b, θ, and β are illustrated in Figure 2.5

$S_{1\phi} = \lambda_2 \tan \Omega \tan \beta \, [(\tan \theta \tan \beta + 1)(3 + 4 \tan \phi \tan \beta) - (2 \tan \phi \tan \beta)]$
      $/ (\tan \theta \tan \beta + 1)^2$

$S_{2\phi} = 2 \, \lambda_2 (1 + \tan^2 \phi) / (\tan \theta \tan \beta + 1)$

$S_{3\phi} = (\tan \phi - \tan \Omega) \, [\tan \beta - (\tan^4 \beta \tan^3 \theta + \tan^3 \beta \tan^2 \theta) / (\tan \theta \tan \beta + 1)^3\,]$

$S_{1c} = 2 \tan \Omega \tan \beta \, [\lambda_1 (1 + 2 \tan \theta \tan^2 \phi + \tan \beta) + 2 \tan \beta(\tan \theta \tan \beta + 1) - \tan \beta]$
      $/ (\tan \theta \tan \beta + 1)^2$

$S_{2c} = \lambda_1 + (1 + \lambda_1 \tan \phi) / (\tan \theta \tan \beta + 1)$

$S_{3c} = \tan \beta - [(\tan^3 \beta \tan^2 \theta + \tan^2 \beta \tan \theta) / (\tan \theta \tan \beta + 1)^2\,]$

$\lambda_1 = K_1 K_{pc}$

$\lambda_2 = K_1 (K_{p\phi} + K_2 / \cos \beta) / 2$

$K_{pc} = 1 / [(\tan \theta \sin \beta + \cos \beta)(\sin \beta - \cos \beta \tan \phi)]$

$K_{p\phi} = \tan \beta (\cos \beta + \sin \beta \tan \phi) / [(\tan \theta \tan \beta + 1)(\sin \beta - \cos \beta \tan \phi)]$

$K_1 = \cos \beta (\tan \theta \sin \beta + \cos \beta) / H$

$K_2 = \tan \beta \sin \beta / (\tan \theta \tan \beta + 1)$

K_o = At rest earth pressure coefficient

K_a = Active earth pressure coefficient

c = Soil Cohesion
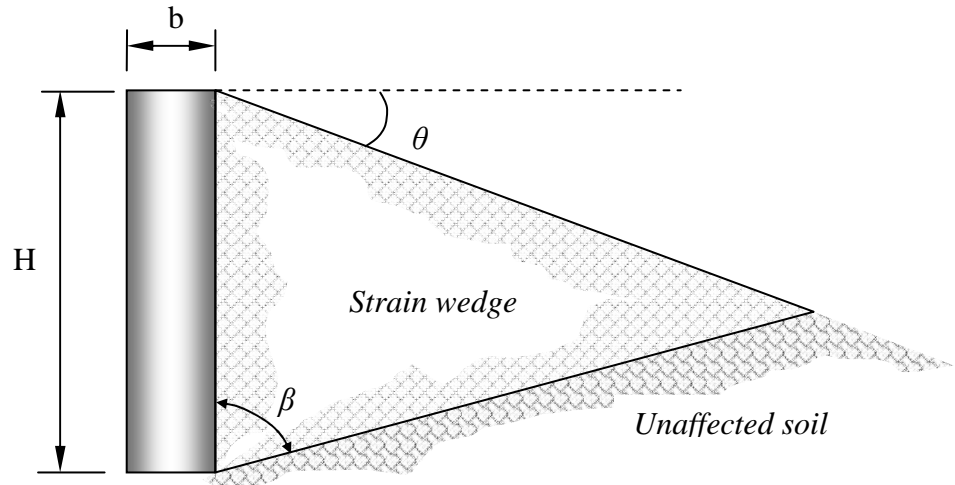
Figure 2.5 Strain Wedge Geometry.

Results of the analytical method show that the ultimate resistance ratio, Ψ, of the pile in a slope to the pile in horizontal ground (P_u slope/P_u flat) is dependent on the friction angle of the soil. In particular, as the soil friction angle increases, the ratio Ψ decreases, which was shown to be true for both cohesionless and cohesive soils. In general, cohesionless soils were predicted to have much higher Ψ ratios than cohesive soils of the same friction angle as shown in Figure 2.6, which also shows the relationship between the slope angle, Θ, and Ψ. In both cohesive and non-cohesive soils, Ψ decreased as the angle of slope increased; the greatest rate of decrease in Ψ occurring between 0° and 10° angle slopes. The Ψ factor slowly decreases for subsequently higher angles of slope. The decrease, however, is not as pronounced in soils with cohesion. Because of the difference in the rates of decline, the Ψ factor relationships for the cohesionless soils and cohesive soils appear to converge for values of Θ between 30° and 35°. The analytical method presented by Gabr and Borden predicts a Ψ of 0.5 for a pile located at the crest of a 30° slope ($\phi = 40^o$).

To verify the results from the analytical method, Gabr and Borden conducted large scale field tests on 2 to 3 foot diameter piers in both cohesive and cohesionless soil profiles cut to a slope of 2.2H : 1V ($\theta = 24.4^o$) . The lengths of the piers varied from 6 to 8 feet and were all placed at the crest of the slope. With a length to diameter ratio of only 3, the piers are likely behaving as short piles. A moment was applied to the piles at the ground level by pulling a cable attached to a pole which was then attached to the piers. A schematic representation of the loading is shown in Figure 2.7. The results of the field tests showed that the point of rotation occurred at a depth of about 2/3 of the embedment depth, H.
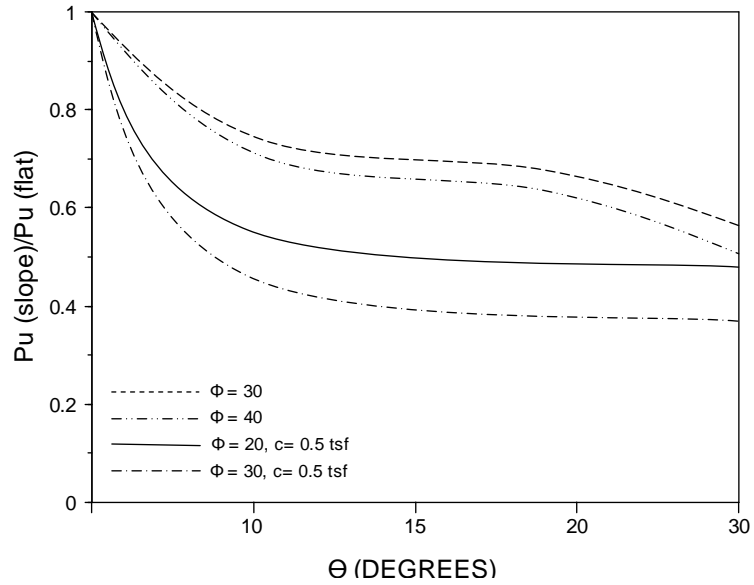
Figure 2.6 Ultimate Resistance Factor Ψ as a Function of Ө.
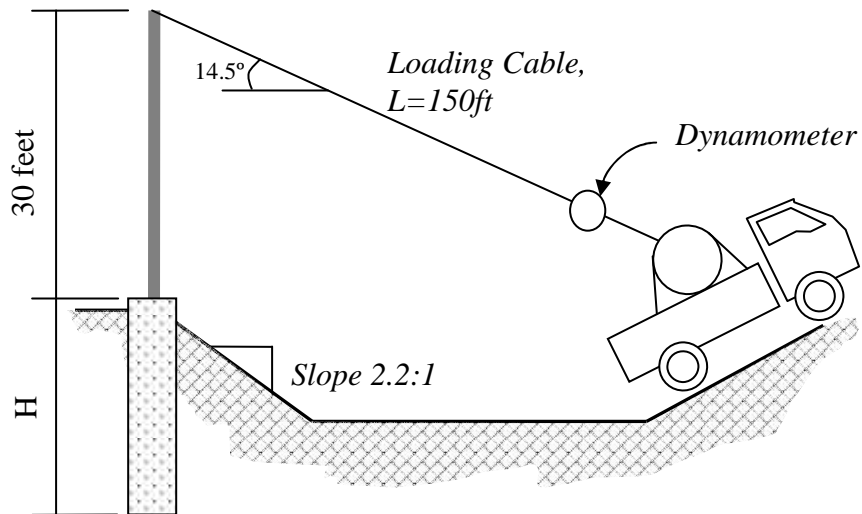
Figure 2.7 Large-scale Test Layout.

Although a close similarity in the results was observed between the analytical method and the field tests, overall, the analytical method underpredicted the applied moment at a given deflection for cohesive soils. For cohesionless soils, the analytical

model overpredicted the applied moment causing small deflections, between 0 and 2.5 inches, but then underpredicted the applied moments for subsequent deflections. Gabr and Borden attributed the discrepancies between the analytical and field results to the observation made in the field of a gap forming between the back side of the pile and soil due to the lateral displacement of the pile, which stayed open during the entire test. The gap was observable for both cohesive and cohesionless soils, suggesting that the assumption made in the analytical model of active pressure acting behind the pile was erroneous for both cohesive and cohesionless soils. This observation of a gap forming between pile and soil was also made and discussed by Davidson (1982).

Gabr and Borden concluded that the analytical method was within 15-25% of the measured results. They stressed, further, the need for more field tests to better understand the effects of a slope on the lateral resistance of piers.

2.3.3   Research Conducted Between 1991 - 2000

Boufia and Bouguerra (1995) conducted tests on small-scale model piles in dense sand in a centrifuge to determine the effects of pile distance from the slope crest on the lateral resistance of the pile. The distance from the slope crest, t, considered in the study were 0, 2, 5, 7, 13.1, 14.8, and 20.5 pile diameters, B. In addition, a pile in horizontal ground was tested. The soil profile was composed of dense sand (SP with D_r of 95%) and the slope was cut to 2H : 1V ($\theta = 26.6°$). Boufia and Bouguerra observed that the closer the pile was to the crest of the slope, the greater the bending moment of the pile although the increase was relatively small. The results of maximum bending moment for the pile in horizontal ground as well as at crest (0B) and two pile diameters (2B) from the

20

slope crest are summarized in Table 2.1. The results showed that the pile at the slope

crest experienced 1.15 times the bending moments of the pile in horizontal ground.

Table 2.1 Maximum bending moments and bending moment ratios.

Pile location, t	Mmax, kN-m	$M_{max}/M_{max\ horiz}$
Horizontal	370	1
2B	400	1.08
0B	425	1.15

Figure 2.8 shows the ratios, IM_{max}, of maximum bending moment of piles near the

slope to the maximum bending moment of the pile in horizontal ground, from which the

IM_{max} ratio for a pile at 3B from slope crest can be interpolated as 1.07. The bending

moment results suggest that for piles placed 10 to 15 pile diameters or more from the

crest of the slope, the effect of the slope on bending moments of the pile becomes

negligible.

With regard to the lateral load and deflection, Boufia and Bouguerra observed that

for a given load, piles closer to the crest of the slope experienced greater deflections in

the direction of the applied load relative to the case with horizontal ground. The lateral

load and deflection relationship is shown in Figure 2.9 and the ratios, I_{YH}, of horizontal

displacement of piles near slope to pile in horizontal ground for different pile locations

are shown in Figure 2.10, which shows I_{YH} values of 1.81 and 1.66 for piles place at the

slope crest and 3 pile diameters from slope crest, respectively.
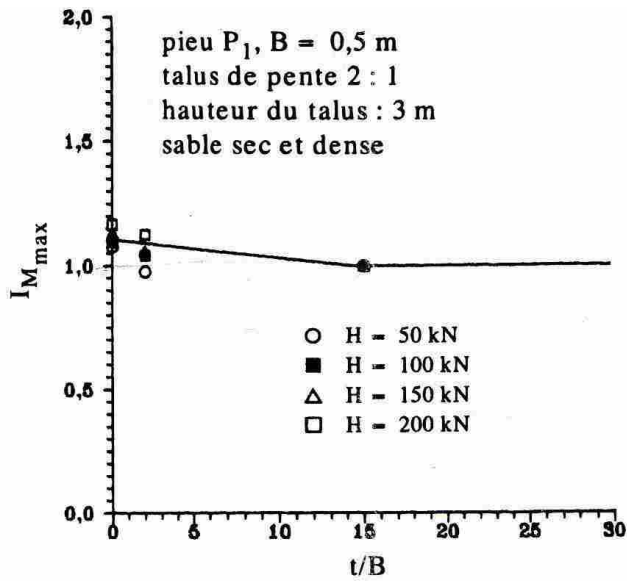
Figure 2.8 I_{Mmax} Ratios as a Function of Pile Location (Boufia and Bouguerra, 1995).
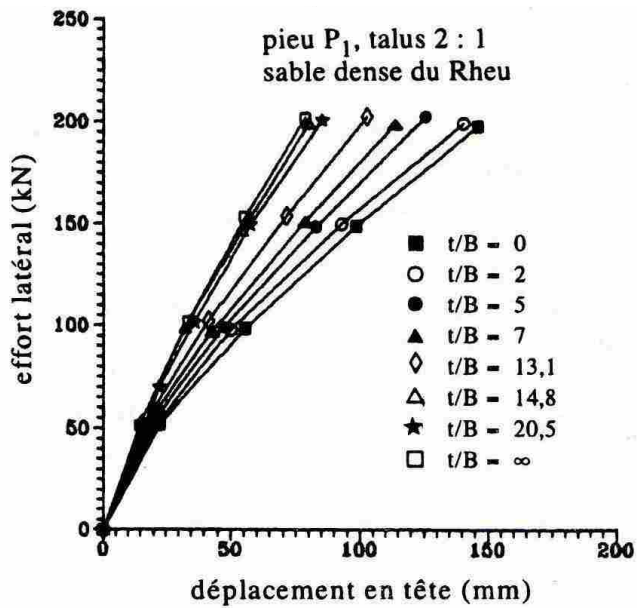
Figure 2.9 Lateral Load and Deflection Relationships for Different Pile Locations (Boufia and Bouguerra, 1995).

22
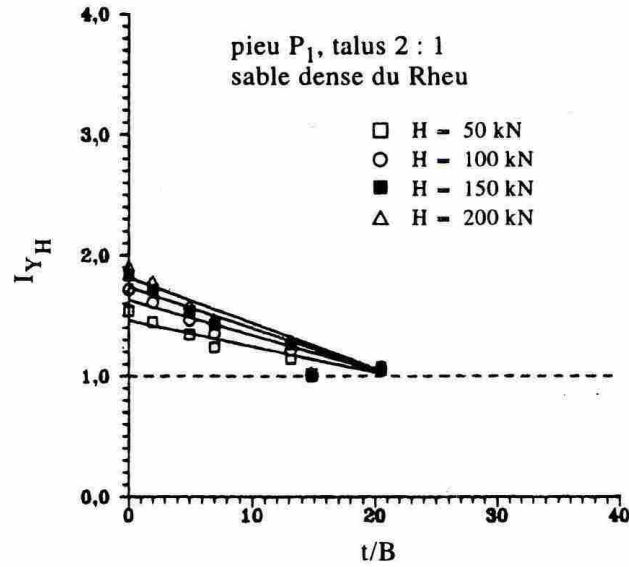
Figure 2.10 I_{YH} Ratios as a Function of Pile Location (Boufia and Bouguerra, 1995).

The lateral load vs. deflection curves suggest that for piles placed 15 to 20 pile diameters or more from the crest of the slope, the effect of slope on lateral resistance is negligible. The results further suggest Ψ factors of 0.62 and 0.69 for piles at the slope crest and three pile diameters from slope crest, respectively, where Ψ is the lateral resistance ratio of the pile in slope to the pile in horizontal ground (P_u slope/P_u flat).

Mezazigh and Levacher (1998) also conducted tests on model piles in a centrifuge to determine the slope effect on the lateral resistance of long flexible piles. The model piles were driven into fine white Fontainebleau sand. Two relative densities (D_r) of sand were used, 81% and 58%, to evaluate the effects of sand density. The piles were aluminum tubes with dimensions that were set to represent an outside diameter of 720 mm and a length of 12 m at prototype scale with a 40g acceleration of the centrifuge. The pile distances from the slope crest considered in the study were 0, 1, 2, 3, 4, 8, 10 and 12 pile diameters, B. In addition, three piles in horizontal soil profiles were tested to

23

provide reference points. Two soil slopes, 2H : 1V (θ = 26.6º) and 3H : 2V (θ = 33.7º),
were considered in the study.

Test results reported by Mezazigh and Levacher agree with the conclusion
reached by Boufia and Bouguerra (1995) that piles closer to the crest of the slope
experience somewhat greater bending moment. Mezazigh and Levacher conclude that
for a slope of 2H : 1V (θ = 26.6º), the distance beyond which the slope has negligible
effect on the bending moment of the pile is 6 pile diameters and 12 pile diameters for a
slope of 3H : 2V (θ = 33.7º).

Table 2.2 summarizes the measured bending moments of the piles under
maximum loading for the pile in horizontal ground and piles located 0 and 2 pile
diameters from the 2H : 1V slope crest.

Figure 2.11 shows the ratios, m(t/B)/mREF, of the normalized bending moments
of the piles at different locations, m(t/B), to the normalized bending moments of the piles
in horizontal ground, mREF. The bending moments have been normalized by the applied
load causing the moment. Figure 2.11 shows that the ratios of the normalized bending
moments were 1.25 and 1.06 for a piles placed at the slope crest (t/B = 0) and at three pile
diameters from the slope crest (t/B = 3), respectively. These values are comparable to
those of 1.15 and 1.07 obtained by Boufia and Bouguerra (1995).

With respect to lateral load-deflection behavior, Mezazigh and Levacher's (1998)
and Boufia and Bouguerra's (1995) conclusions again agree in that piles nearer to the
slope crest experienced greater deflections as seen in Figure 2.12. They disagree,
however, with respect to the location of the pile relative to the slope crest, beyond which,
the slope has no effect on the lateral displacement of the pile. Mezazigh and Levacher

observed a distance of 8 to 10 pile diameters–about half the distance reported by Boufia
and Bouguerra's (1995).

Table 2.2 Maximum bending moments and bending moment ratios.

Pile location, t	M_{max}, kN-m	$M_{max}/M_{max\ horiz}$
Horizontal	1450	1
2B	1675	1.15
0B	1945	1.34
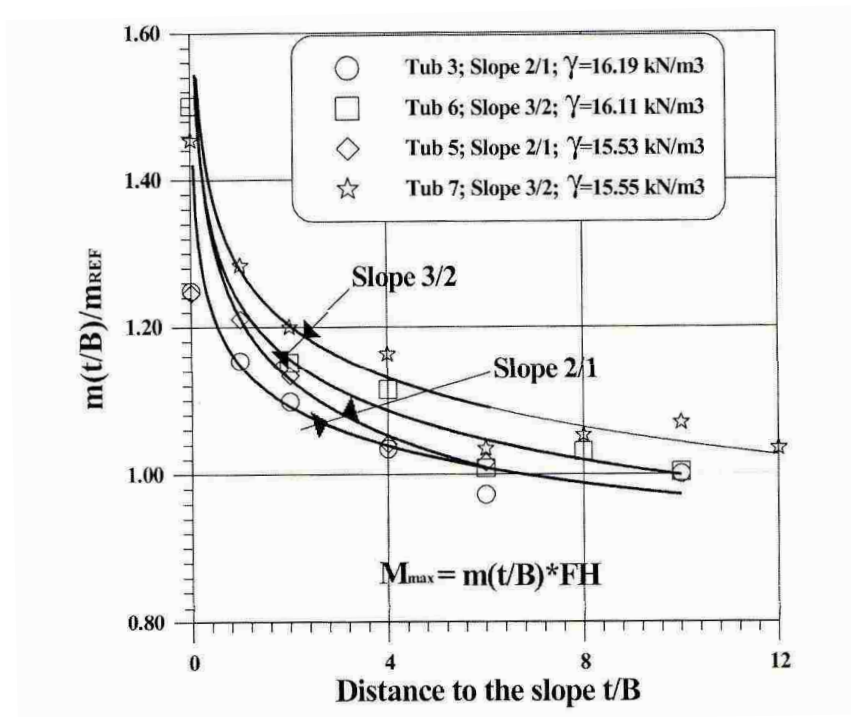
Figure 2.11 Normalized Bending Moment Ratios as a Function of Pile Location (Mezazigh and Levacher 1998).
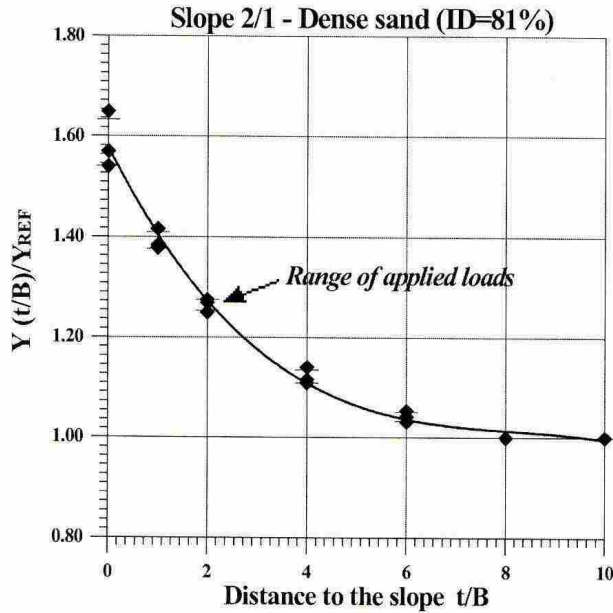
Figure 2.12 Deflection Ratios as a Function of Pile Location Relative to Slope Crest(Mezazigh and Levacher 1998).

Mezazigh and Levacher's results show that the pile located at the crest of the slope experienced about 1.6 times the deflections of the pile in horizontal ground. As shown in Figure 2.12, the pile at three pile diameters from the slope crest was predicted to have experienced 1.16 times the deflections of the pile in horizontal ground for a given load. The relationships between lateral load and displacement for the piles tested by Mezazigh and Levacher is nearly linear, which suggests that the displacement ratios of the pile at slope crest and at three pile diameters from the slope crest correspond with Ψ factors of 0.62 and 0.86, respectively.

Mezazigh and Levacher (1998) suggest a P-multiplier, r, to reduce the p-y curve for the soil to account for the slope of the soil and the pile placement relative to the crest of the slope. The P-multiplier, r, is given by Equation 2-2.
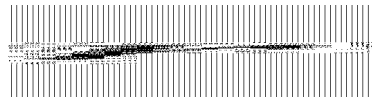
where β = Slope angle, B is the pile diameter, and t is the distance from the crest to the center of the pile. Based on Equation 2-2, a 30º slope would yield an r value of 0.21 and 0.46 for piles at the slope crest and at three pile diameters from the slope crest, respectively.

Mezazigh and Levacher (1998) indicated that the coefficients used in Equation (2-2 have been validated by comparing the experimental curves to curves computed using PILATE (Frank et al., 1990, 1994), and that the sand density and mass were not significant factors contributing to the slope effect.

2.3.4   Research Conducted Between 2001 - Present

Chen and Martin (2001) conducted extensive Finite Element analyses of piles located near slope crests to asses the effects of slope and pile proximity to slope crest on the lateral resistance and p-y curves of the soil-pile system. The study involved a c-ϕ type soil with a cohesion of 30kPa (4.4 psi) and a friction angle, ϕ, of 20º. Various slopes were considered in the study and reaffirmed the conclusions reached by other researchers regarding the inverse relationship between slope angle and soil-pile capacity. Figure 2.13 shows Ψ values as a function of pile distance from slope crest for various slope angles. Here again Ψ is the ratio of ultimate resistance of a pile near slope to pile in horizontal profile (Pu $_{slope}$/Pu $_{horiz.}$). Chen and Martin state that for slope angles less than 45º the effect of slope on ultimate load capacity becomes less than 10% for distances greater than 6 pile diameters, and therefore the slope effect beyond that can be neglected.
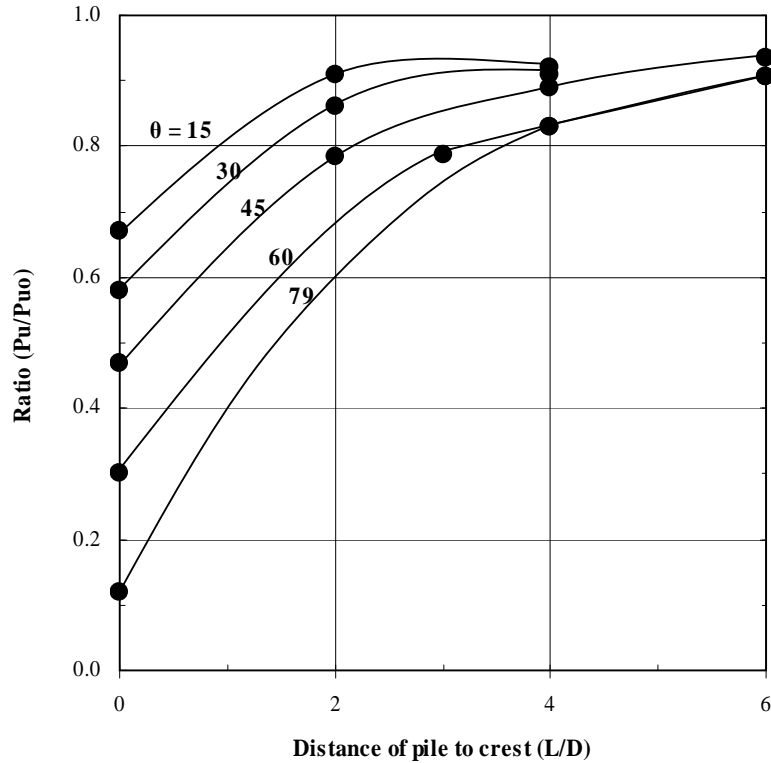
Figure 2.13 Ultimate Resistance Ratios for Various Slope Angles.

Chae et al. (2004) conducted a series of Finite Element (FE) analyses as well as small scale model tests to determine the effects of slope and pile placement relative to a slope on the behavior of short piles subject to lateral loads.

The soil used in the small scale model tests was Onahama sand with a relative density, D_r, of 90% and friction angle, ɸ, of 47.5°. The tests were performed on piles located 0, 2, and 4 pile diameters from the crest of a 30° angle slope. In addition, a test was performed in horizontal ground to compare to the piles in sloped soils.

Similar to the results of the other studies, the results presented by Chae et al. (2004) show that the piles closest to the slope experienced the greatest deflection and the highest bending moments. The results of the small scale model tests showed that the maximum bending moments for the pile at the crest of the slope under a load of 195N

were 1.15 to 1.24 times larger than the bending moments experienced by the pile located four pile diameters from the crest of the slope. Such a value is comparable to a factor of 1.2 obtained by Mezazigh and Levacher (1998) and 1.1 obtained by Boufia and Bouguerra (1995).

With respect to the lateral load-deflection relationships, Chae et al. (2004) model test results show that the piles at the crest of the slope had Ψ factors of 0.4, 0.6 and 0.9 for piles located at the crest (0D), two diameters from crest (2D), and four diameters from the crest (4D), respectively. Results are summarized in Figure 2.14 and Figure 2.15, which show the lateral load-deflection relationships and Ψ factors, respectively, for different pile-slope geometries. By linear interpolation, Ψ for the pile located three pile diameters form the crest of the slope was predicted to be 0.75 based on the model tests and 0.85 from the FE analysis.
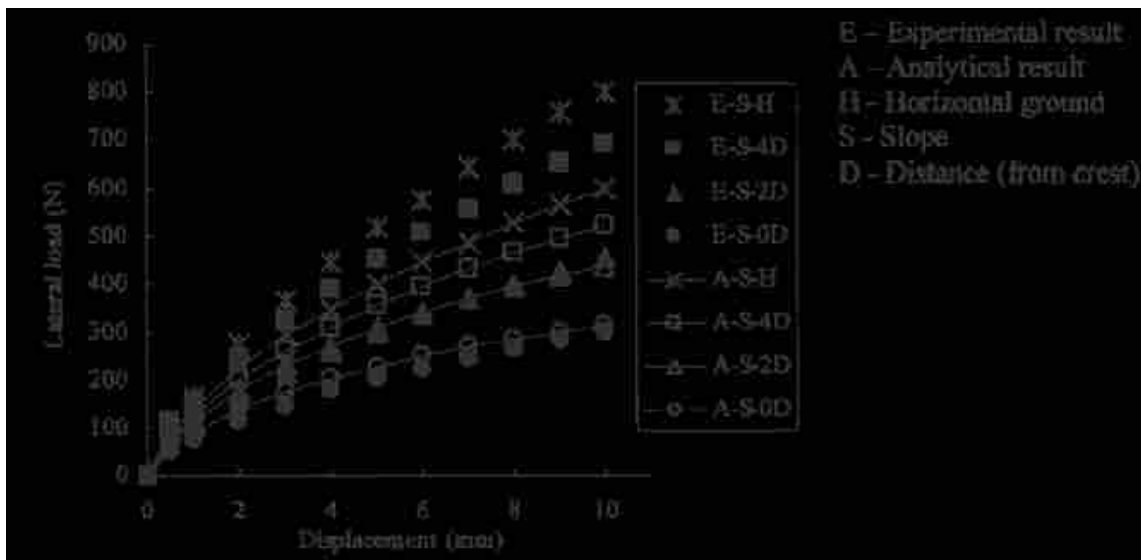
Figure 2.14 Lateral Loads and Deflection Relationships for Different Pile Locations (Chae et al., 2004).

29

To validate the FE analysis, Chae et al. (2004) report the results of a full scale test on a 10m pier with a 3m diameter conducted by Takeuchi and Okada (1996) and make an attempt to simulate the results using the FE method. The results of the field test and the corresponding FE analysis are summarized in Figure 2.16 and Figure 2.17, which show the subgrade reactions and the lateral load-deflection results, respectively.
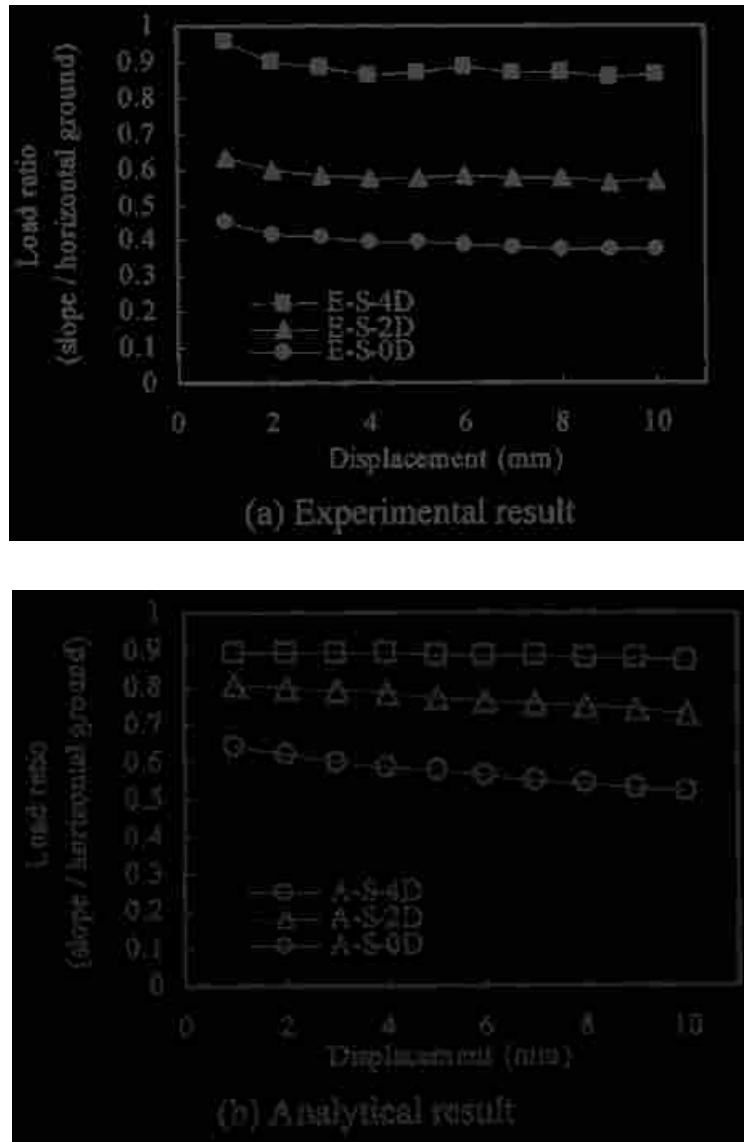
Figure 2.15 Load Ratios From a) Model Tests and b) From FE Analyses (Chae et al., 2004).

(a) Observed result [22]

(b) FE analytical result
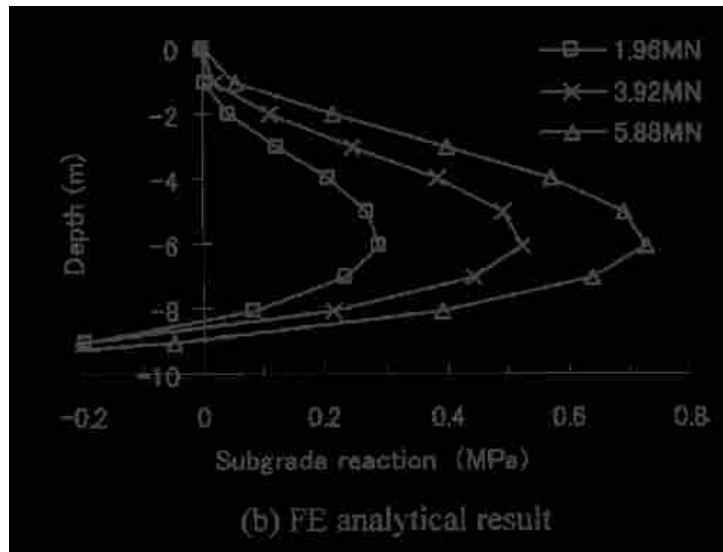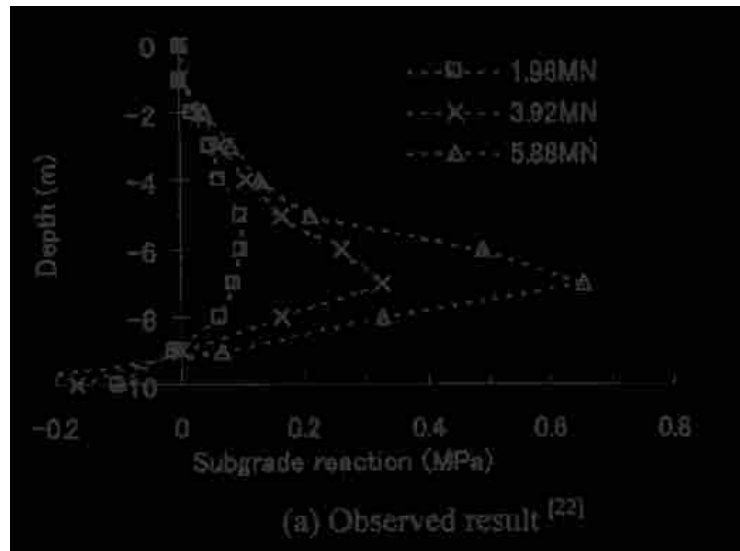
Figure 2.16 Subgrade Reactions from a) Full-scale Tests and b) FE Analysis (Chae et al., 2004).
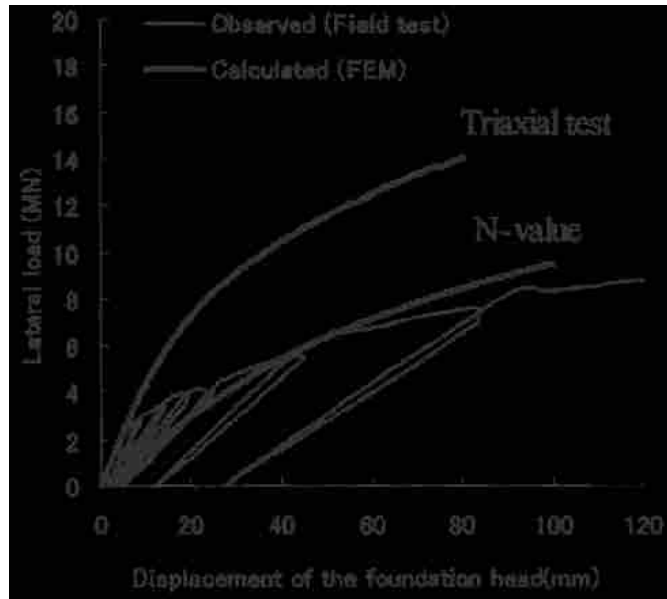
Figure 2.17 Full Scale and FE Results of Lateral Load and Displacement (Chae et al., 2004).

The bold lines in Figure 2.17 represent the results of the FE analyses using different soil elastic moduli (from a Triaxial test and from the SPT N value correlations). The results show that for small loads and deflections, the elastic modulus of the soil, E_s, was best estimated by the triaxial test, while the modulus from the SPT N value correlation provided the best estimate for large loads and deflections.

Although Chae et al. (2004) acknowledge that a discrepancy exists between the results of small scale model tests and FE Analysis (especially for piles located at 2D from the slope crest and in horizontal ground), they conclude that the FE model shows a reasonable agreement with the experimental model.

El Sawwaf (2006) conducted a series of 36 small scale model tests on short rigid piles and intermediate length piles in sand slopes with a relative density, D_r, of 80%. The primary goal of the test program was to examine the effects of geogrid reinforcement on the lateral strength of piles in a slope. He also studied the effects of pile placement

relative to the crest of a non-reinforced 1.5H : 1V ($\theta = 33.7°$) slope. The pile locations considered in the study were 0, 2.5, 5, and 10 pile diameters from the crest of the slope.

The results of the tests showed that the Ψ factor of the pile immediately at the slope crest was 0.57. By polynomial interpolation, Ψ for the pile located three pile diameters form the crest of the slope was predicted to be 0.93.

Results also show that the point beyond which the slope of the soil had no effect on the lateral load and deflection relationship was five pile diameters. Therefore, the test results for the pile 10 pile diameters from the slope crest can be safely assumed to be identical to the results of a pile in horizontal ground, which was not included, and have been used in place of the results from the pile in horizontal ground in determining Ψ factors.

To account for the effect of the slope on the strength of deep pile foundations at the crest of the slope, in its 2006 GEO Publication, the Hong Kong Geotechnical Engineering Office provides Equation 2-3 as means for calculating the lateral resistance factor, Ψ, based on full scale tests on drilled piers in stiff clay conducted by Bhushan (1979).

(2-3)

where θs = Slope angle

Equation 2-3 yields a Ψ of 0.63 for a pile at the crest of a 30° angle slope. Although the equation was developed from research involving full-scale tests on drilled

piers in stiff clays, the suggested Ψ value correlates very well with values suggested for sands by other researchers.

Reese et al. (2006) used Equation 2-3 to account for the effects of slope on long piles in clays and suggested a complex equation to account for the effects of slope on the lateral strength of piles placed in a continuous sandy slope. The equation they suggest for sands, Equation 2-4, provides an ultimate soil resistance per foot of pile length as a function of the angle of slope, θ; soil friction angle, ϕ; at-rest earth pressure coefficient, K_o; and other soil and pile properties.

$$p_{usa} = \gamma H \left| \begin{array}{l} \dfrac{K_o H \tan\varphi \sin\beta}{\tan(\beta-\varphi)\cos\alpha}(4D_1^3 - 3D_1^2 + 1) \\[2em] + \dfrac{\tan\beta}{\tan(\beta-\varphi)}(bD_2 + H\tan\beta\tan\alpha D_2^2) \\[2em] + K_o H \tan\beta(\tan\varphi\sin\beta - \tan\alpha) \\[1em] (4D_1^3 + 3D_1^2 + 1) - K_A b \end{array} \right| \qquad \textbf{(2-4)}$$

where

$$D_1 = \frac{\tan\beta\tan\theta}{\tan\beta\tan\theta + 1}$$

$$D_2 = 1 - D_1$$

$$K_A = \cos\theta\frac{\cos\theta - \sqrt{(\cos^2\theta - \cos^2\varphi)}}{\cos\theta + \sqrt{(\cos^2\theta - \cos^2\varphi)}}D_1$$

Ko = At rest pressure coefficient
$\alpha = \phi$ for dense sands $\phi/2$ for loose sands
$\beta = 45° + \phi/2$
b = Pile diameter

To obtain the relationship between ultimate soil resistance of pile in slope and in horizontal ground, Ψ, a series of computations were made with general soil and pile properties using the equations suggested by Reese et al. (2006) for slope and horizontal ground. The analysis showed that, although the relationship was not affected by the unit weight of the soil, it was somewhat sensitive to K_o and ϕ and highly sensitive to θ. The analysis further showed that the relationship was relatively insensitive to the pile dimensions.

Figure 2.18 shows the Ψ relationship as a function of θ for different ϕ values obtained with the equation developed by Reese et al., as well as, values obtained from Equation 2-3 suggested by the GEO Publication (2006) for comparison.
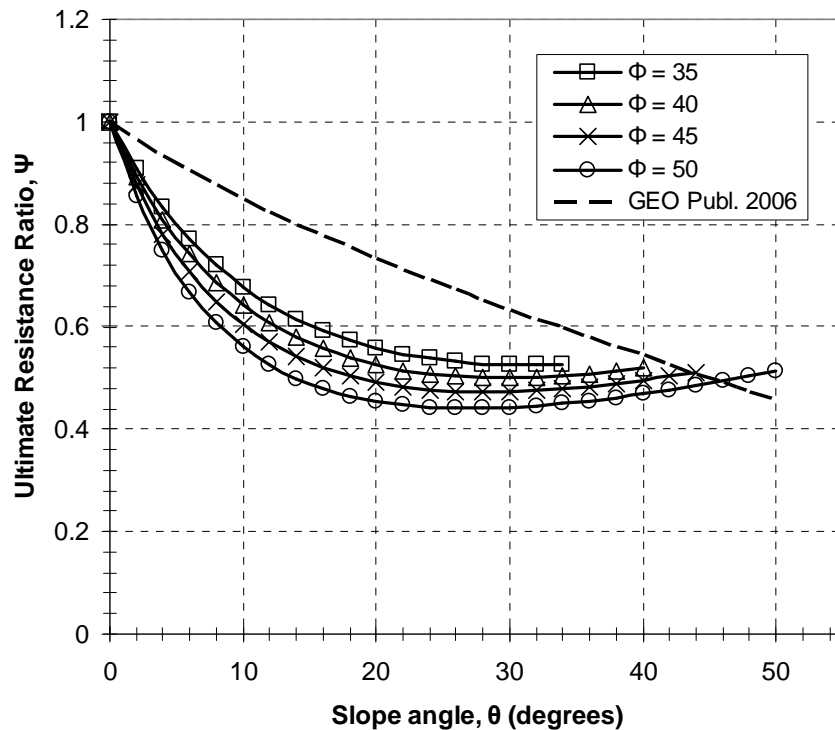
Figure 2.18 Ultimate Resistance Ratios as a Function θ for different ϕ values.

For a 30° slope in sand with a friction angle of 40°, the equation suggested by Reese et al. (2006) yields Ψ a value of 0.5 with the assumption of 0.5 for the value of the at-rest earth pressure coefficient, K_o.

It is interesting to note that according to the equation proposed by Reese et al. (2006), the slope to horizontal ultimate resistance relationship is inversely proportional to the friction angle. This is in accord with the results obtained by Gabr and Borden (1990), whose mathematical analysis results are illustrated in Figure 2.19. One fundamental difference between the suggestions by Reese et al. (2006) and Gabr and Borden (1990) is that while Gabr and Borden predict a continuously decreasing ultimate resistance ratio, Ψ, with the increase of slope angle, θ, Reese et al. predict a slight increase in Ψ for larger θ's. The increase is most evident in soils with high friction angles. For example, a pile in sand with a ϕ of 50° is predicted to have greater load capacity on a 50° angle slope than on a 30° angle slope.
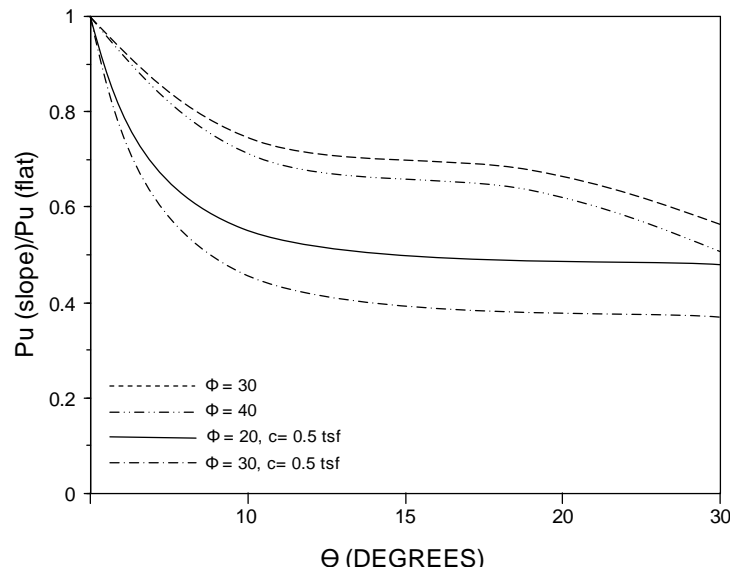
Figure 2.19 Ultimate Resistance Ratios as a Function of θ (Gabr and Borden 1990).

36

2.4   SUMMARY

Table 2.3 provides a summary of significant findings from the different studies that have been conducted to analyze the effects of slope and pile placement relative to slope crest on the behavior of single piles subjected to lateral loading. Additionally, results of ultimate resistance ratios from the different studies have been combined into Figure 2.20 for comparison.

Although a general agreement exists between the results of the different studies, the factors quantifying such effects vary significantly from study to study. The differences can be attributed to the many factors involved such as the type of materials used in the laboratory tests and the assumptions made in analytical models that differ between studies. However, without an adequate amount of full-scale field tests to verify the methods, it is difficult to come to a consensus on the method to be used in analysis and design of piles in or near sloped soil profiles.

It should be acknowledged that full and large scale tests have been performed to analyze the slope effects, namely, Bhushan (1979), Gabr and Borden (1990), and Takeuchi and Okada (1996). However, most of the above mentioned full and large scale research has been conducted on short rigid piers; hence, a deficiency of full scale data exists for long flexible piles, which are a more common application of deep foundations.

The results of the research presented in this thesis will be a valuable addition to the knowledge base on the effects of soil slope and pile placement relative to slope on flexible piles.

Table 2.3 Summary of significant findings.

Researcher(s)	Soil Type	D_R	ϕ, su	Test Type	Θ	X_{LIM}	Ψ, 0D	Ψ, 3D	IM_{max}, 0D	IM_{max}, 3D	r, 0D
Poulos (1976)	Clay	---	0, 6.6 psi	Small-scale model	30°	5D	- - -	0.69	- - -	- - -	- - -
Gabr & Borden (1990)	Sand	---	41°, 0	Mathematical model	30°	- - -	0.5	- - -	- - -	- - -	- - -
Boufia & Bouguerra (1995)	Dense Sand	95%	---	Small-scale model*	26.6°	10-20D	0.62	0.69	1.15	1.07	- - -
Mezazigh & Levacher (1998)	Fine Sand	81%	---	Small-scale model*	26.6°	6-8D	0.62	0.86	1.25	1.06	0.47
		58%			33.7°	12D	0.42	- - -	1.5	1.16	0.33
Chen and Martin (2001)	Silt	---	20°, 4.4 psi	FE Analysis	30°	6D	0.58	0.91	- - -	- - -	0.43
Chae et al. (2004)	Dense Sand	90%	47.5°, 0	Small-scale model	30°	- - -	0.4	0.75	- - -	- - -	- - -
		---		FE Analysis	30°	- - -	0.6	0.85	- - -	- - -	- - -
El Sawwaf (2006)	Sand	80%	43°, 0	Small-scale model	33.7°	5D	0.57	0.93	- - -	- - -	- - -
GEO Publication (2006)	Stiff Clay	---	---	Full-scale	30°	- - -	0.63	- - -	- - -	- - -	- - -
Reese et al. (2006)	Sand	---	40°, 0	Mathematical model	30°	- - -	0.5	- - -	- - -	- - -	- - -

* - indicates centrifuge tests
Θ = Slope angle in degrees from horizontal.
X_{LIM} = Distance of pile from slope for negligible slope effect.
Ψ = Ratio of slope and horizontal pile lateral resistance.
D = Diameter of pile.
D_R = Relative Density.

IM_{max} = Ratio of maximum slope and horizontal pile bending moments.
su = Soil cohesion, psi
ϕ = Angle of internal friction
r = P-multiplyer to account for slope effect
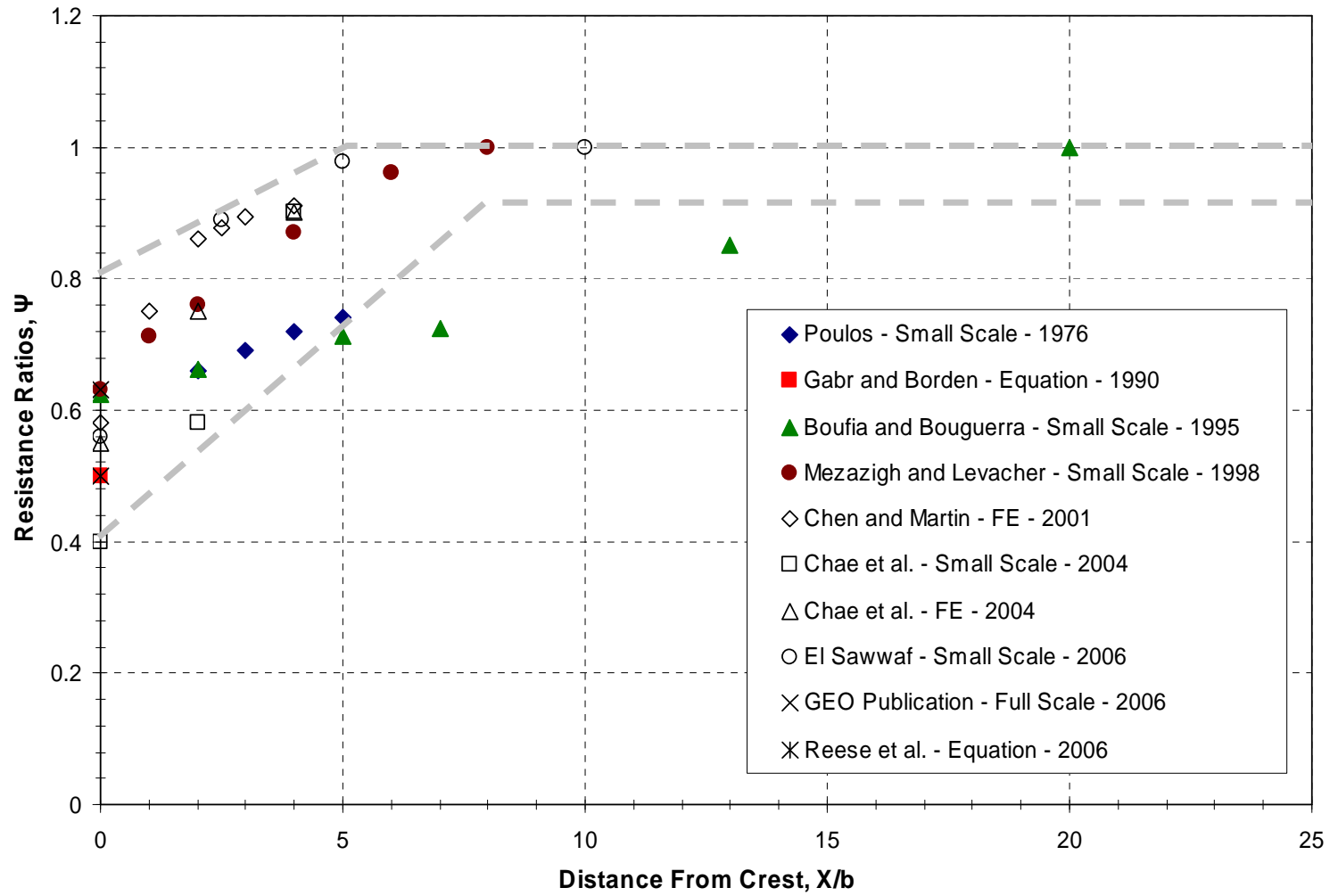
Figure 2.20 Comparison of Resistance Ratios from Past Research.

CHAPTER 3 - GEOTECHNICAL INVESTIGATION

3.1   INTRODUCTION

The site chosen for the tests in this study is located about 300 yards north of Salt Lack City International Airport's control tower.   The primary factors governing the choice of the site for the testing were its accessibility, manageable terrain, and the wealth of geotechnical information available regarding the site.   Figure 3.1 is an aerial photograph of the site.

The site has served as a testing ground for numerous studies on single and grouped drilled shafts and piles. The first test conducted at the site was on a 3 x 3 group of driven piles in 1995. In 2002, an additional 26 piles were driven north of the existing piles and more tests were performed. At that time, about 5 feet of the native sandy gravel were removed exposing the native clay layer underneath, in which the piles were tested to investigate lateral behavior of pile groups in clay. In 2004, about 3 more feet of the native exposed clay layer were removed and the entire site was backfilled with washed concrete sand, making the topmost layer of soil around the piles composed of sand 8 ft-thick. The sand was backfilled in lifts of about 8 to14 in. Each lift was compacted with a track hoe with a compactor attachment and with a hand operated jumping jack compactor. After the compaction of each lift, a nuclear density gage was used to check

the relative compaction, moisture content, and densities of the compacted profile, the results of which are presented in Section 3.3.1. The general condition of the site at the time of the tests conducted for this study had remained unchanged since the alterations made in 2004.
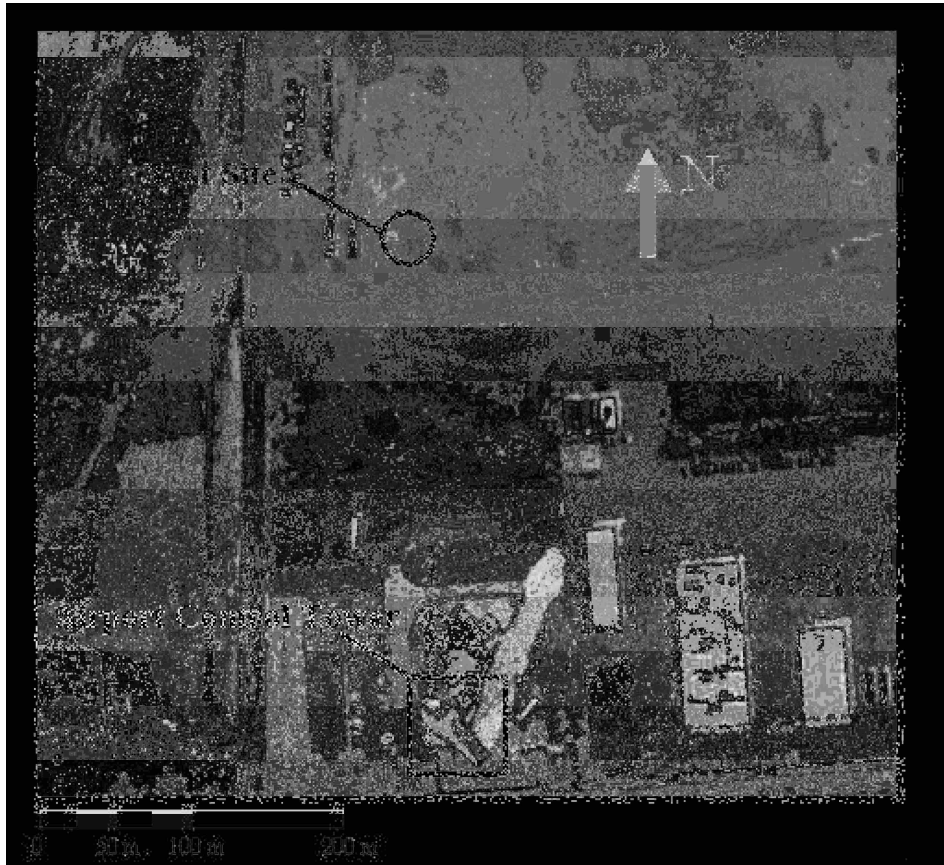
Figure 3.1 Aerial Photograph from the USGS of the Site Taken in 1998 (Walsh 2005).

This chapter is a summary of the numerous geotechnical investigations, both in-situ and laboratory, that have been conducted on the layers of soil surrounding the test piles and shafts. Emphasis is given to investigation conducted in a close proximity to the single pile tested in this study.

3.2   HISTORY OF INVESTIGATIONS

As part of the 1995 research conducted by Peterson (1996) on the first piles installed on the site, a series of surface and subsurface investigations were made. These included cone penetrometer testing (CPT), pressuremeter testing (PMT), standard penetration testing (SPT), and vane shear testing. In addition to the in-situ tests, laboratory test were performed on undisturbed and disturbed samples of the soil. These tests yielded useful information such as particle size distribution, soil classification, consolidation characteristics, shear strength, and Atterberg limits. To confirm the results of the 1995 investigations, two more CPT tests were conducted on the site in 1998.

The next wave of geotechnical investigation was conducted after the addition of more piles and shafts to the site in the summer of 2002. The areas subject to the new investigations in 2002 were around the new 15 pile and 9 pile groups. The 2001 investigations consisted of CPT tests and laboratory tests on samples retrieved from hand augering. In 2004 and 2005, additional tests were carried out focusing on the top layer of sand backfill that surrounds both the 15 and 9 pile groups.

In addition to the vast amount of geotechnical investigation conducted in the past, additional investigative tests were performed in this study, which included nuclear density gage testing and direct shear testing. These tests were carried out to confirm results of key properties and to ensure that the site characteristics had not changed significantly. Figure 3.2 is a plan view of the site, showing the locations of major geotechnical investigations conducted in the area.
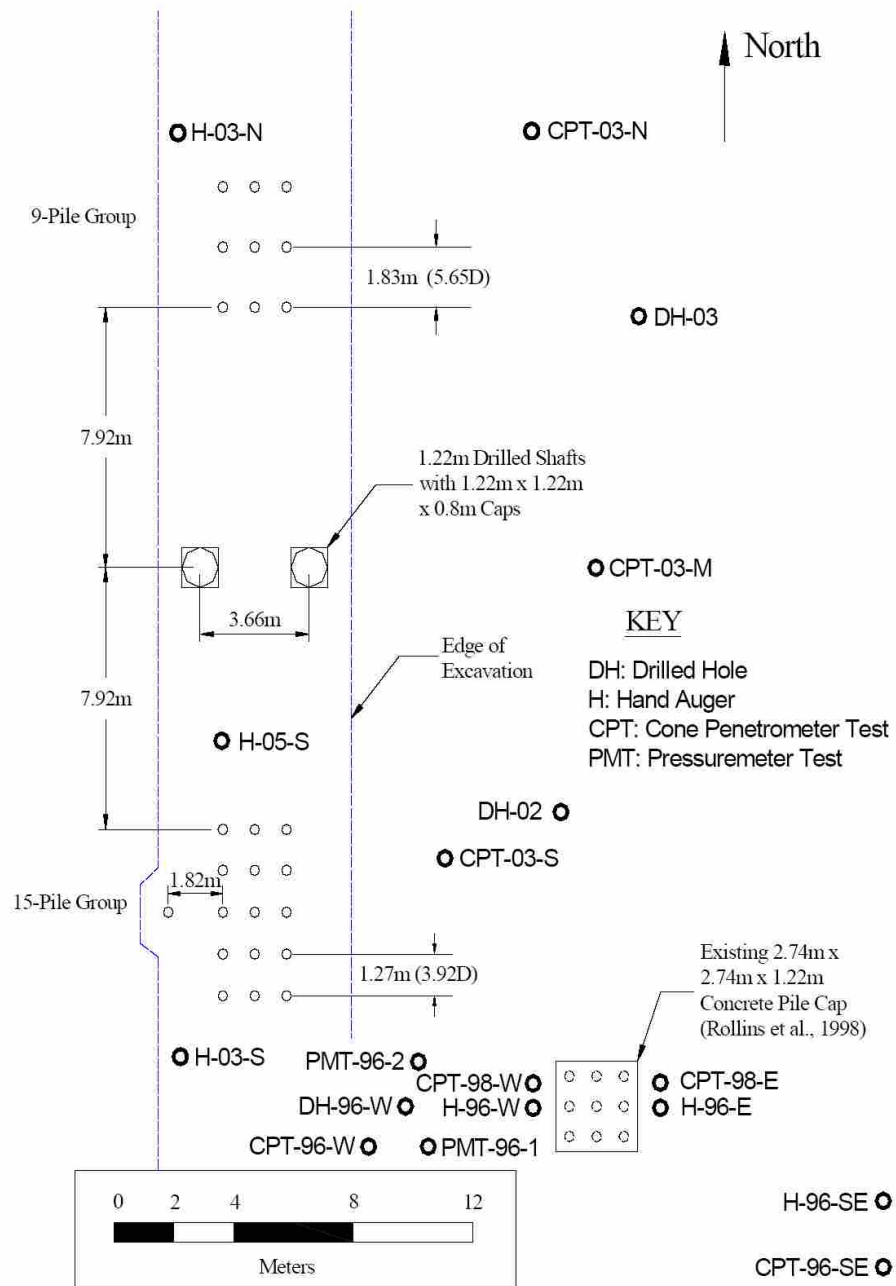
Figure 3.2 Plan View of Site with Locations of Soil Tests (Walsh 2005).

3.3   IDEALIZED SOIL PROFILE

Results of in-situ and laboratory tests have been combined to generate an idealized soil profile illustrated in Figure 3.3. Development of the idealized soil profile has relied heavily on the work of Walsh (2005) and Christensen (2006), as well as work conducted in this study. Figure 3.3 shows that the top layer, extending 8 feet below ground surface, was composed of Well Graded Clean Sand. The sand layer was underlain by alternating layers of silts, clays, and sands. These layers, however, played a relatively minor role in the overall lateral response of the pile because most of the lateral resistance soil resistance is developed in the upper 5 to 10 pile diameters of the soil profile. Hence, the focus of in-situ and laboratory tests in this study was on the top sand layer. Figure 3.3 also shows a water table in the sand layer between 6 and 7ft below ground surface. This was a governing factor in the recompaction of soil, discussed in later chapters, extending only to 6 ft below ground surface. The soil profile presented here was used, with some modifications, in modeling of the tests in the computer program LPILE. These modifications are discussed in a later chapter.

3.4   CONE PENETRATION TESTING (CPT)

The primary advantage of the CPT is its ability to provide continuous readings of skin friction (f_s), tip resistance (q_c) and pore water pressure (u). This allows for the identification of layer boundaries and thus the depth of each layer. Correlations with tip resistance and side friction allow for an identification of each layer. A large tip resistance and relatively low skin friction readings, for example, indicate dense sand, where as, large skin frictions and low tip resistance indicate clayey soils. For combinations of tip
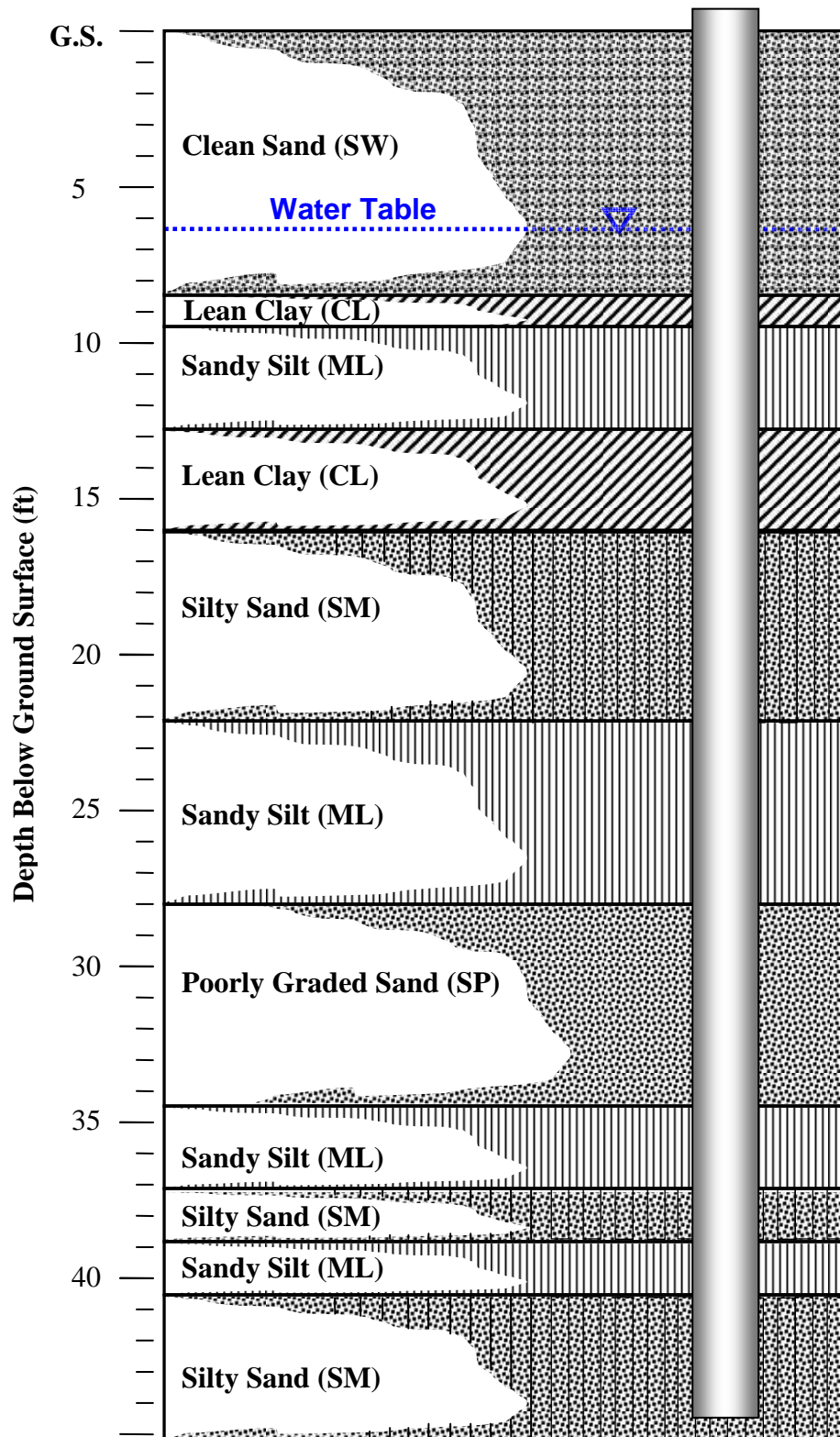
Figure 3.3 Idealized Soil Profile Around Single Pile

46

resistance and skin friction, correlations such as the one provided by Robertson and Campanella (1993) exist, which can help identify the layer. In addition, correlations such as the one provided by Tatsuoka et. al (1990) can be used with tip resistance data from a CPT reading to obtain the relative density of a sandy layer. These correlations have been a key component in the compilation of the idealized soil profile presented in Figure 3.3.

Cone Penetration Testing has been performed at the site for a total of 11 times. The area directly around the 15-pile group has been the focus of only one such test, conducted in 2001 shortly after the installation of the new 15-pile group. This test is labeled CPT-03-S in Figure 3.2. Two previous tests, labeled CPT-96-W and CPT-98-W, conducted in the vicinity provide comparable results. A comparison of the 15-pile group CPT test and CPT tests conducted in the vicinity is provided in Figure 3.4. Data to a depth of 8ft is nonexistent in the plots in Figure 3.4 because, at the time of testing, the profile had been excavated to a depth of 8ft.

CPT-03-S and CPT-98-W were conducted by ConeTec, Inc. using a 180-kN truck mounted electric cone, while CPT-96-W was conducted by RB&G Engineering with an electric cone mounted drill rig.

3.5   INDEX TESTING

3.5.1   Particle Size Distribution

A particle size distribution analysis was performed in the Soils Laboratory of the Clyde Building at Brigham Young University on the top sand layer. The soil, which had been brought from the site, was left to air dry for 4 days. The purpose of the experiment
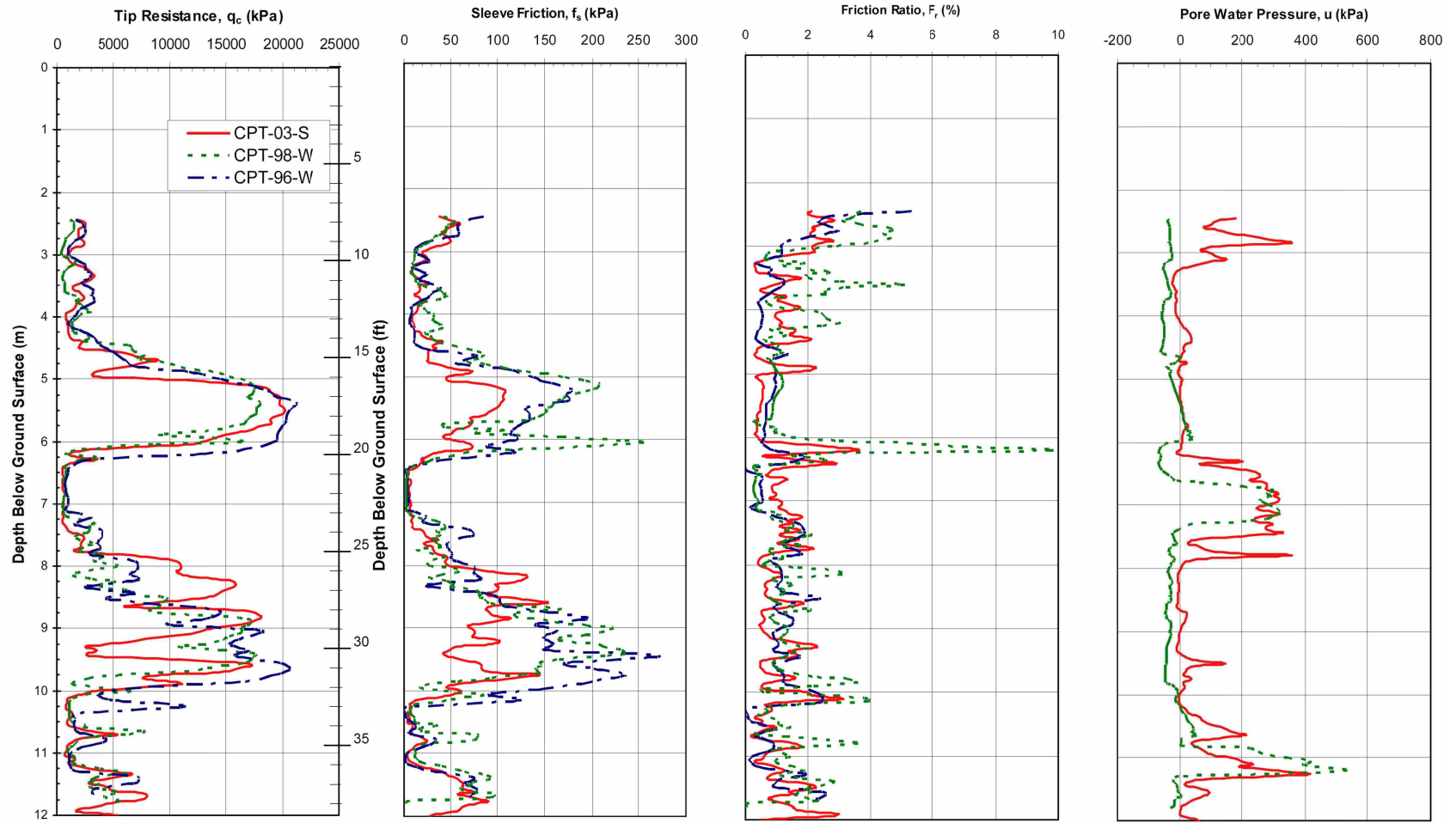
Figure 3.4 Comparison of Results from Three Different Soundings Performed at Different Times Around the 15-pile Group.

was to measure the size distribution of the particles in the soil sample and to classify the soil. All work was performed in general accordance with ASTM D 421, Practice for Dry Preparation of Soil Samples for Particle-Size Analysis of Soils (the use of No. 100 and No. 50 sieves is a variation from ASTM D 422 standard procedures). Figure 3.5 shows the percent finer by weight as a function of grain size. Upper and lower bound curves of ASTM-C33 are also included in the plot.
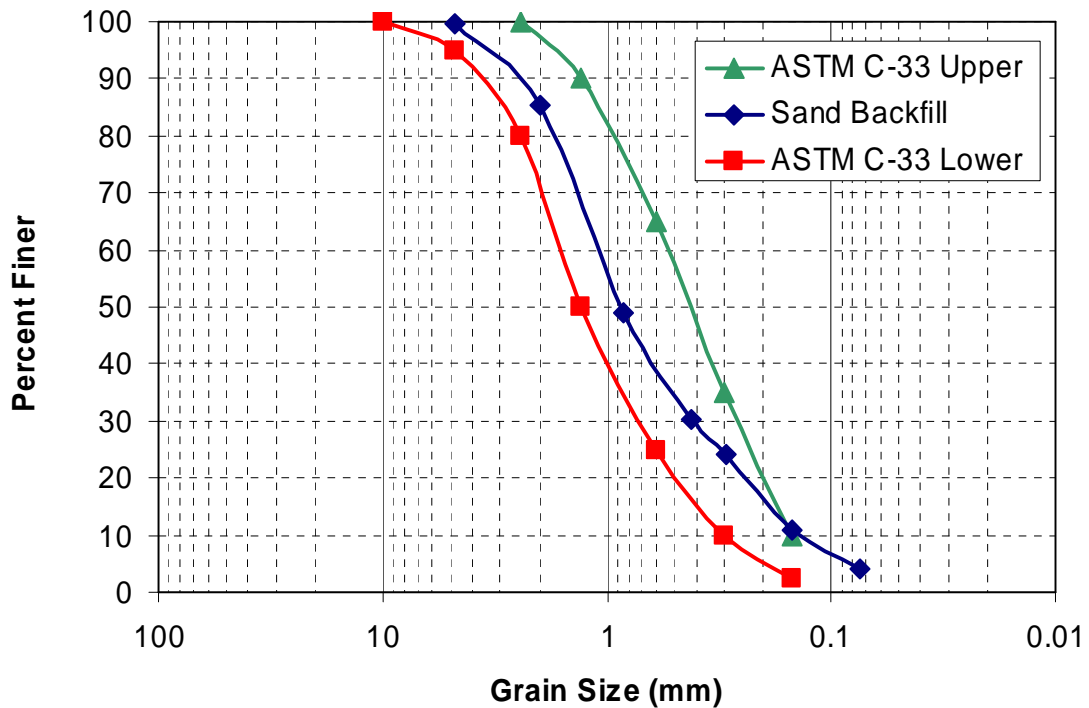
Figure 3.5 Grain Size Distribution of Sand Backfill.

A slight variation from the ASTM C-33 upper bound is observable due to the high percent of particles smaller than 0.2 mm; the predominant particle size in the soil sample was between 2 and 0.5 mm's and the largest particle size was about 5 mm. Table 3.1 is a detailed breakdown of the particle composition of the sand backfill. The table clearly

shows that a majority of the material is composed of medium to fine sand with a significant amount of coarse sand and fines, which suggests that the soil is relatively well graded. The soil sample also does not contain any particles larger than fine gravel.

Table 3.1 Percentage of material present.

Particle Description	Size Range	U.S. Sieve Size	Percent Present
Boulder	>300 mm	>12-in	0
Cobbles	75 mm to 300 mm	3-in to 12-in	0
Gravel	4.75 mm to 75 mm	No.4 to 3-1n	0.2%
Coarse	19 mm to 75 mm	¾-in to 3-in	0
Fine	4.75 mm to 19 mm	No.4 to ¾-in	0.2%
Sand	0.075 mm to 4.75 mm	No.200 to No.4	95.7%
Coarse	2 mm to 4.75 mm	No.10 to No.4	14.6%
Medium	0.425 mm to 2 mm	No.40 to No.10	55.1%
Fine	0.075 mm to 0.425 mm	No.200to No.40	26.2%
Fines	< 0.075 mm	< No.200	3.9%

Table 3.2 shows the diameters of particles at points of interest, from which the indices Cu and Cc were calculated as 8.6 and 2, respectively. The values are taken directly from the grain size distribution plot, Figure 3.5. According to the AASHTO Soil Classification System (AASHTO M 145, 1995), the soil is classified as an A-1-b soil. According to the Unified Soil Classification System (USCS), the soil is classified as a Well Graded Sand (SW). This correlates with the conclusion reached by Christiansen (2006) and Walsh (2005).

Table 3.2 Diameter of particles according to percent finer.

Percent Finer	Diameter (mm)
D_{10}	0.13
D_{30}	0.42
D_{50}	0.85
D_{60}	1.13

3.5.2 Atterberg Limits

Atterberg limit tests were performed on samples of soils from below the sand layer to classify the cohesive layers. The samples came from sites labeled H-05-S and H-03-S. Testing was conducted at the soils laboratory of Brigham Young University and in general accordance with the applicable ASTM standards. Results of the Atterberg limit tests and resulting soil classification of cohesive layers is presented in Table 3.3.

Table 3.3 Grain size distribution and Atterberg limits of soil samples (Walsh, 2005).

Depth Below Ground Surface (ft)	Natural Moisture Content (percent)	Grain Size Distribution		Atterberg Limits		Classification of Soil Layer (USCS)
		Sand (percent)	Fines (percent)	Liquid Limit (percent)	Plasticity Index (percent)	
0	---	96	4	N/A	NP	Well Graded Clean Sand (SW)
9	36	38	62	24	1	Sandy Silt (ML)
10	30	38	62	23	3	Sandy Silt (ML)
11	33	61	39	N/A	NP	Fine Sand w/ Silt (SM)
12	30	24	76	25	3	Sandy Silt (ML)
13	31	22	78	N/A	NP	Sandy Silt (ML)
14	27	38	62	24	3	Sandy Silt (ML)
15	32	41	59	N/A	NP	Sandy Silt (ML)
16	31	62	38	N/A	NP	Silty Sand (SM)
17	30	67	33	N/A	NP	Silty Sand (SM)
17.6	26	71	29	N/A	NP	Silty Sand (SM)

3.6   MODIFIED PROCTOR TESTING

In 2004, two modified proctor tests were performed by Walsh (2005) on the backfilled sand layer, the results of which are shown in Figure 3.6. Test results indicated that the average dry unit weight of the material is about 111 lb/ft^3. The dry unit weight was shown by both Proctor tests to be relatively independent of the moisture content. This, Walsh (2005) notes, is relatively unusual, as the dry unit weight typically varies

with the moisture content, peaking at a specific moisture content which would provide the maximum compaction. The results suggest that for moisture contents between 5 and 12 percent, the maximum unit weight of compaction stays independent of the moisture content. Such behavior is typical of relatively clean sands.
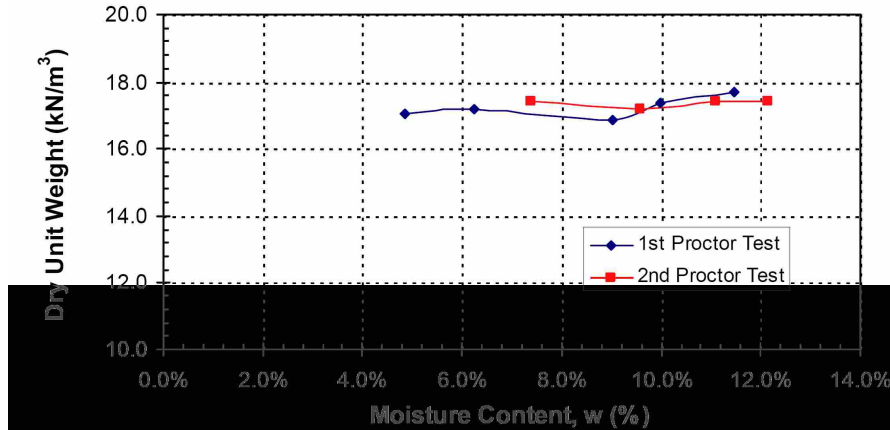
Figure 3.6 Results of Modified Proctor Tests, Walsh (2005).

3.7   IN-SITU DENSITY TESTING

A series of nuclear density gage tests were conducted at various depths to ensure consistency in moisture content, unit weight, and compaction of the surface sand layer throughout all three tests (Figure 3.7 and Figure 3.8). The results for tests one, two, and three are summarized in Table 3.4, Table 3.5, and Table 3.6, respectively. The average dry unit weights for the three tests were 105.9, 105.8, and 106.0 pcf, respectively, which is very consistent. This dry unit weight corresponds to an average relative density, D_r, of 76% and an average relative compaction, R_c, just above 95%. In calculating D_r and R_c values, maximum and minimum dry densities were obtained from Cole (2003), who conducted standard and modified Proctor tests on a sample of the clean sand used in this

52

study.   The average moist unit weight was approximately 115 pcf.   The standard

deviation of the dry unit weight decreases with each test, but is less than 2.7 pcf even for

the first test, which had the most erratic distribution of dry unit weights at various depths.

Figure 3.7 Photograph of Soil Compaction During Test Three.

Figure 3.8 Photograph of Nuclear Density Testing During Test Three.

Figure 3.9 and Figure 3.10 summarize the dry unit weight and moisture content results, respectively, as a function of depth for of all three tests. Dry unit weight results, presented in Figure 3.9, show that between the three tests the dry unit weight varied between 103 and 109 pcf. The moisture content results as a function of depth are presented in Figure 3.10, which shows that during the sloped tests the moisture content varied between 6 and 12%, resulting in an average moisture content of about 8.2%. The spread of moisture content results was more dramatic in the case of the horizontal profile test, where the moisture content varied between 3 and 16%, resulting in an average moisture content of about 7.5%. However, as indicated by the Proctor test results, the maximum dry unit weight for this sand is not strongly correlated to the natural moisture content.

Table 3.4 Nuclear density gage test results for test 1.

Depth Below Ground (ft.)	Dry Unit Weight (pcf)	Moisture Content (%)	Moist Unit Weight (pcf)	Relative Density (%)	Relative Compaction (%)
0.8	109.4	3.2	112.9	93.0	98.6
3.1	105.2	4.3	109.7	73.6	94.8
3.8	106.2	6.1	112.7	78.4	95.7
5.2	102.9	16.4	119.8	62.4	92.7
Average:	105.9	7.5	113.8	76.8	95.4
Standard Deviation:	2.7	6.1	4.3	12.7	2.4

Table 3.5 Nuclear density gage test results for test 2.

Depth Below Ground (ft.)	Dry Unit Weight (pcf)	Moisture Content (%)	Moist Unit Weight (pcf)	Relative Density (%)	Relative Compaction (%)
1.4	108.4	6.9	115.9	88.5	97.7
1.8	104	6.9	111.2	67.8	93.7
2.3	103.1	11.5	115.0	63.4	92.9
2.7	103.5	10.4	114.3	65.4	93.2
3.1	107.8	9	117.5	85.8	97.1
3.7	106.4	5.4	112.1	79.3	95.9
4.5	105.8	8.7	115.0	76.5	95.3
5.2	107.7	8.6	117.0	85.3	97.0
Average:	105.8	8.4	114.7	76.5	95.3
Standard Deviation:	2.1	2.0	2.2	9.9	1.9

Table 3.6 Nuclear density gage test results for test 3.

Depth Below Ground (ft.)	Dry Unit Weight (pcf)	Moisture Content (%)	Moist Unit Weight (pcf)	Relative Density (%)	Relative Compaction (%)
0.0	105.7	5.5	111.5	76.0	95.2
0.6	105.6	6.5	112.5	75.6	95.1
1.0	106.8	7.8	115.1	81.2	96.2
1.4	105.3	10.3	116.1	74.1	94.9
2.0	104.5	10.8	115.8	70.3	94.1
2.4	105.1	7.7	113.2	73.2	94.7
2.9	109.3	6.3	116.2	92.6	98.5
3.3	105.9	7.1	113.4	77.0	95.4
4.1	105.6	6.3	112.3	75.6	95.1
4.5	106.1	7.4	113.9	77.9	95.6
Average:	106.0	7.6	114.0	77.3	95.5
Standard Deviation:	1.3	1.7	1.7	6.1	1.2
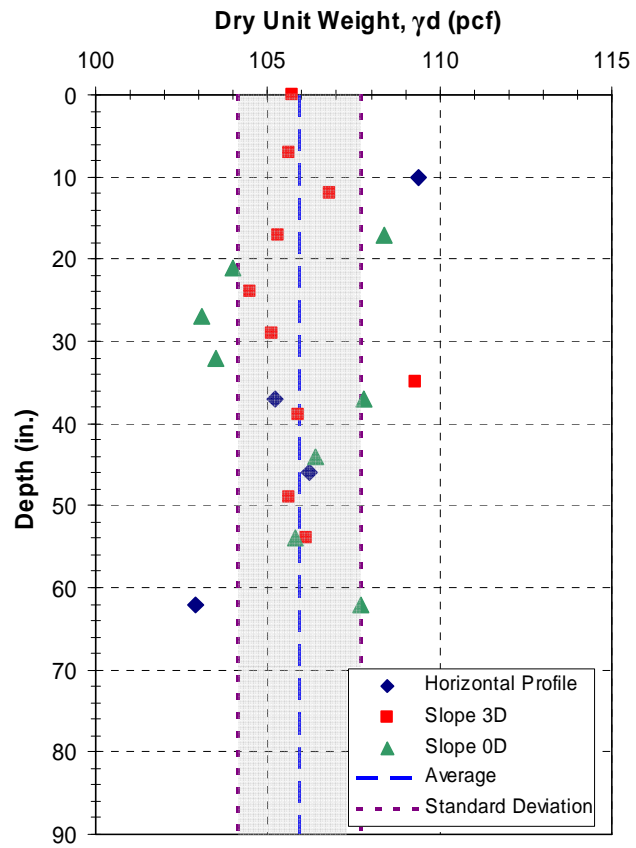
Figure 3.9 Unit Weight Results as a Function of Depth.
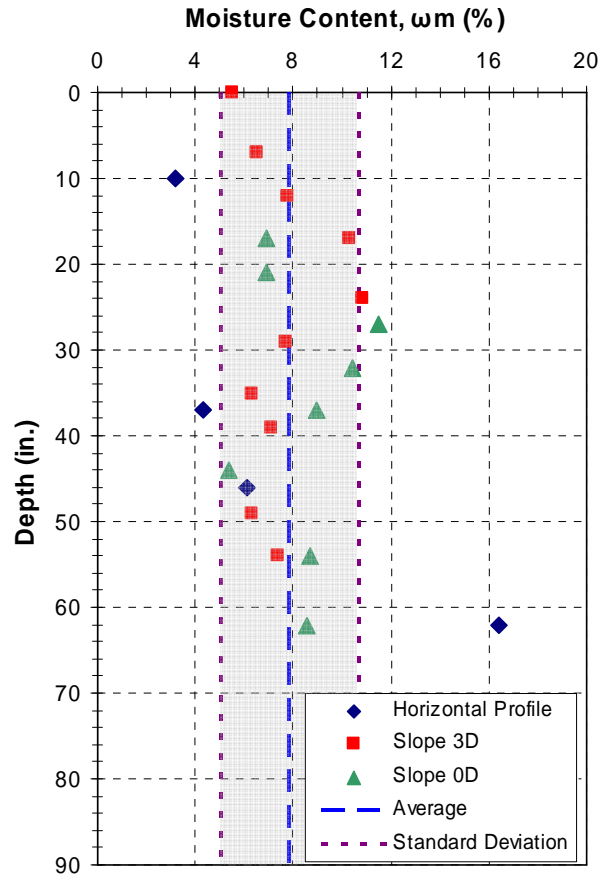
Figure 3.10 Moisture Content Results as a Function of Depth.

3.8   STRENGTH TESTING

3.8.1   Direct Shear Testing

A direct shear test was performed on the top sand layer near the single test pile located west of the 15-pile group. For this test, an 18 inch square steel shell was fitted around the sand, taking great care not to disturb the soil. This was achieved by placing the box on top of the soil and carefully digging under the box, allowing it to slowly and evenly settle around the sand. The box was allowed to settle until the soil in the box was level with the top of the box. A steel plate, slightly smaller than the inside dimension of

57

the box, was placed over the soil inside and weights were placed on top. The box was then loaded laterally using a manually operated hydraulic jack. The load was measured with a calibrated dial gage and the lateral displacement of the box was measured with a dial gage accurate to a thousandth of an inch. The lateral load was applied at an average rate of 0.2 inches per second until the soil failed along the interface between the soil in the box and soil below. The test was conducted in stages with four progressively higher loads to provide an indication of the shear strength as a function of normal stress. The shear stress as a function of displacement for all four tests is shown in Figure 3.11, while the shear stress is plotted versus normal stress in Figure 3.12.
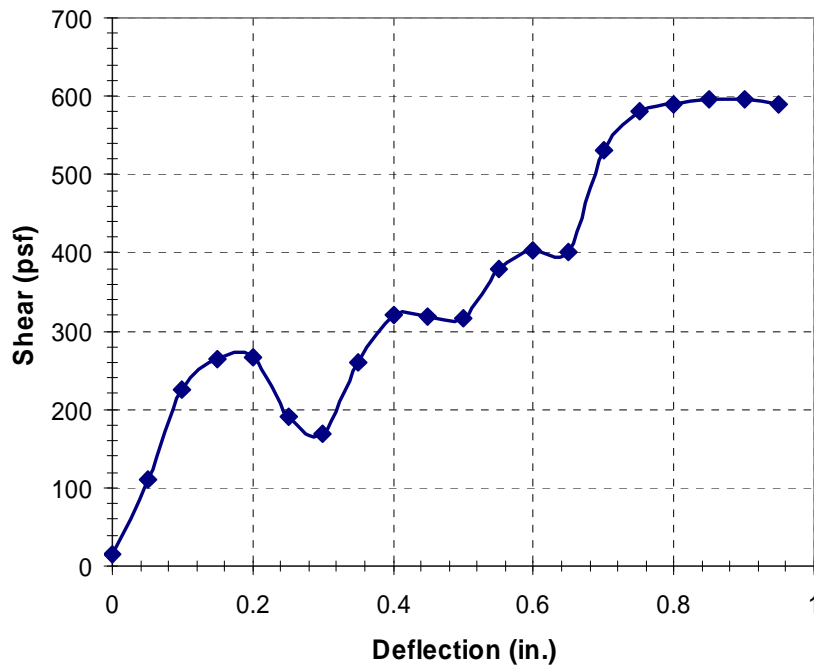
Figure 3.11 Shear vs. Lateral Deflection Results of Field Test.

The primary purpose of the direct shear test was to determine the angle of internal friction, ϕ, of the soil. To do this, the shear stress was plotted as a function of the normal
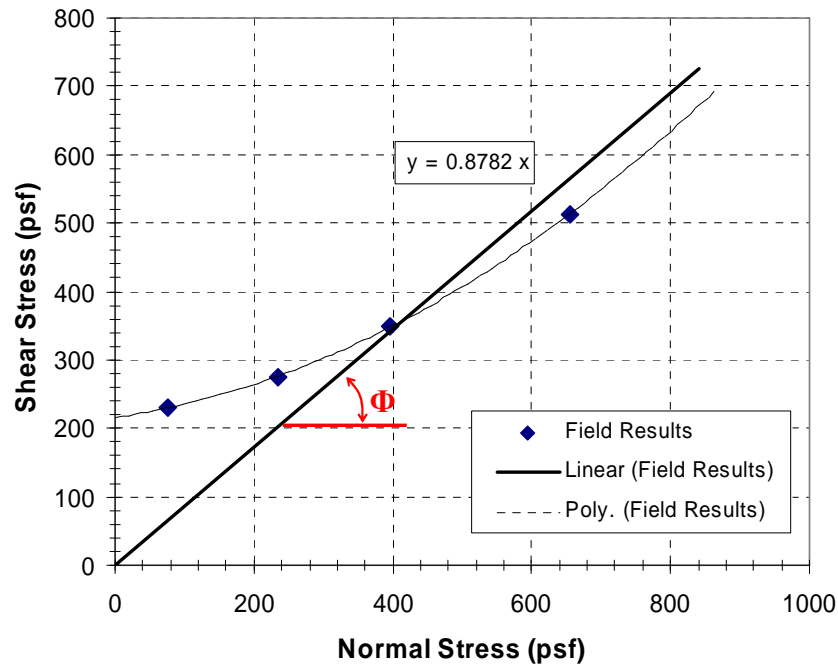
Figure 3.12 Shear Stress vs. Normal Stress Field Results.

stress. The friction angle, then, is taken as the slope of the shear stress and normal stress relationship. Because of the scattered nature of the data points, a linear trendline was fitted to the four points, which is shown in Figure 3.12. The trendline was forced through the origin as there is no significant cohesion in the soil tested–clean washed concrete sand. The friction angle, taken as the inverse tangent of the trendline slope, was determined to be approximately 41.3°.

Figure 3.12 appears to show a quadratic relationship between the shear stress and normal stress, which suggests that there may be some apparent cohesion in the sand owing to partial saturation effect. It further appears that for higher stresses the relationship asymptotes to the trendline; thus, validating the use of a linear trendline passing through the origin to represent the stress relationship at higher stress levels. One significant potential drawback of the staged in-situ direct shear test is that shearing is

repeatedly taking place on the same shear plane for each test. When dense sand is sheared, dilation typically leads to a decrease in density along the shear plane. As a result, the shear strength from subsequent tests could be less than that for the initial test. Ideally, separate in-situ tests should be performed at each normal stress to obtain better results; however, the time and effort associated with these in-situ direct shear tests makes such methodology difficult.

Laboratory direct shear tests were conducted by RB&G Engineering on a sample of the top sand layer. The laboratory test results are presented in Figure 3.13, form which a friction angle of approximately 38.1° is obtained. The slight discrepancy between the field and laboratory results may be due to some inconsistency between field and laboratory soil sample properties such as relative density and compaction. Therefore, a friction angle, φ, of 40° is used-the rounded average of the field and laboratory results.
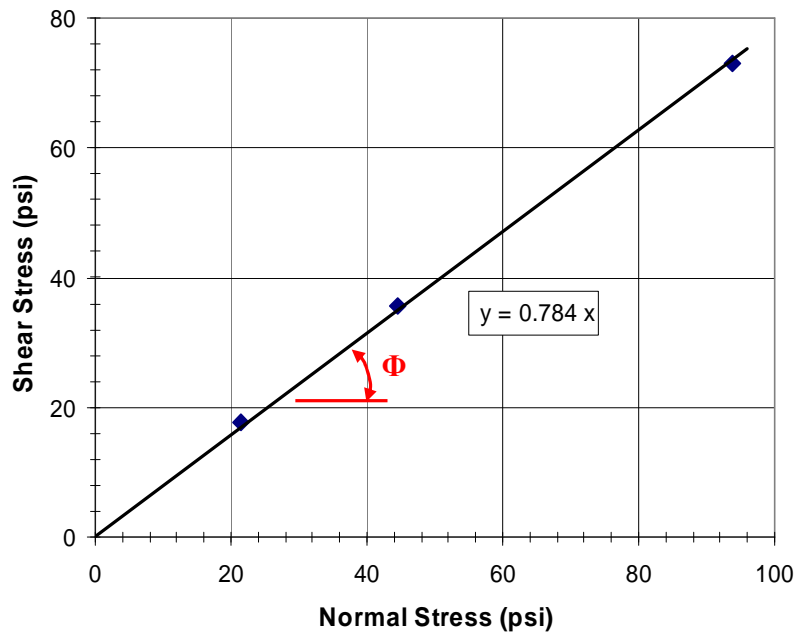
Figure 3.13 Shear Stress vs. Normal Stress Laboratory Results.

3.8.2 Vane Shear Testing (VST)

Vane shear testing was performed at the location labeled DH-96-W on the clay layers located at depths between 8-16 ft and 22-28 ft below ground surface. The recorded shear strength values were corrected using the methods prescribed by Bjerrum (1972) to account for the plasticity index (PI). Three of the four vane shear tests fell within the range of 420 to 1250 psf, while the fourth test reported a shear strength of 2300 psf. As can be seen in Figure 3.14 a majority of the shear strength results obtained from the vane shear tests are within the general range of shear strengths obtained from other tests performed in the site.
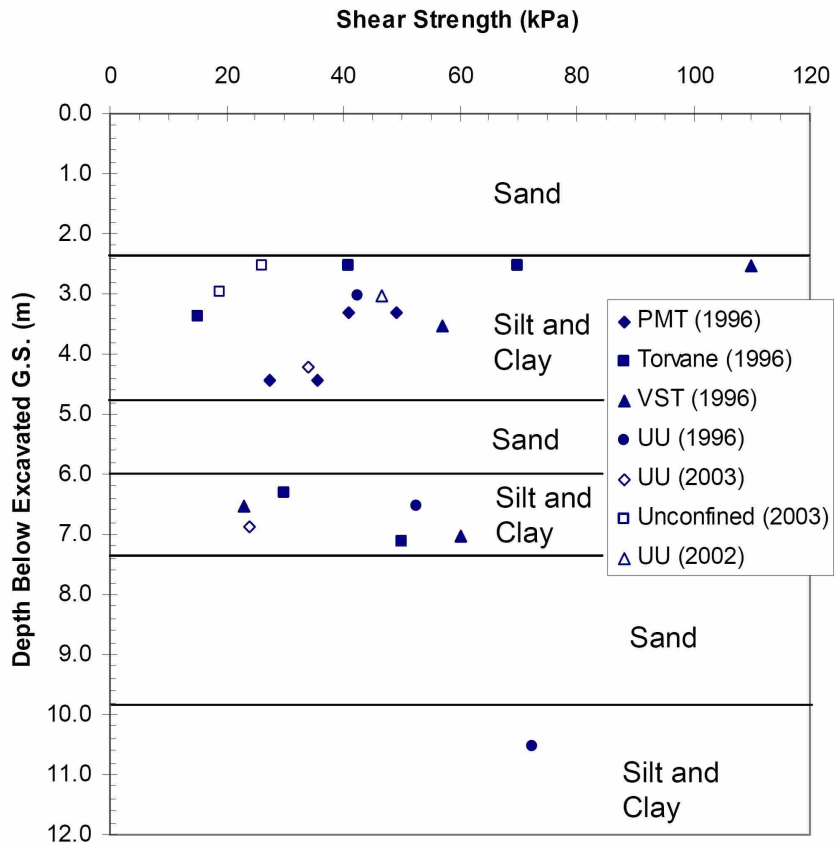
Figure 3.14 Shear Strength of Clay Layers from Various Tests (Walsh 2005).

Figure 3.14 also shows a wide scatter of shear strength results at a depth even within a test group. This is primarily due to unconformities within the layer and the variations in soil properties between the locations of the samples tested.

3.8.3   Shear Strength Tests

Laboratory shear tests were conducted on soil samples of the clay layers below the backfilled sand layer. The tests performed included Unconsolidated-undrained (UU) triaxial tests, on samples from borings DH-96-W, DH-02, and DH-03; Pocket torvane shear tests on samples from DH-96-W; and an unconfined compression test on a sample from DH-03 (see Figure 3.2 for boring locations). Results from the shear tests performed on the clay layers were used to obtain input values for the computer analysis using the program LPILE.

CHAPTER 4 - SINGLE PILE FIELD LOAD TEST

4.1   INTRODUCTION

Full-scale lateral load tests on a single driven steel pipe pile were carried out at a site near the Salt Lake International Airport to observe the effects of sloping ground and pile distance from slope crest on the lateral resistance of the pile-soil system. The slope of 1.75H : 1V (30º angle) was chosen for this research as it is the most commonly used slope in practice and literature, particularly with respect to abutments. All field tests were carried out between August 20th and September 20th of 2006. General ASTM standards for testing were followed and precautions were made to acquire results as accurate as possible from which useful information regarding the slope effect on the pile strength could be obtained.

This chapter is a summary of the test layout, instrumentation, procedures, results, and observations made during and after testing. The results and observations of the tests involving piles adjacent to a slope are compared to the results of the test for the pile in horizontal ground.   In addition, recommendations and explanations of observed phenomenon are presented in this chapter.

4.2   TEST LAYOUT

Figure 4.1 shows a detailed layout of the site, including the tested single pile and the 15-pile group used in the testing. Before the installation of the piles, approximately 5 feet of the gravel fill at the site was excavated to a distance of 6 feet around the pile. The single pile was driven closed-ended on June 2, 2002, leaving approximately 7 feet of the pile head exposed. Subsequently, approximately 3 feet of clay was excavated around the top of the pile. Washed concrete sand was then backfilled and compacted around the pile level with the original ground surface before any excavation. This resulted in a sand layer approximately 8 feet thick at the surface around the pile.
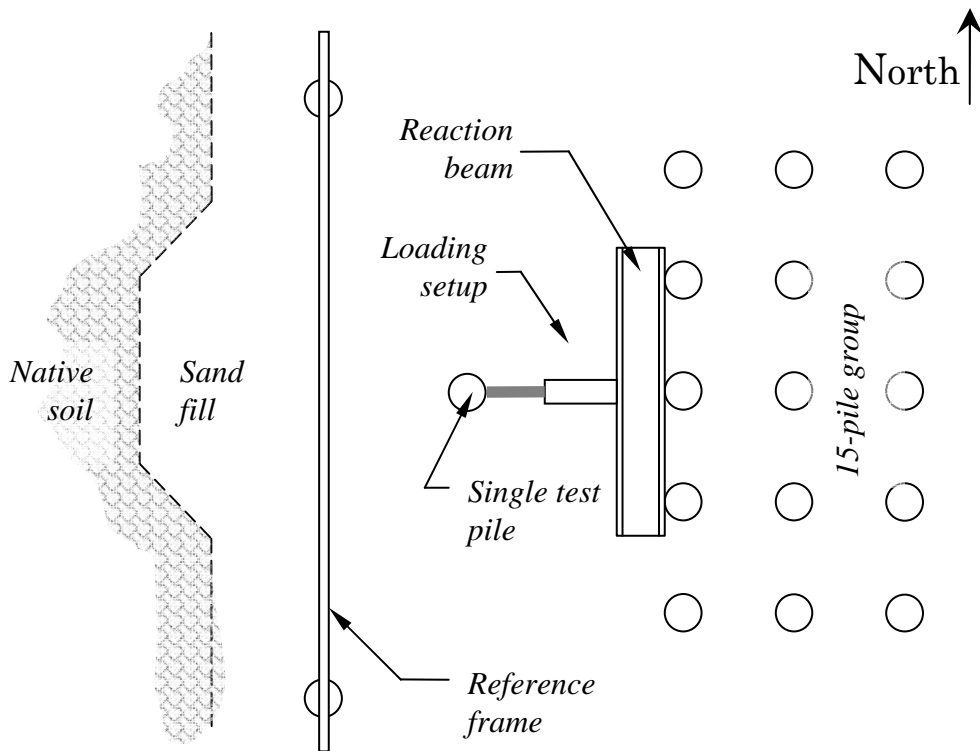
Figure 4.1 Test Layout.

In preparation for the tests conducted in this study, the washed concrete sand around the pile was again excavated to a depth of 6 feet where groundwater was typically encountered. The excavated zone extended about 6 feet west of the pile, 2 ft east of the pile, and was about 12 ft wide transverse to the direction of loading. The excavated sand was then backfilled and compacted in 6 to 9 inch lifts to a density of about 95% of the modified Proctor value. The procedure was performed to ensure that disturbed soil was not being used from the tests conducted in 2005 on the site. After each test, the same zone was again excavated to minimize differences in soil properties within this critical region for lateral resistance. Analysis indicates that the lateral pile deflections below 6 ft for the horizontal test would likely be less than 0.2 inch and a gap would not form in sand below the water table. Therefore, the influence of soil variations below 6 ft would likely be relatively minor compared to the soil behavior above this depth.

The single pile was loaded laterally for all tests by applying a point load approximately 19.5 inches above the ground surface. The load was applied by the expansion of a 150-ton hydraulic jack connected to the pile as shown in Figure 4.2. The reaction was provided by three piles from the 15-pile group on the east side of the single pile. A reaction beam was welded to the reaction piles and the jack was bolted to the beam. The reaction piles were at least six feet away from the test pile to minimize any interference. To connect the jack to the pile, a channel section was welded to the pile head and a one-directional swivel was bolted onto the channel; the jack, then, was connected to the swivel. The swivel was placed between the jack and the pile to ensure that the pile was loaded under a "free head" (zero-moment) condition, greatly reducing the potential for eccentric loading and applied moments. A potential problem associated

with the loading setup was the possibility of applying the load at an angle; thus, applying axial loads on the pile, which would alter the results. Such potential problem was mitigated during the testing by taking great care to place the hydraulic jack orthogonal to the pile. Figure 4.2 b) is a photograph of the actual loading setup used throughout the research.

a)
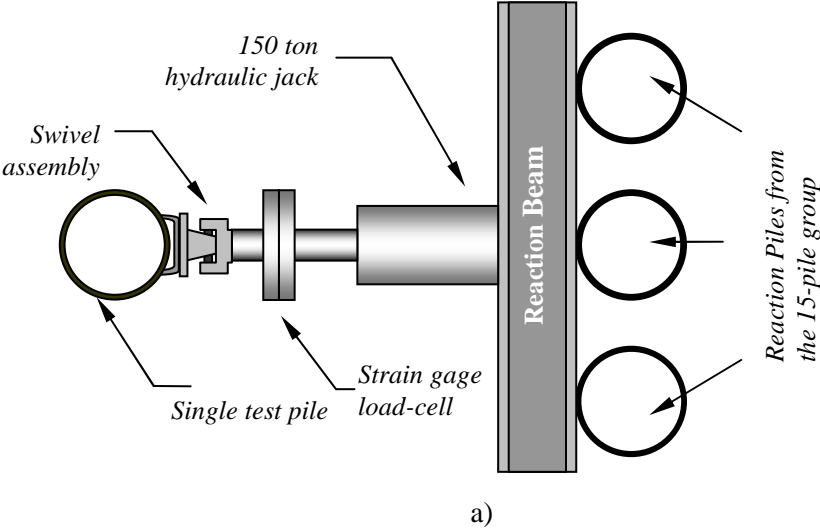
b)

Figure 4.2 a) Schematic Diagram and b) Photograph of the Loading Setup Used in the Tests.

4.3   MATERIALS

The reaction beam placed between reaction piles and the jack was a W12 x 45 steel section. Preliminary analysis showed that the beam would not undergo significant deformation from the loading; and therefore, no alterations were made to the beam.

The single pile used in the testing conformed to the ASTM 252 Grade 2 specifications. The pile had an outer diameter of 12.75 inches and a wall thickness of 0.375 inches. Figure 4.3 shows the cross-sectional dimensions of the pile. The figure also shows the steel angles that were welded onto the pile to protect the attached strain gages, which are discussed further on in this chapter.   The angles altered the moment of inertia of the pile, increasing it from 279 in^4 to 344 in^4. Because of the significant difference, all calculations of bending moment in this research use the altered moment of inertia. Yield strength tests on 192 similar piles performed by the Geneva Steel Company suggest that the average yield strength of the pile is 58,700 psi with a standard deviation of 2,200 psi. The tests also suggest that the average tensile strength of the pile is 84,700 psi with a standard deviation of 2,560 psi. Analysis of the pile strength was done using the 0.2 % strain offset method.

Calculations indicate that the yield bending moment of the single pile with the welded angle irons is about 264 kip-ft (3,166 kip-in). All previous tests performed on the pile have resulted in bending moments less than the yield moment and therefore the pile has been considered elastic throughout this research.

Strain gages

Welded angle iron with leg lengths of 1.5 in. and thickness of 0.2 in.

Direction of Force

Closed-ended steel pipe pile with OD of 12.75 in. and thickness of 0.375 in
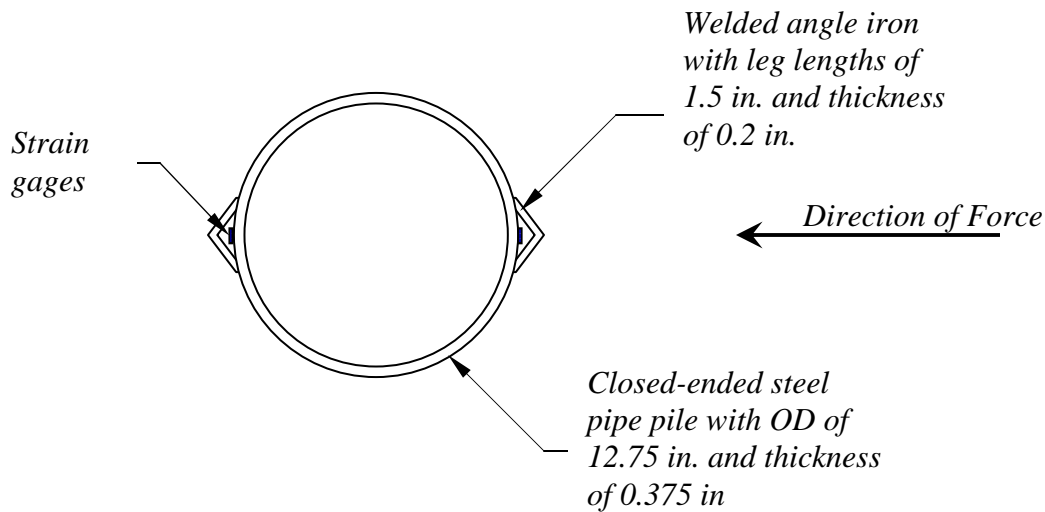
Figure 4.3 Cross-section of the Single Pipe Pile Used in the Testing.

4.4   INSTRUMENTATION

A variety of instruments were used to measure the response of the pile to the lateral load. To ensure accuracy and reliability of data, checks were performed on the various instruments. The responses of most interest in the research were the pile head deflection, pile head rotation, and pile bending moments as a function of pile head load.

The pile head deflections were measured by digital string potentiometers, accurate to a hundredth of an inch. The extendible string of the potentiometer was connected to the side of the pile head at an elevation level with the point of load application. An independent reference frame was constructed in front of the pile with supports a sufficient distance from the pile to ensure independence from the soil movement due to loading. The potentiometer was attached to the reference frame at an elevation level with the point of application. To ensure accuracy and redundancy, two string potentiometers

were used, one on each side of the pile. Because no anomalies were detected, the two deflection measurements were zeroed and averaged for use in analyses. Data from the potentiometers were digitally transferred to a computer data acquisition system. Figure 4.4 is a close-up photograph of the instrumentation setup used during the tests.
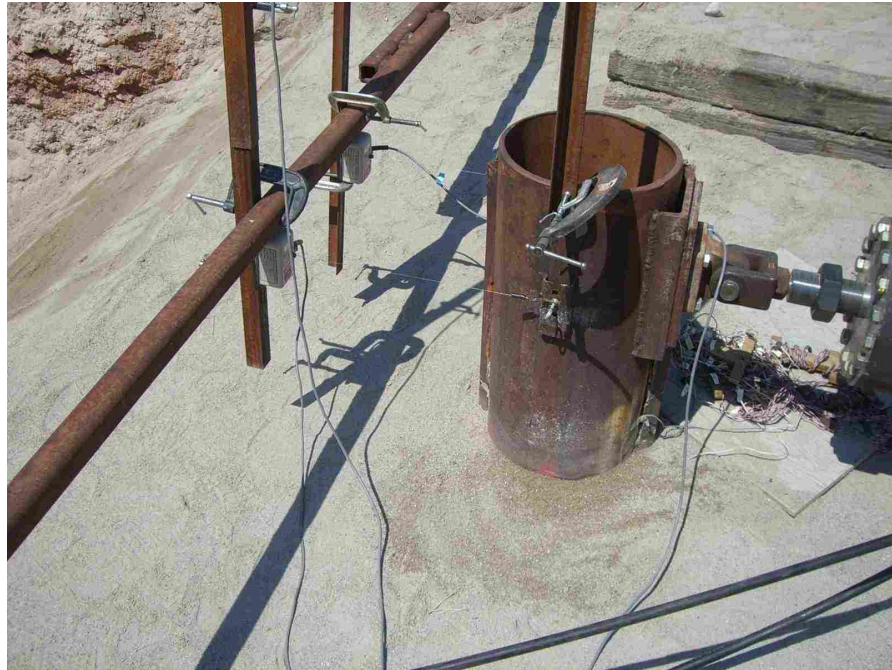
Figure 4.4 Photograph of the Instrumentation Setup.

The rotation of the pile head was obtained by measuring the differential deflection of two points some distance apart. The first point was the point of load application, data for which were provided by the two string potentiometers used for measuring pile head deflections. The second was a point 36 inches above the point of load application, for which deflection was measured by a third string potentiometer. The extendible string of the third potentiometer was connected to a steel angle, which was then connected to the

pile head. The third potentiometer was also connected to the reference frame by a second angle iron.

Bending moments in the pile were obtained from measured strains on opposite sides of the pile in the direction of the loading. Strains were measured by waterproof electrical resistance type gages, model WFLA-6-12, manufactured by Texas Measurements, Inc. The gages were placed on opposite sides of the pile at the same level along the length of the pile. A total of 42 gages were used with varying distances between successive gages. The top 6 gages were placed 2.5 feet apart, the middle 26 were placed 1.5 feet apart, and the bottom 14 were placed 3 feet apart as illustrated in Figure 4.5. Strain gages near the top were placed closer together since the top half of the pile was expected to experience the greatest bending moment fluctuations; hence, more data were necessary.

Before the installation of the gages, the locations where the gages would be attached were sanded smooth and rinsed with acetone to prevent the separation of the gages from the pile during testing. The gages were then glued to the pile with an epoxy-based glue.   After the installation of the gages, the angles were welded to the sides of the pile, covering the strain gages to protect them from damage during driving of the pile. In addition, water resistant foam was injected into the cavity formed between the angle and the pile to protect the gages against damage during driving and interference from water. Despite these precautions, a number of strain gages had failed and provided either no data or unreliable data. In such cases, the data from faulty gages were not included in the analyses. A sufficient number of gages survived, however, to provide adequate results of bending moments along the length of the pile. As a check for accuracy of the gage data,

moments derived from the strains at the surface level were also compared to the moment at ground level using general statics principles – applied load multiplied by the distance to point of load application. Data from the strain gages was digitally transferred to the data acquisition system.

.
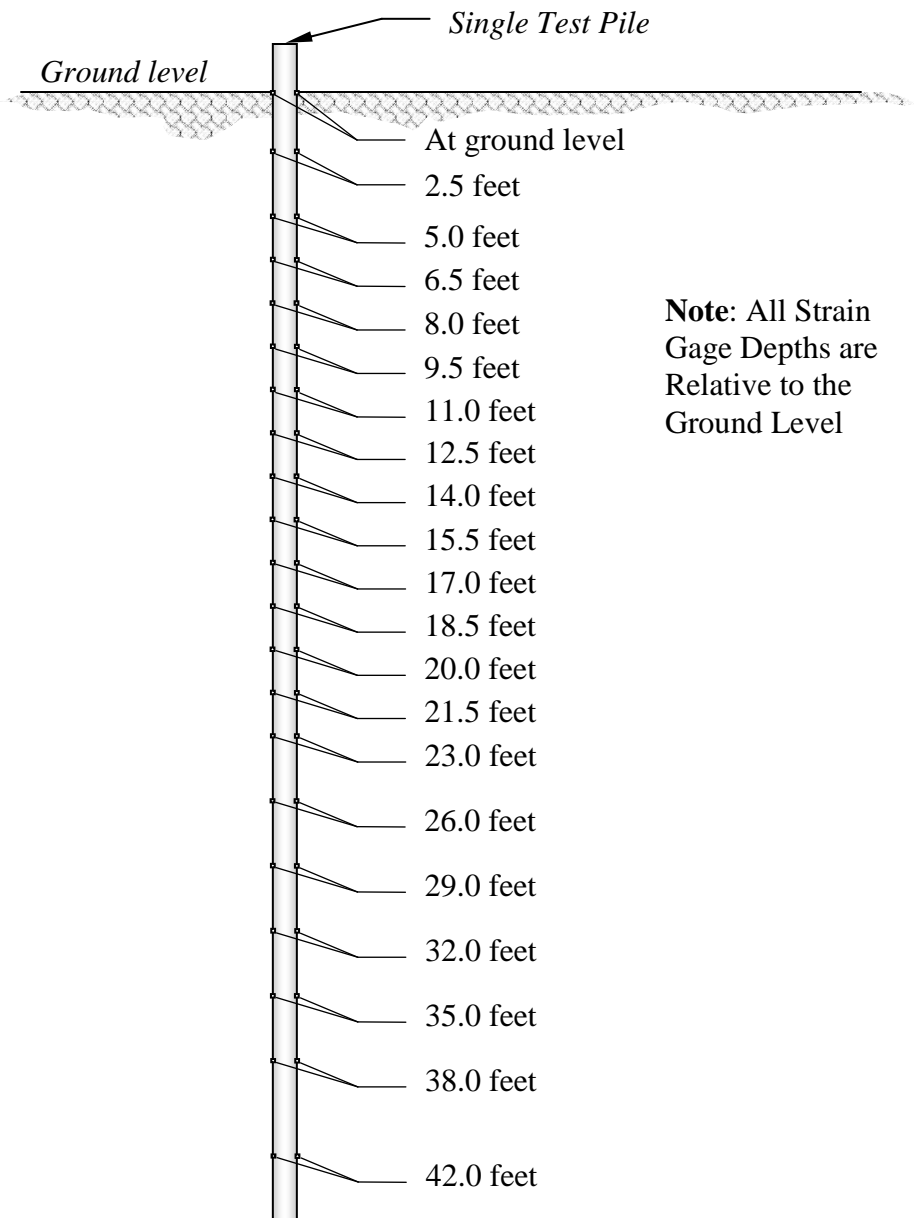
Figure 4.5 Strain Gage Locations Relative to Ground Surface.

The applied loads were measured by a load-cell placed between the jack and the pile. As a check for accuracy of the load-cell, readings were compared to pressure data from the jack multiplied by the area of the piston. Load-cell data was digitally transferred to the acquisition system.

The data from all string potentiometers, strain gages, and load-cell were digitally transferred in 1.0 second intervals to an Optim Megadac data acquisition system. The system allowed for live monitoring of acquired data, giving the researchers an opportunity to check data for reasonability. All data was then transferred to a spreadsheet for analysis.

4.5   TEST PROCEDURE

Testing started on August 20, 2006. The fill sand 6 feet in front and 6 feet to each side of the pile was excavated out in 6 to 12 inch layers to a depth of about 6 feet. Densities at each layer were measured with a nuclear density gage and recorded. The excavated fill sand was later put back into the excavation and compacted to the previously recorded densities in about 6 inch lifts and the sand was brought to the level of the surrounding soil. The compaction was achieved using a jumping-jack type hand operated hydraulic ram. After the compaction, the instruments and loading apparatus were set up and connected to the data acquisition system. The instruments were checked and the first test, pile in horizontal soil profile, was performed. The single pile was pushed laterally at an average rate of 0.2 inches per second to target deflections of 0.125, 0.25, 0.5, 0.75, 1.0, 1.5, 2.0, 2.5, and 3.0 inches with pauses between successive

deflection targets for manual readings. After the last target deflection, the pile was pulled back to its original position.

The second test, pile at the crest of a 1.75H : 1V (30º angle) slope, was performed the following day. The soil 6 feet in front and on each side of the pile as well as 2 feet behind the pile was excavated to a depth of about 6 feet and recompacted back into the excavation in about 6 inch lifts to the same density as the first test. The sand was compacted into place at an inclination and later was shaped into the desired slope of 1.75H : 1V (30º angle) with the crest of the slope intersecting the center of the pile at ground level. After the setup was complete, the pile was pushed at an average rate of 0.2 inches per second to the same target deflections as in the first test with the addition of a 3.5 inch target deflection. After the last target deflection, the pile was brought back to its original position.

The third test, pile located three pile diameters from the crest of a 1.75H : 1V (30º angle) slope, was conducted the same day as the second test. The same steps were performed as in the second test with the only difference being the location of the crest of the slope relative to the pile. Figure 4.6 shows a schematic drawing of the three tests performed.

4.6   TEST RESULTS

This section presents the results of the response of pile and soil to the lateral loading. Particular emphasis has been placed on the lateral deflection and bending moments experienced by the pile as a function of applied load. In addition, the shear

failure patterns during each test were carefully mapped and photographed in an effort to gain insight into the failure mechanism.
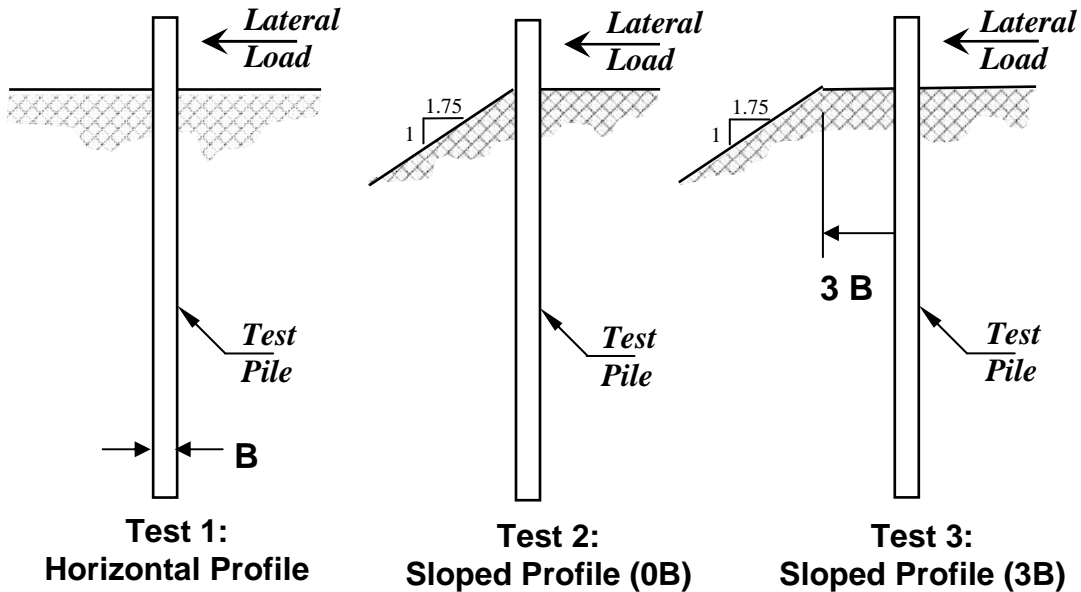
Figure 4.6 Schematic Representation of Tests Performed.

4.6.1   General Observations

A gap formed behind the pile as the pile head deflected under the lateral load as seen in the photograph in Figure 4.7. The same phenomenon in cohesionless soils was observed by Gabr and Borden (1990) and Davison (1982). The visible portion of the gap remained open throughout the testing of all three tests, suggesting a) that the sand had some apparent cohesion, which was likely due to its partially saturated condition, and b) that the material behind the pile had little effect on the pile response for the depth to which the gap extended. Previous test on the same single pile and soil profile conducted a year prior, also reported a gap forming behind the pile; however, as Walsh (2005)

74

reports regarding the testing, the gap collapsed and filled up with the sand behind the pile. The difference in these results can be attributed to the fact that the soil in the 2005 test had a slightly lower relative compaction and cyclical loading was applied to the soil, which caused a loosening of the sand allowing it to fill the gap. The potential for collapse may also be related to the moisture content of the sand. Dry sands or saturated sand would be more likely to collapse, while the partially saturated sand would be more likely to maintain a gap.
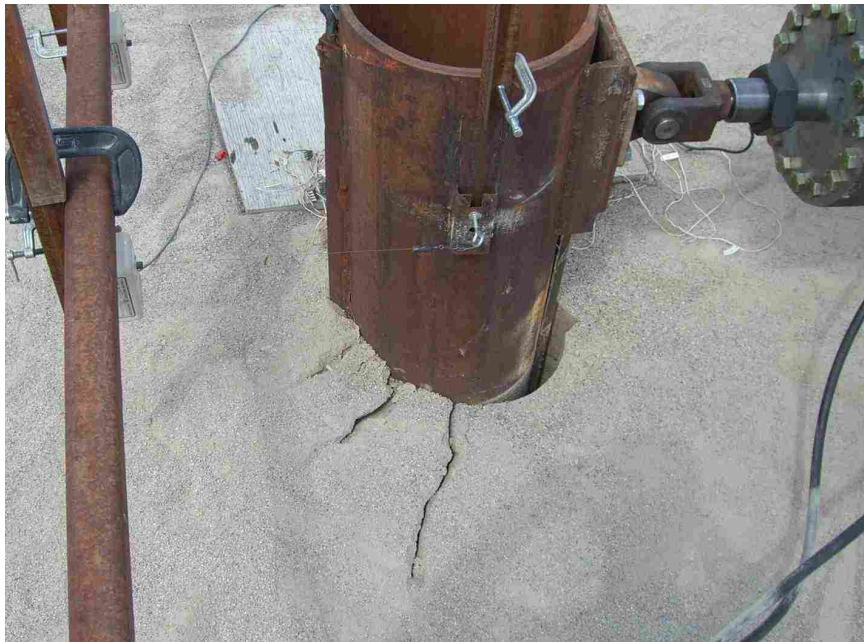
Figure 4.7 Photograph of Gap Behind the Pile.

4.6.2   Load and Deflection

Figure 4.8 through Figure 4.10 show the complete lateral load and deflection relationship of the pile during the three tests. The load and deflection data has been adjusted to account for arbitrary initial values recorded by the instruments prior to

loading. The results show that no anomalies took place during testing. Because the data used to generate the plot was in agreement with the checks discussed earlier in the chapter, the relationship is considered accurate.
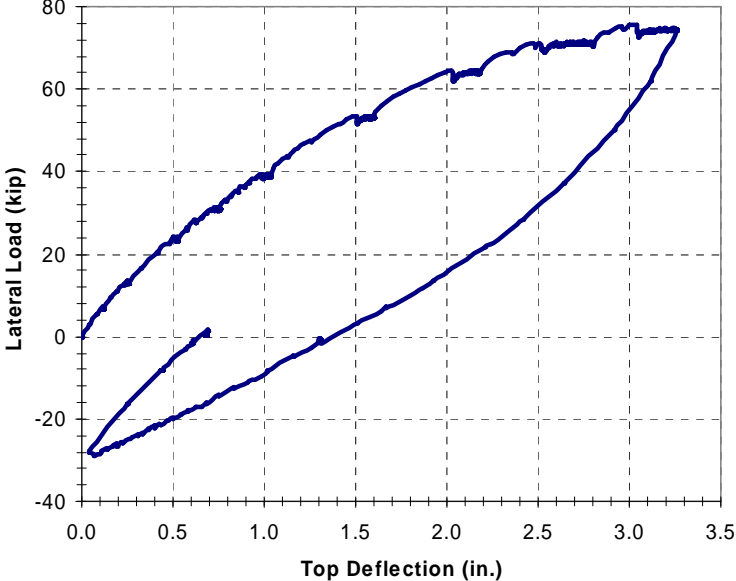
Figure 4.8 Unreduced Load and Deflection Results of Test One.
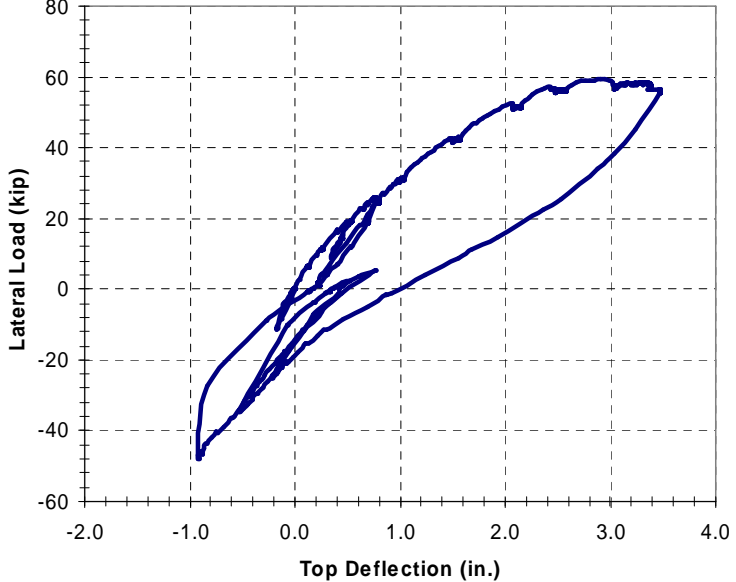
Figure 4.9 Unreduced Load and Deflection Results of Test Two.
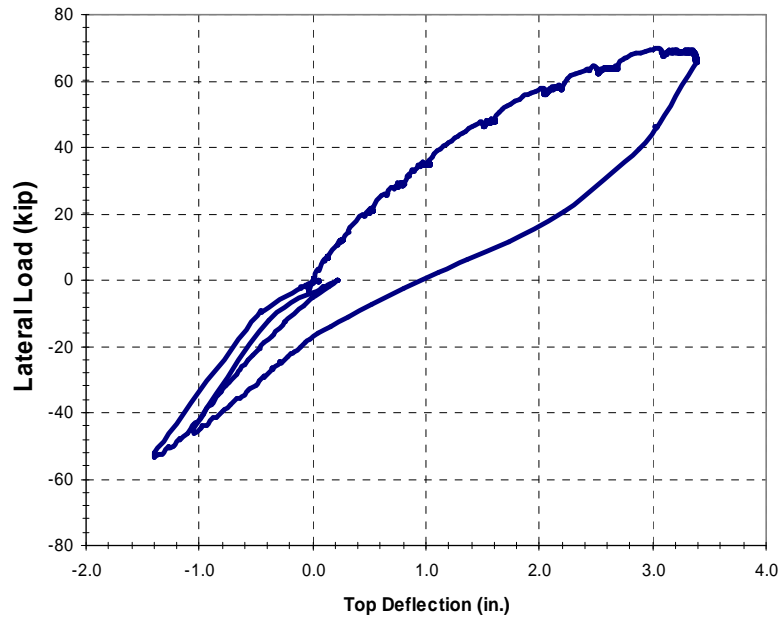
Figure 4.10 Unreduced Load and Deflection Results of Test Three.

The pile in all three load tests did not return to its original position after all load was removed. Christensen (2006) reported a similar observation, attributing it to sand filling in behind the pile preventing it from returning to its original position. In this case, however, it is likely due to yielding of the pile because the gap behind the pile remained largely open through the test. Typically, it was necessary to pull back on the pile to move it back to its original position. The pile's inability to return to its original position without additional load had no significant effect on subsequent tests, as the soil around the pile was excavated to a depth of about 6 feet and recompacted after each test. However, the effects of yielding were accounted for in the analysis of the strain data as described subsequently.

The load vs. deflection curve of test two, Figure 4.9, shows that after target deflections of 0.5 and 0.75 in., the pile was momentarily pulled back then pushed forward. This was not done intentionally; instead, was due to operator error. Although

the pull and push would induce cyclical loading action, which Christiansen (2006) shows reduces the strength of the soil-pile system, the remainder of the load vs. deflection curve shows strong agreement with the curve prior to that point. Therefore, the accidental unloading had no significant effect on the outcome of the results.

Figure 4.11 shows plots of the peak loads at each target deflection for all three tests. It is readily observable from Figure 4.11 that the sloped profile negatively affected the ultimate lateral strength of the pile-soil system, which is particularly true for the pile located closest to the crest of the slope. This observation is in strong agreement with previous research. However at small deflections the load-deflection curves for the three tests are very similar. At these small deflection levels, the shear zones radiating out from the pile have not likely encountered the slope face.
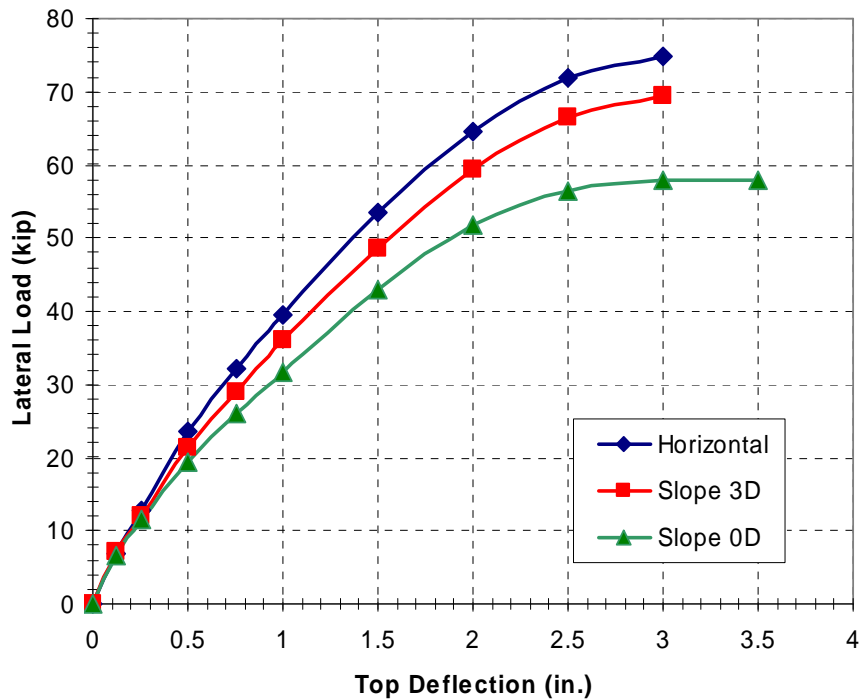
Figure 4.11 Reduced Load vs. Deflection Curves of All Three Tests.

Table 4.1 is a summary of the peak loads at each target deflection for all three tests and the ratios, ψ, of load on pile in the sloped profile to the load on pile in the horizontal profile at each target deflection. The average ψ values and standard deviations are also shown for both sloped profile tests. A plot of ψ values for each target deflection is shown in Figure 4.12, which indicates that the effect of slope on the response of the pile-soil system is near constant past a certain deflection point. For both sloped profile tests, this point appears to be at a deflection of 0.5 in., suggesting that it takes a deflection of about 0.5 in. for the shear zones to be effected by the slope in front of the pile. For this reason, average and standard deviation calculations in Table 4.1 omit values from target deflection less than 0.5 in. The relatively small standard deviations given in Table 4.1 reaffirm the observation that the reduction of strength due to the slope is near constant and independent of the load applied or deflection past the point of engagement.

Table 4.1 Load ratios at target deflections.

Defl [in.]	Horiz Load (kip)	Slope 0D Load (kip)	Slope 3D Load (kip)	ψ 0B	ψ 3B
0.125	6.85	6.56	7.10	0.96	1.04
0.25	12.85	11.55	12.09	0.90	0.94
0.5	23.45	19.28	21.32	0.82	0.91
0.75	32.14	25.90	29.07	0.81	0.90
1	39.51	31.66	36.02	0.80	0.91
1.5	53.52	42.86	48.61	0.80	0.91
2	64.64	51.82	59.29	0.80	0.92
2.5	71.78	56.42	66.42	0.79	0.93
3	74.85	57.93	69.42	0.77	0.93
Average:				0.80	0.91
Standard Deviation:				0.02	0.01
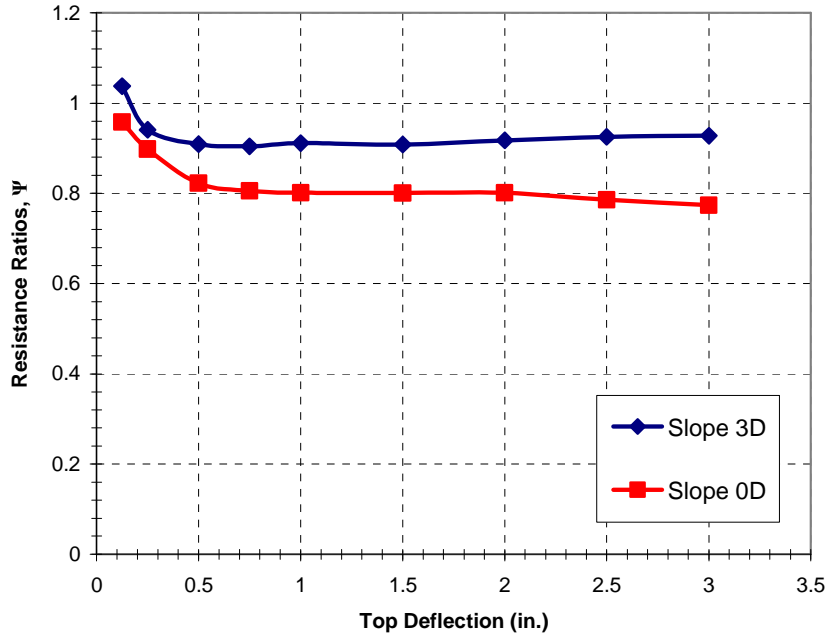
Figure 4.12 Resistance Ratios at Each Target Deflection.

The ultimate resistance ratio, Ψ, taken as the ratio of ultimate load of pile in slope to pile in horizontal profile (P_u slope/P_u flat), was calculated as 0.93 for the pile located three pile diameters from the crest of the slope and 0.77 for the pile located at the crest of the slope. These values are significantly higher than the values suggested by most of the small scale-model tests and mathematical models discussed in Chapter 2. However, the results are in reasonable agreement with centrifuge test results in dense sand reported by Mezazigh and Levacher (1998) and 1-g model tests in dense sand reported by El Sawwaf (2006). A comparison of Ψ values as a function of pile distance from slope crest for a slope of about 30º is shown in Figure 4.13, which indicates that the values obtained from the full scale tests in this study are generally higher than most of the values from other studies.
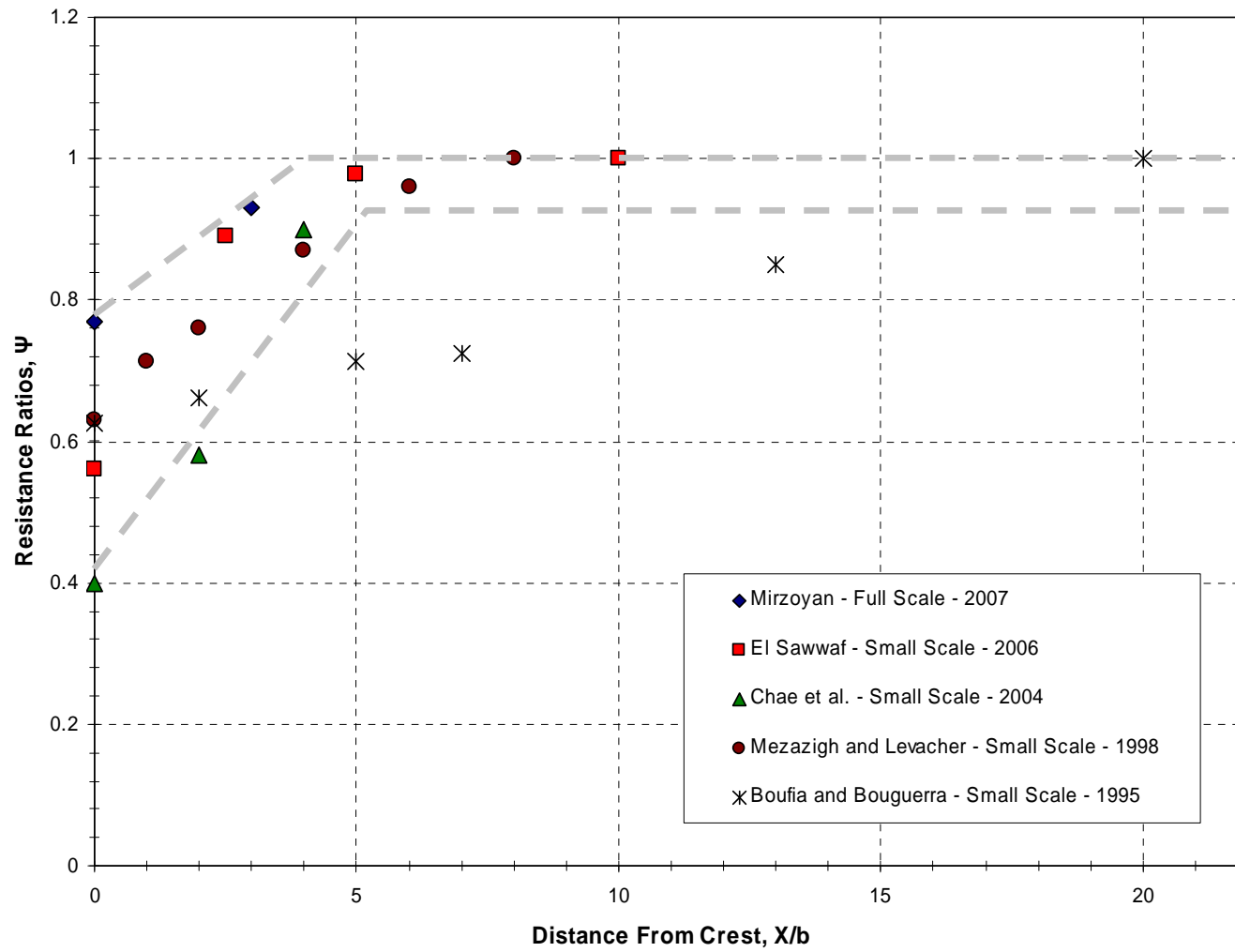
Figure 4.13 Comparison of Ultimate Lateral Resistance Ratios for Sands.

The significant discrepancy could be due to effects of the pile-soil interaction not accounted for in mathematical models and not obtainable in small-scale model tests. The discrepancy could also be due to the fact that in both sloped profile tests (tests two and three), the slope was cut only 6 feet horizontally and 3.64 feet vertically. Assuming a soil failure plane angle, β, of 45°+ϕ/2, as suggested by Reese (2000), and a depth of significance, H, of 9 pile diameters (Reese and van Impe suggest 5 to 10 pile diameters for piles in sand), calculations show that the failure wedge in front of the pile would not have been entirely contained in the slope. However, the near constant relationships between the capacities of the sloped and horizontal profile pile-soil systems strongly suggest that the shallow depth of the slope did not play a significant role in the results of either sloped profile test. This concept is illustrated in Figure 4.14.
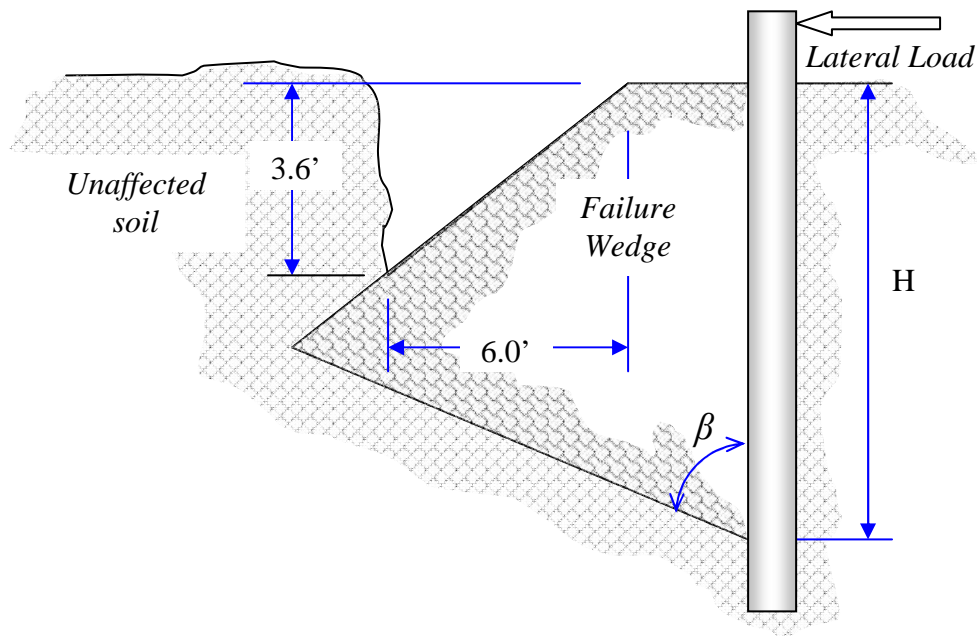
Figure 4.14 Illustration of Failure Wedge Not Contained in Slope.

4.6.3   Bending Moments and Depth

In choosing a pile cross-section, it is important to know the value and where the maximum bending moment developed in the pile will be. To determine this and the effect of the slope on the location and magnitude of the maximum bending moment, strain data from gages attached along the length of the pile were used to generate bending moment vs. depth curves for all three tests. The bending moment, M, at each depth was computed using the equation

$$M = \frac{EI(\varepsilon_T - \varepsilon_C)}{\Delta h} \tag{4-1}$$

where   E = Young's modulus of elasticity of steel = 29,000 ksi
             I = Moment of inertia of pile cross-section = 344 in^4
             ε_T = Strain in the extreme tension face of pile
             ε_C = Strain in the extreme compression face of pile
             Δh = Distance between extreme tension and compression fibers.

Some alterations were made to the above equation for cases where strain data for a given depth was only available from either the tension face or the compression face. In these cases, the missing strain value was assumed to have the same value as the measured one with its sign adjusted accordingly. Because of the symmetry of the pile cross-section and because the modulus of elasticity of steel is more or less the same in compression and in tension, the strains on the tension and compression faces should be equal in magnitude; and therefore, the alteration discussed above presents a valid solution to the problem. This method was also applied to points where data from one of the sides was present but significantly differed in magnitude from the other side. In this case, the side with the greater magnitude of strain was typically used.

Because of the factors discussed earlier in the chapter, cases where only one of the pairs of gages at a depth functioned properly were quite common. Some gages were operational for some tests and were completely erratic in subsequent tests. There were even cases where both pairs of gages malfunctioned at a given depth. Such was the case for gages at depths 2, 4.5, 13, 14.5,16, 17.5, 22, 28, 31, 37, and 40 from the top of the pile. In such cases the data points at those levels were completely omitted and bending moments were interpolated by the algorithms built into the spreadsheet program generating the bending moment vs. depth curves. This potentially poses problems with accuracy of results especially since the gages at depths 2, 4.5, and 7 ft, from which no data was available, fall within the depth of significance of the pile (Reese and van Impe 2001). Table 4.2 is a summary of the operational state of the gages at their labeled depths. The letter B indicates that gages on both sides of the pile at that labeled depth were operational and gave reasonable data. The letters E and W indicate that only data from the East or West side, respectively, was collected and considered reasonable. Cells left blank in the table indicate that no data from those depths was available or reasonable.

Table 4.2 Summary of the operational state of strain gages.

Label [ft]	2	4.5	7	8.5	10	11.5	13	14.5	16	17.5
Test 1	W			B	W	E				B
Test 2		E		W	W	E	W		W	W
Test 3		E		W	W	E	W	W		

Label [ft]	19	20.5	22	23.5	25	28	31	34	37	40	44
Test 1	B	W	B	B	W	W	W	B	W	W	B
Test 2	W	W		W	B	W		W	W		B
Test 3	E	W		W	B		W		W	W	W

84

Initial calculations showed bending moments far below the expected values. For example, bending moments at the ground surface calculated from the strains were about 4 times lower than values obtained from statics or the supplementary gages attached to the pile at the ground surface. Through supplementary laboratory experiments and an in-depth look at the data reduction process, it was discovered that the problem rested in the data acquisition. The voltage used to collect the strain data differed from the required by a factor of two; this then, caused the device to record strains that were lower than the actual by a factor of four. To solve the problem, all of the strain data was multiplied by a factor of four. All of the results and conclusions based on the results presented in this and other sections that deal with bending moments are based on the corrected strain values.

Given the limitations of the data available and procedural discrepancies discussed above, the results of the bending moment analysis will primarily be considered for comparison purposes and qualitative rather than quantitative observations will be the focus of this section. This is a valid approach since the limitations and procedural discrepancies were applied to all three tests and thus the results, although not absolute, are comparable.

Figure 4.15 shows the bending moments developed in the pile along its length for different deflections. The figure shows that for all three tests, the location of maximum bending moment increased with the increase in applied top deflection. It is interesting to note that the slope had very little, if any, effect on the location of maximum bending moment. The figures also show that the slope had very little apparent effect on the magnitude of moment at a target deflection.

Bending Moment (kip-in)

a) 0.125 in.

b) 0.5 in.

c) 1.0 in.
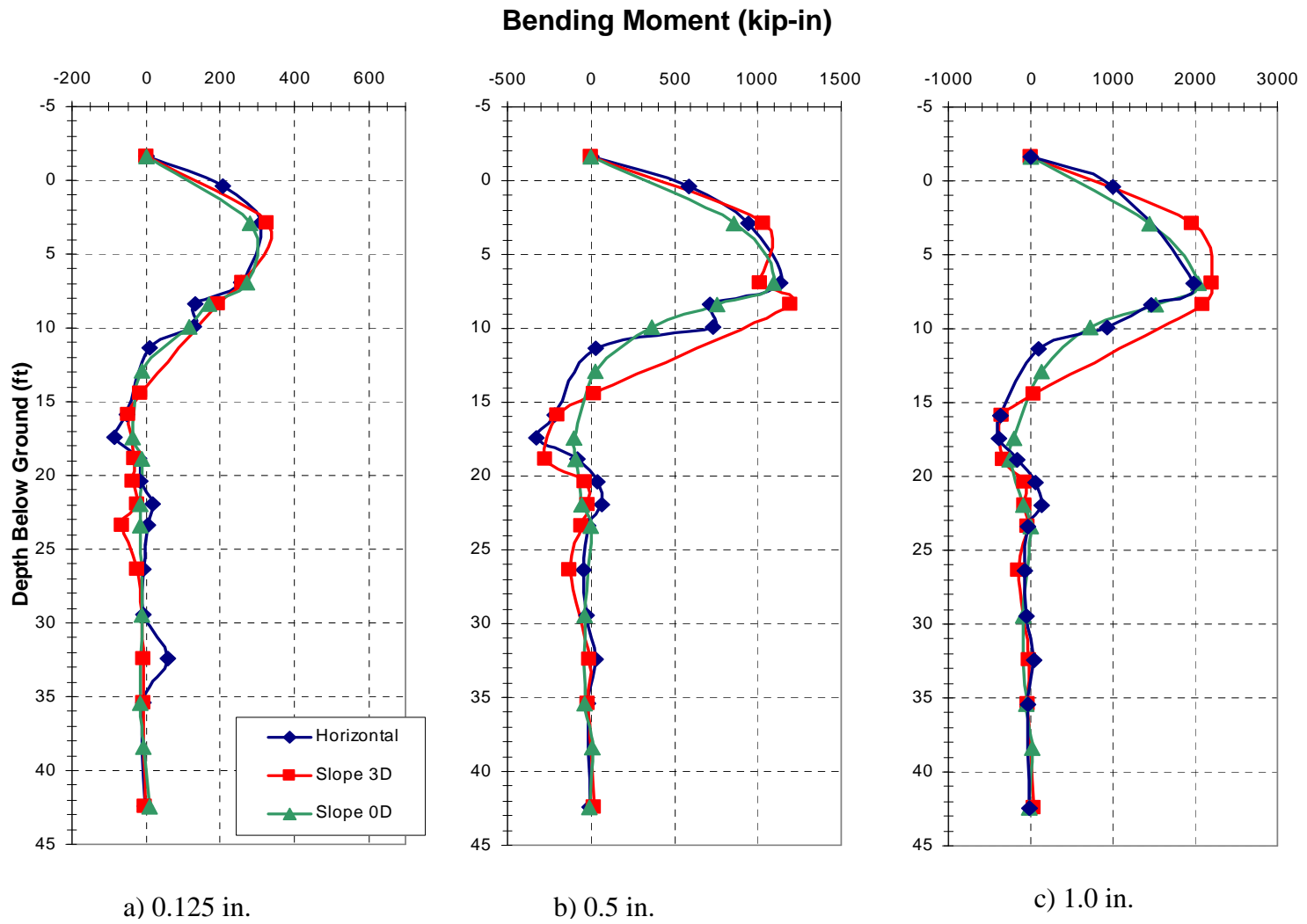
Figure 4.15 Bending Moment vs. Depth Curves for Various Target Deflections.

Figure 4.16 shows a comparison of depths to maximum bending moment from each test. It can be readily observed that in all three tests, the location of maximum bending moment decreased with the increase of applied load. This is because as the applied load increases, the soil in front of the pile fails leaving the top of the pile unsupported and thus altering the depth to maximum bending moment. It appears that the depth converges to a value at high applied loads. This depth appears to be between 7 and 8 ft below ground surface for all three tests.

The slope had no readily observable effect on the depth of maximum bending moment. This, however, could be due to the lack of an adequate amount of strain gages at the location of maximum bending moment to provide enough data for a comparison to be made.
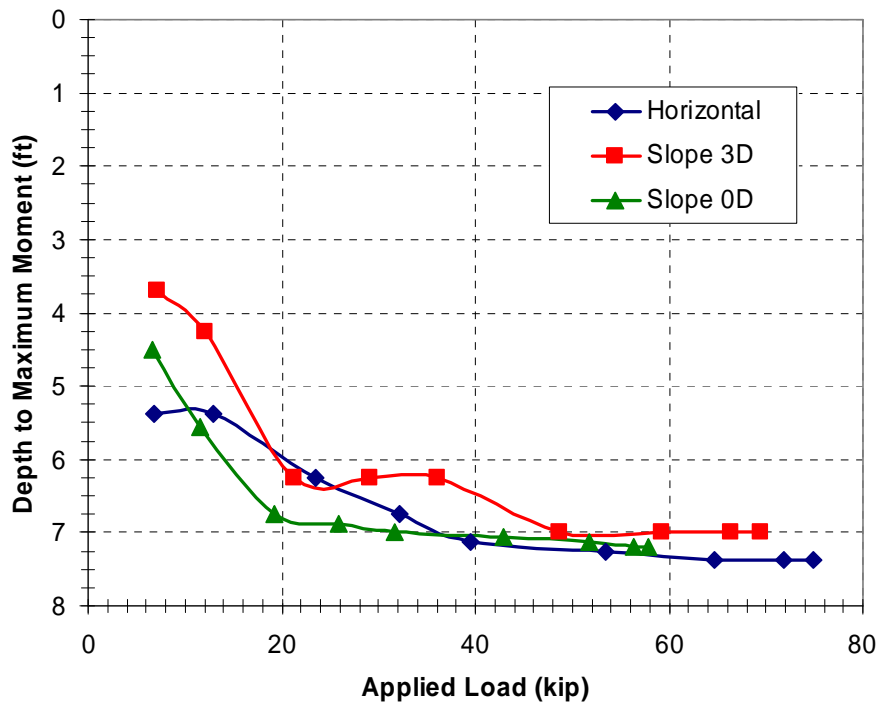
Figure 4.16 Comparison of Depth to Maximum Bending Moments.

Figure 4.17 is a plot of maximum bending moments at each target deflection for all three tests. A comparison of the maximum bending moment curves for the three tests shows little apparent change due to the slope for a case where the pile is placed at the slope crest and only a slightly greater change for the pile located 3 pile diameters form the slope crest. This is particularly true for deflections less than 0.75 in. These, somewhat, counter-intuitive results occur because piles near the slope resist less lateral load for a given deflection than the pile in horizontal ground. Because the applied load is lower, the maximum bending moment is lower than might be expected considering the reduction in lateral restraint due to the slope which would otherwise increase the maximum bending moment.
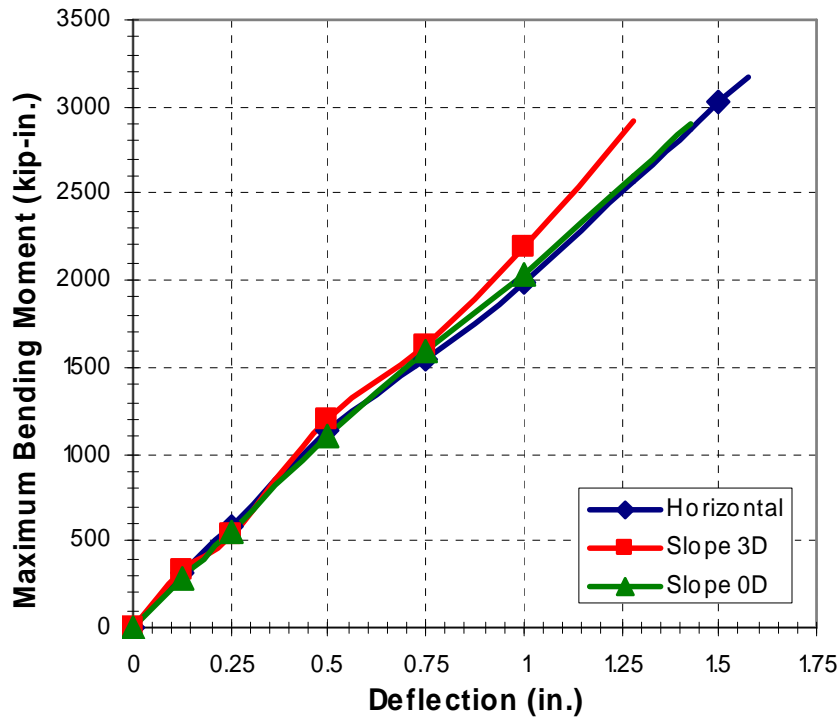
Figure 4.17 Maximum Bending Moments at Each Target Deflection.

Figure 4.18 shows plots of the ratios, IM_{max}, of maximum bending moment of sloped profile to horizontal profile as a function of top deflection, which shows that, on average, the pile located 3 pile diameters from the slope crest experienced 10 to 15 % higher moments than the pile in the horizontal profile. For the pile located at the crest of the slope, the figure shows an increase of less than 10 % in maximum bending moments.
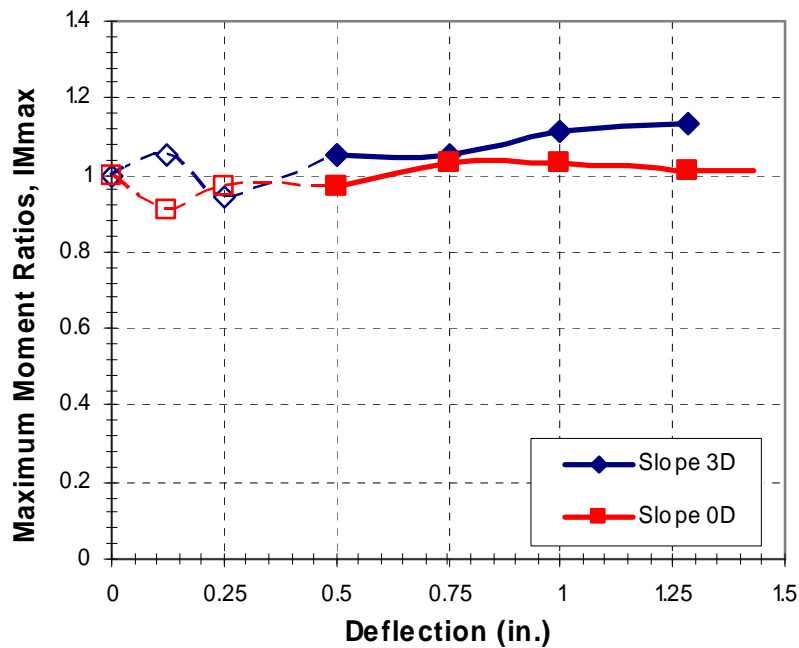
Figure 4.18 Maximum Bending Moment Ratios at Each Target Deflection.

A more accurate representation of the slope effect on the bending moments developed in the pile would be one that considered the applied load rather than the top deflection as the domain. Figure 4.19 is a plot of maximum bending moments as a function of applied lateral load. The applied lateral loads are taken as the maximum loads recorded at the target deflection causing the moment. Figure 4.19 shows that for a given applied load, the slope has a significant effect on the maximum moment

experienced by the pile. And, as expected, the effect is greater for the pile located closest to the crest of the slope. These results are consistent with the concept that placing a pile near a slope reduces the lateral restraint on the pile relative to a pile in horizontal ground and leads to a greater bending moment for a given applied load. It is interesting to note that the slope effect becomes apparently predominant after an applied load of 20 kips, which corresponds to a target deflection of about 0.5 in. This supports the conclusion reached in the load vs. deflection section that a movement of about 0.5 in. is required for the shear zone to reach the slope surface and fully engage the resistance of the soil.
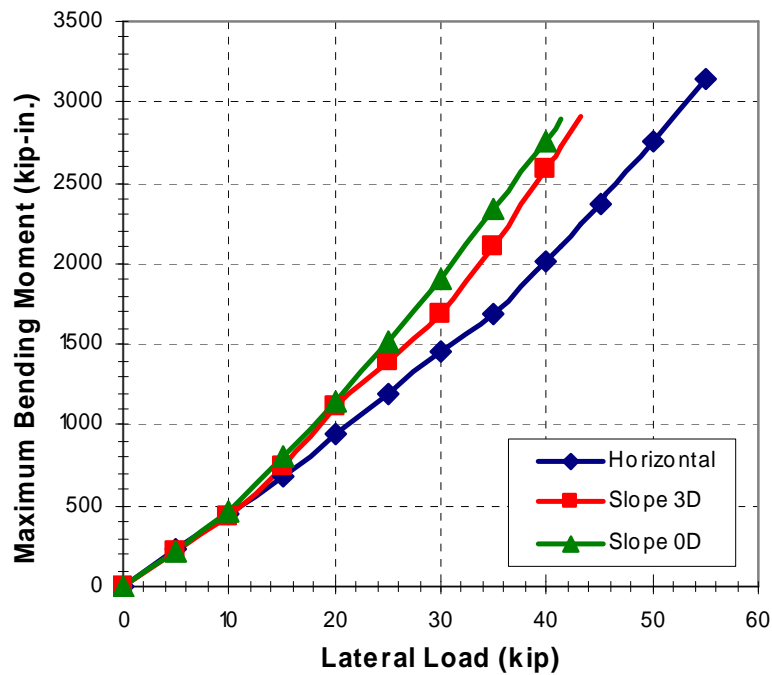

Figure 4.19 Comparison of Maximum Bending Moments vs. Applied Load.

Figure 4.20 shows plots of the ratios, IM_{max}, of maximum bending moment for the pile in a sloped profile to that in a horizontal profile as a function of applied load. These curves indicate that the effect of slope is not constant with respect to the applied load;

90

instead, it gradually increases and apparently converges to a value. Again, it should be

noted that at loads less than 20 kips the full resistance of the soil has not been engaged,

resulting in the unreasonable response observable in Figure 4.20. Considering, therefore,

only the curve past the point of engagement (20 kips), it can be observed that the IM_{max}

ratio of the pile located at the crest of the slope converges to a value of 1.4; whereas, in

the case of the pile located 3 pile diameters from the crest of the slope, it converges to a

value of 1.3. These values are both significantly higher than the values reported by other
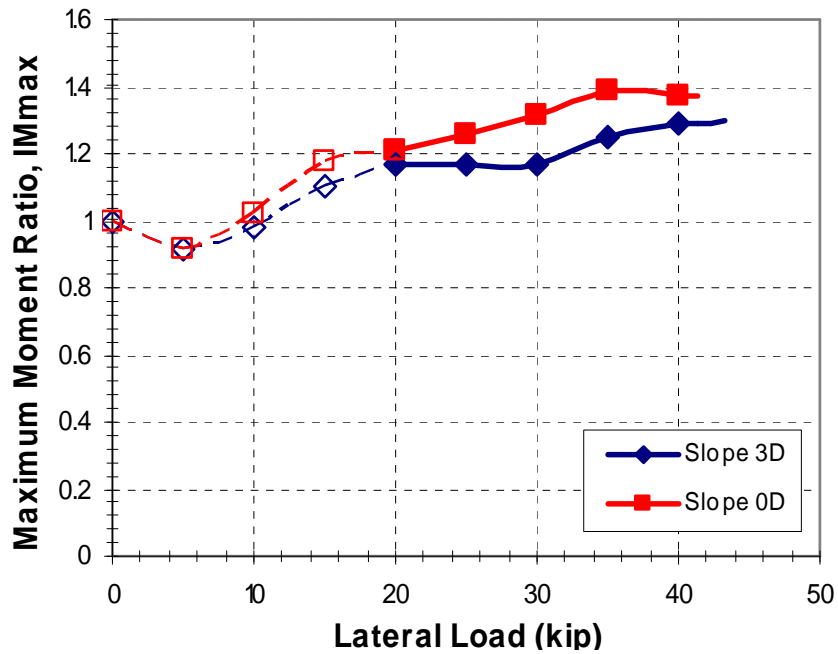
researchers as summarized in Table 2.3.

Figure 4.20 Comparison of Maximum Moment Ratios vs. Applied Load.

In summary, although the accuracy of the bending moment results are

questionable due to the factors discussed earlier in the section, they are useful in making

comparisons and determining the effects of slope on the location and magnitude of

maximum bending moment developed in the pile. Comparisons of bending moment results for the three tests conducted showed that the slope has no significant effect on the location of maximum bending moment. The slope does, however, have a significant effect on the magnitude of the maximum bending moment developed in the pile at an applied load; the effect being more pronounced for the pile closest to the crest. It was shown that, relative to the pile located in the horizontal profile, the pile located at the crest of the 30º slope experienced approximately 40% higher bending moments, while the pile located 3 pile diameters from the crest of the slope experienced approximately 30% higher bending moments. Although, these values are higher than values reported by other researchers, they provide an agreement with their conclusions regarding effects of slope on bending moments developed in a pile.

4.6.4   Load and Head Rotation

Head rotations were determined by taking the inverse sine of the ratio of the differential deflection of the two string potentiometers at different elevations and the distance between them, as illustrated in Figure 4.21. Such a method is only an approximation since the geometry involved is more complex. However, for the small deflections and rotations experienced in the tests, it is a reasonable approach. Lateral load vs. head rotation results are given in Figure 4.22, which shows that for a given load, piles near a slope experienced greater head rotations. The cause is the direct relationship between head rotation and lateral deflection, which as shown in Figure 4.11, was greater at a given load for piles located near a sloped profile.
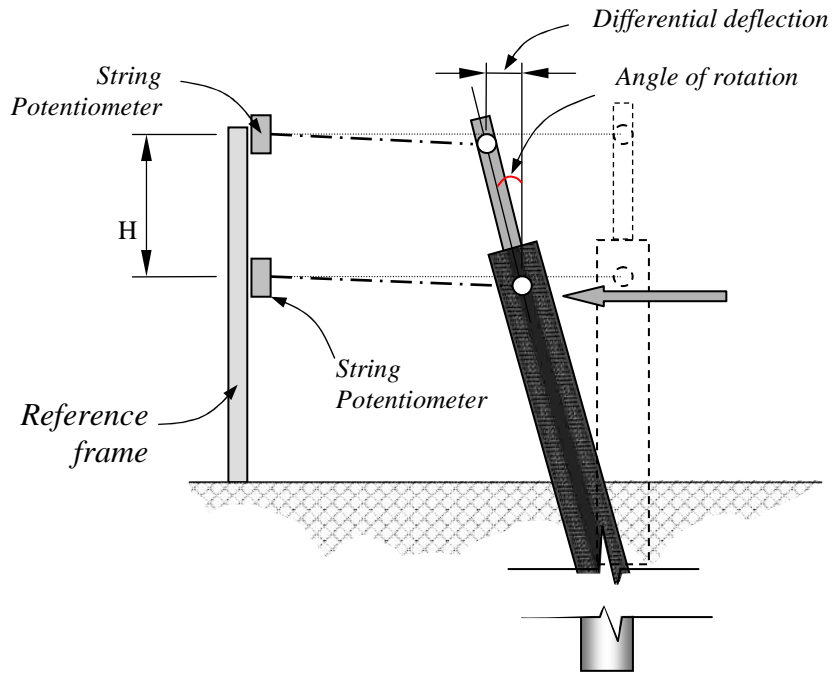
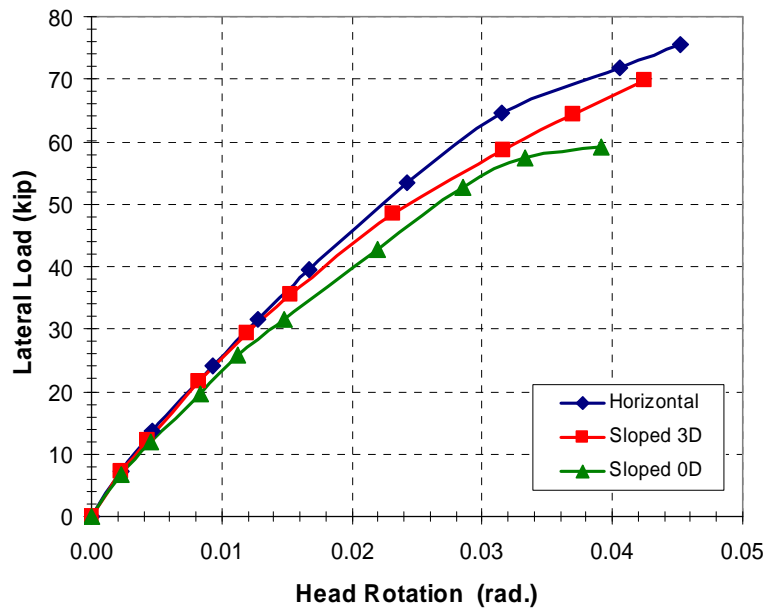**Figure 4.21 Illustration of Calculation of Head Rotations.**

Figure 4.22 Load vs. Head Rotation Curves of All Three Tests.

93

4.6.5   Shear Failure of Soil

To better understand the behavior of the soil under lateral loading, attention was given to the shear failure patterns visible in the soil profile during and after each lateral load test. The shear failure patterns were carefully mapped and photographed. The information gained in the analysis of the failure patterns played an important part in the development of the mathematical model discussed in Chapter 6.

Failure lines in the soil profile were clearly visible after and during each of the load tests but were most pronounced in tests two and three, where the pile was close to the crest of the slope. Failure lines were observed to start at the sides of the pile and extend perpendicular to the direction of loading as shown in Figure 4.23 a. The lines then curved parabolically and gave the failure shape the wedge appearance noted by other researchers. This suggests that the assumption that the failure planes of the resisting wedge are flat made in deriving the mathematical model in this study, as well as studies done by other researchers, is incorrect. The assumption is made, however, to simplify the mathematics involved in deriving the equations. In the case of both sloped profile tests (tests two and three) the failure lines extended into the slope and were clearly visible. In the horizontal profile test (test one), the failure lines extended a short distance in front of the pile then became undetectable. Figure 4.23 through Figure 4.25 present photographs and illustrations of the observed failure patterns in all three tests. The illustrations of the failure lines are based on the measurements taken during and after the tests.

Figure 4.23 shows the pattern of failed soil of test one at the ultimate load. The numbers next to the lines in Figure 4.23 b) indicate the chronological order of the appearance of the cracks. It is difficult to determine the shear failure angle, Ω, for test
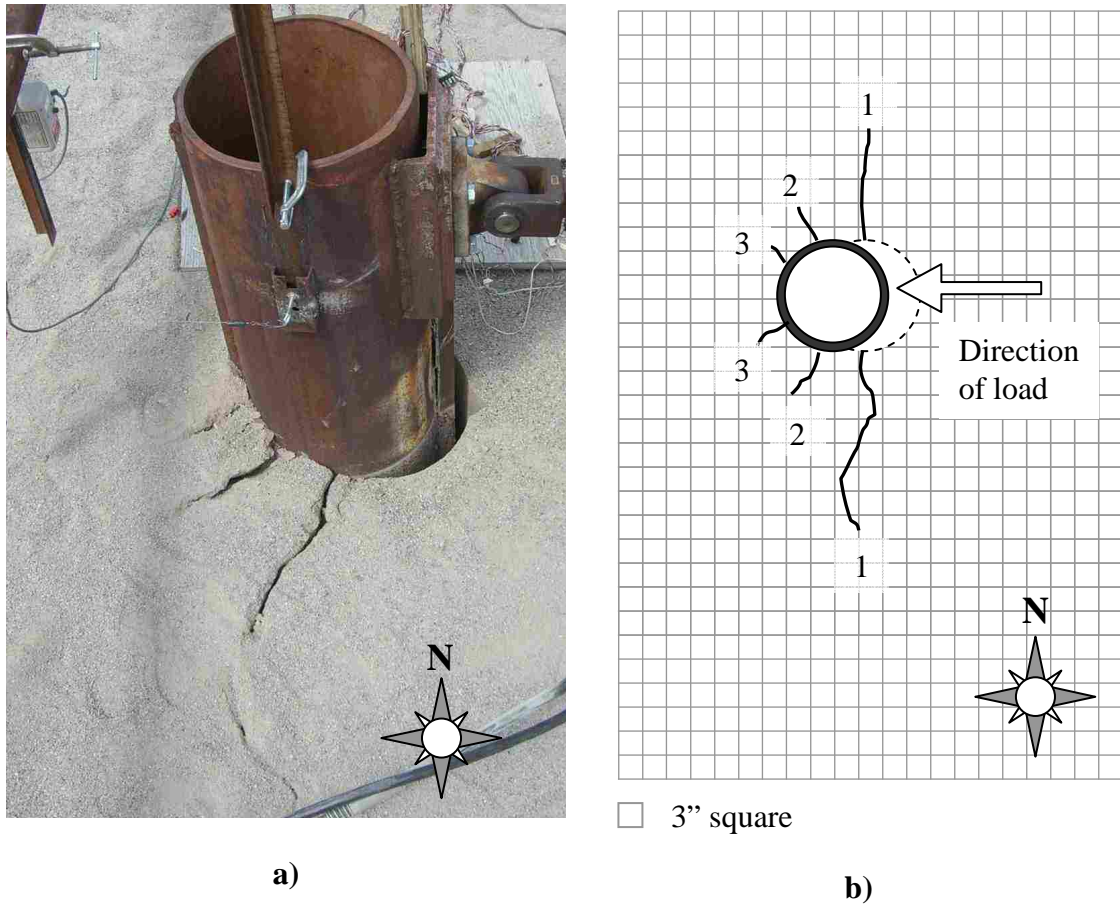
Figure 4.23 a) Photograph and b) Illustration of Final Failure Pattern of Test One.

one as the full extent of the failure lines was not visible. It is, however, interesting to note that the angle Ω decreased as the applied load and deflection increased. This suggests that the failure angle Ω may be dependent on the deflection of the pile.

The failure lines of the soil wedge were most pronounced in test two. Figure 4.24 shows the final failure pattern of test two at the ultimate load. Measurements taken during and after the test reveal that the shear failure angle, Ω, between a line projected from the side of the pile in the direction of the load to the most extreme failure line was about 29° on the south side of the pile and 33°on the north side. This suggests that angle

Ω for the profile where the pile is at the crest of the slope is about 75% of the angle of internal friction, ϕ.
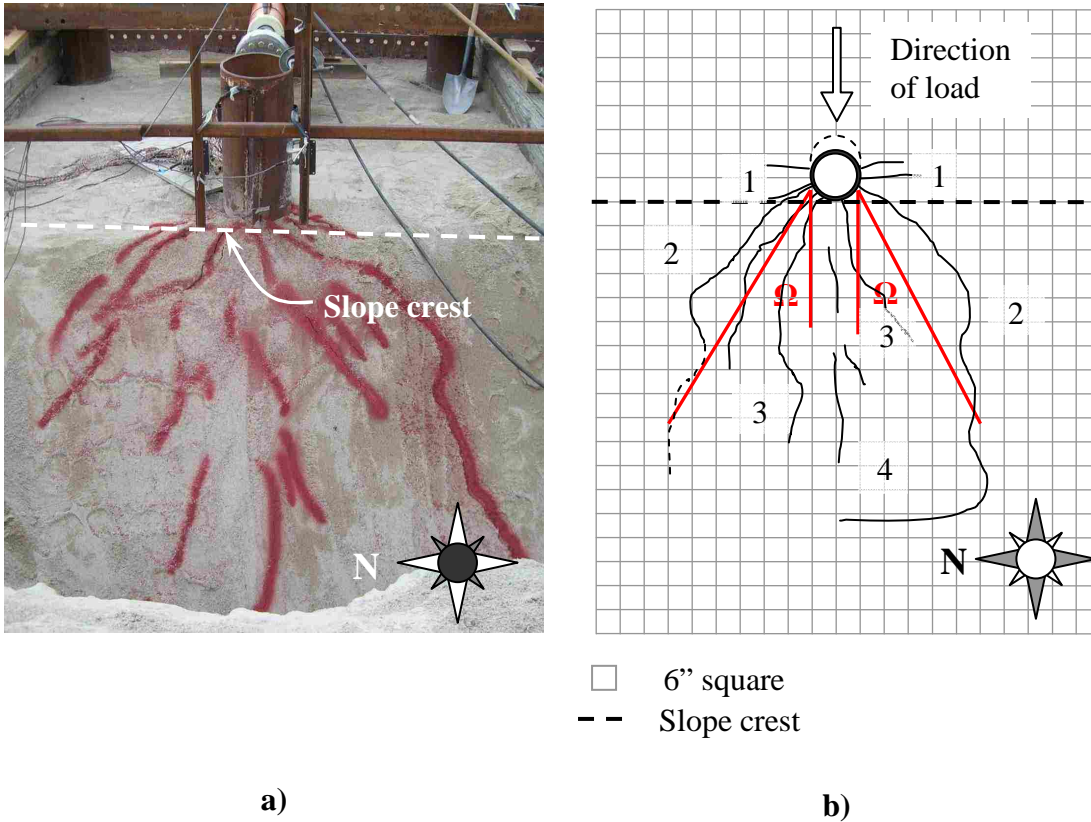
Figure 4.24 a) Photograph and b) Illustration of Final Failure Pattern in Test Two.

The failure wedge of test three, although not as pronounced as in test two, had failure planes extending into the slope. Furthermore, the south side of the pile had more cracks than the north, suggesting somewhat uneven loading or unsymmetrical geometry. Figure 4.25 shows the failure lines of the wedge, which clearly had a smaller angle Ω than test two. Measurements taken during and after the test yield a Ω angle of about 21° on the south side of the pile and about 24° on the north side. This suggests that angle Ω for the profile where the pile is at 3 pile diameters from the slope crest is slightly greater

than half the angle of internal friction, φ, which is a common value of Ω suggested throughout the literature.
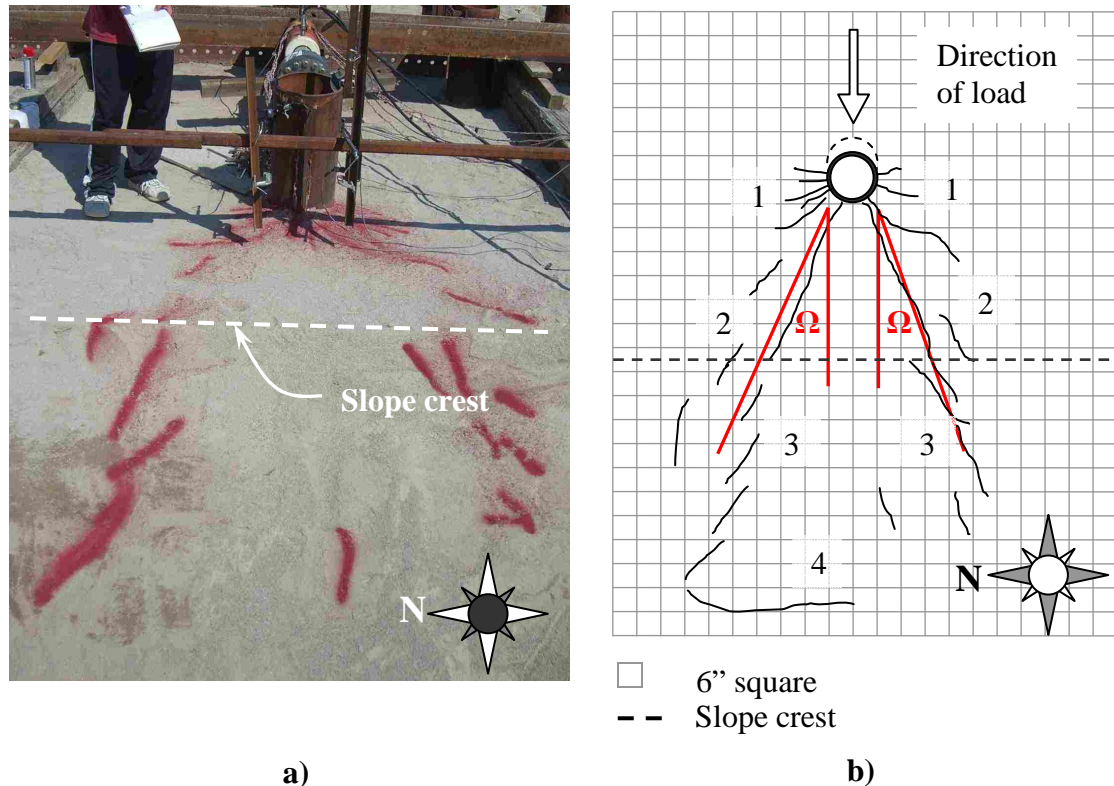
Figure 4.25 a) Photograph and b) Illustration of Final Failure Pattern in Test Three.

In summary, although not as pronounced as in test one, the soil in front of the pile sheared in a wedge pattern as suggested in the literature. The shear wedge geometry differed from test to test. The shear wedge failure angle, Ω, defined as the angle between a line projected from the side of the pile in the direction of the load and the most extreme failure plane, was not constant. Ω was observed to start perpendicular to the direction of load for small deflections and later decreased at higher loads. Also, the proximity of the pile to the crest of the slope affected Ω. The Ω angle of the wedge for the pile located at

the slope crest was much broader than that for the pile at three pile diameters from the

crest.

CHAPTER 5 - COMPUTER ANALYSIS

5.1   INTRODUCTION

The pile was modeled using the computer program LPILE Plus version 4 (Reese et al., 2000), distributed by ENSOFT, Inc.   The current version, as well as its predecessors, was developed by Dr. Lymon C. Reese and his associates at the University of Texas in Austin.   The program, which is widely used in academia as well as in industry to model piles loaded laterally, uses a finite difference method to calculate pile head load vs. deflection curves, bending moments and shear in a pile, as well as pile deflection at any given depth.   The pile can either be modeled as linear-elastic or non-linear.   Pile loading can either be modeled as an applied load, deflection, or moment. LPILE models the pile as a beam and the soil layers as non-linear springs.   The springs are assigned p-y curves, which were derived from a series of instrumented load tests conducted over the years.   This method was introduced in Chapter 1 and later discussed in Chapter 2.   For a more advanced use, the program allows for the use of p-multipliers to more accurately model the pile-soil response.   Past research conducted by Rollins et al. (1998, 2003a, 2000b, and 2005) using LPILE has given validity to the ability of the program to model laterally loaded pile behavior in cohesive soil.   The program also allows the user to input a slope angle in which the pile is driven.   This feature, however,

has not yet been fully validated with full scale tests. The main limitations of the program are the limited number and type of soil layers that one can use to model the soil profile. In the present version the maximum number of layers for modeling the profile is limited to 10. Another limitation of the program is its inability to model cases where the pile is located some distance from the slope crest. In fact, the program does not allow for a slope crest–the slope is modeled as being continuous behind the pile.

Despite its limitations and inconsistency with the field conditions, the program has been used in this study to compare and test its ability to model pile behavior in sloped soil profiles with simple approximations. Because of its limitations discussed above, the soil profile used in the program was first calibrated to match the response of the field results of the pile in horizontal ground. The soil profile was then used with the slope feature and a comparison was made with the field results.

5.1.1   Input Parameters for Pile

The pile input parameters are summarized in Figure 5.1 and Figure 5.2. The cross sectional moment of inertia used here includes the contribution from the angle irons spot welded to the east and west sides of the pile to protect the strain gages. The pile was modeled as a hollow steel tube with a non-linear modulus of elasticity, E, and moment of inertia, I. The E and I values of the steel pile shown in Figure 5.2 are for the linear range of the analysis only.

5.1.2   Input Parameters for Soil

Figure 5.3 is a summary of the soil layers and depths input into LPILE. It should be noted that the profile is different from the idealized soil profile presented in Chapter 3.

This is primarily due to the limitations of LPILE discussed above and the calibration done to match the field results of the case where the pile is in a horizontal profile. The primary difference between the idealized profile derived from geotechnical investigations and the input parameters is in the top most sand layer, which has been modeled as silt in this computer analysis.

Figure 5.1 Pile Input Parameters.

Figure 5.2 Pile Cross Sectional Input Parameters.

Figure 5.3 Idealized Soil Profile Inputs.

Analyses that modeled the top layer as cohesionless sand with a friction angle of 40° significantly underpredicted the strength of the pile in horizontal profile. To provide a reasonable match between the computer and field results it became necessary to increase friction angle of the sand. Sands in LPILE, however, have an upper limit on the friction angle. Therefore, the layer was modeled as silt, which has no upper limit on the friction angle input. A comparison of load vs. deflection curves between the field results and results from using the sand and silt models is presented in Figure 5.4. All subsequent analyses in this chapter are performed considering the top layer as silt.

A detailed view of the silt parameters is provided in Figure 5.5, which shows a friction angle of 54.5°. This is the friction angle that provided the closest match between the field and computed results. To make further adjustments, the cohesion of the layer was

102

manipulated. Each layer also required additional parameters such as unit weight, modulus of subgrade reaction (k), undrained shear strength (s_u), and the strain value at which the soil develops 50% of its shear strength (ε_{50}). Many of these parameters were taken from input parameters used in previous research (Walsh, 2005) to model the profile of the same site in LPILE. These parameters were previously determined by back-analysis from lateral pile load tests in clay (Snyder, 2003). A summary of the layer parameters is shown in Table 5.1. The only difference in inputs between the horizontal and sloped profile tests was the batter angle, which was changed to 30º.
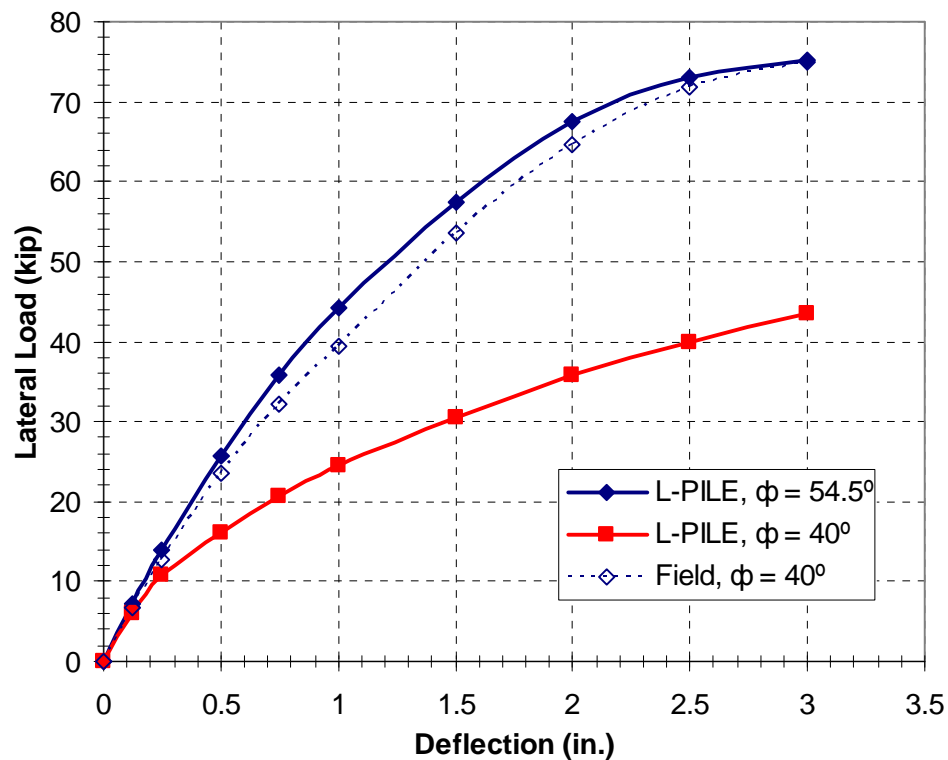
Figure 5.4 Comparison of Load vs. Deflection Curves for Different Soil Models.

Figure 5.5 Top Layer Soil Parameters.

Table 5.1 Soil layer input parameters.

	Soil Type	Unit Weight, γ (lb/in^3)	p-y Modulus, k (lb/in^3)	Cohesive Strength, c (lb/in^2)	Friction Angle, ϕ (deg.)	Soil Strain, $\varepsilon50$
1	Silt	0.0615	275	0.95	54.5	0.01
2	Silt	0.025	125	095	54.5	0.01
3	Soft Clay (Matlock)	0.033	---	6	---	0.01
4	Soft Clay (Matlock)	0.033	---	7.25	---	0.01
5	Soft Clay (Matlock)	0.033	---	5.8	---	0.01
6	Sand (Reese)	0.03	94	---	38	---
7	Soft Clay (Matlock)	0.033	---	8.25	---	0.01
8	Soft Clay (Matlock)	0.033	---	3.63	---	0.015
9	Soft Clay (Matlock)	0.033	---	7.83	---	0.01
10	Sand (Reese)	0.033	55	---	47	---

5.2   RESULTS

5.2.1   Load and Deflection

Figure 5.6 is a comparison of the lateral load vs. top deflection curves measured in the field and computed by LPILE. Although an agreement is reached for the case of a pile in horizontal profile, the sloped profile results differ significantly. On average, LPILE underpredicted the lateral load by about 20%, which is most evident for deflections greater than 0.5 in. Because the soil profile was calibrated and resulted in a match for the horizontal case, LPILE's ability to model the soil may be ruled out as a source of the discrepancy in the results of the sloped test. The source of discrepancy is, therefore, either in the derivation of the mathematical model used to generate the curves or in the differences between field conditions and computer modeling. One such difference was the nature of the slope, which in LPILE is modeled as continuous in front of and behind the pile – a condition clearly not achieved in the field.

As a result of the discrepancy in the load vs. deflection results, the resistance ratios, ψ, obtained from LPILE are lower than the resistance ratios calculated from field results. A comparison of resistance ratios is provided in Figure 5.7, from which the ultimate resistance ratio, the ψ ratio at maximum deflection, is taken as 0.67. This value correlates well with values suggested by the GEO Publication (2006) and research conducted by Boufia and Bouguerra (1995).
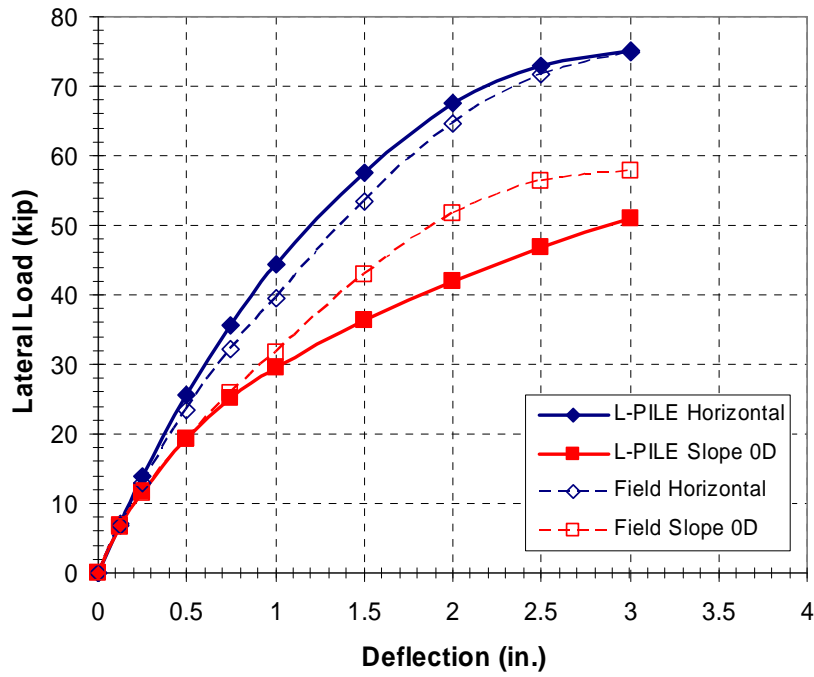
Figure 5.6 Comparison of LPILE and Field Load vs. Deflection curves.
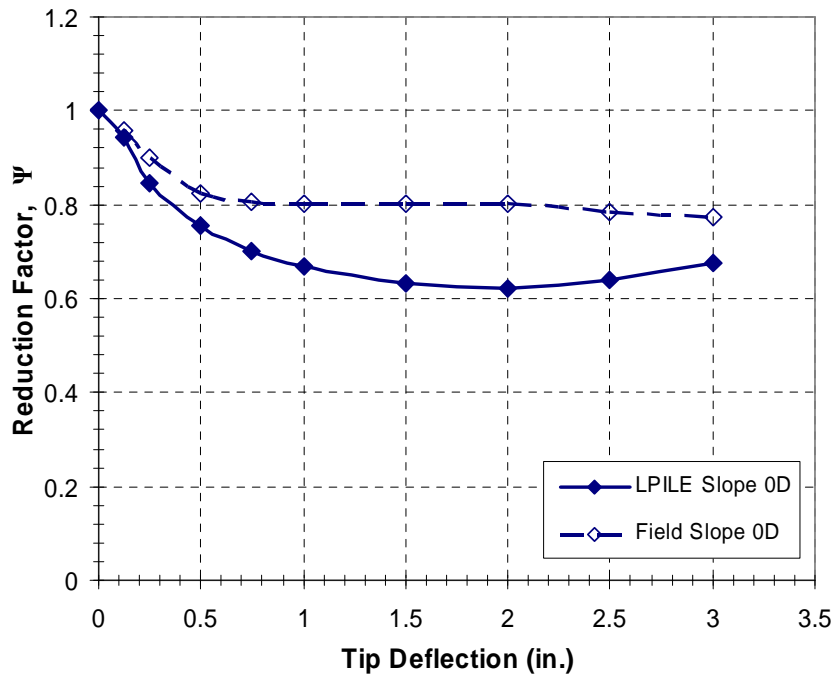

Figure 5.7 Comparison of LPILE and Field Resistance Ratios.

5.2.2 Bending Moment Data

Maximum bending moment vs. applied lateral load was analyzed in LPILE and a comparison was made with the field results and is shown in Figure 5.8, which indicates a striking similarity between the field measured and LPILE calculated maximum bending moments at different applied loads. A comparison of maximum bending moment ratios, $IM_{max,}$ is presented in Figure 5.9. The main discrepancy between the LPILE and field computed maximum slope to horizontal bending moment ratios, $IM_{max,}$ shown in Figure 5.9 occurs within the initial 20 kips of applied load, which, as discussed in earlier sections, corresponds to the amount of deflection needed to engage the resistance of the soil. If we ignore the data points up to 20 kips, the adjustment period, then, on average, LPILE's calculated IM_{max} ratios fall within 6% of the field calculations. This suggests that LPILE can model bending moments vs. applied loads developed in a pile located in a slope reasonably well.

With regards to location of maximum bending moment, however, LPILE significantly underestimated the depth below ground surface, where the maximum bending moments occur. A comparison of field LPILE calculated and depths to maximum bending moments is presented in Figure 5.10. Further, no convergence is apparent in LPILE's calculations of depth to maximum bending moment. LPILE's results do agree with the field results that the depth to maximum bending moment is directly proportional to the applied load; LPILE, however, predicted a significant effect from slope on the location of maximum bending moment. For applied loads greater than about 45 kips, the depth to maximum bending moment in the sloped profile is predicted to occur at over twice the depth of the horizontal profile.
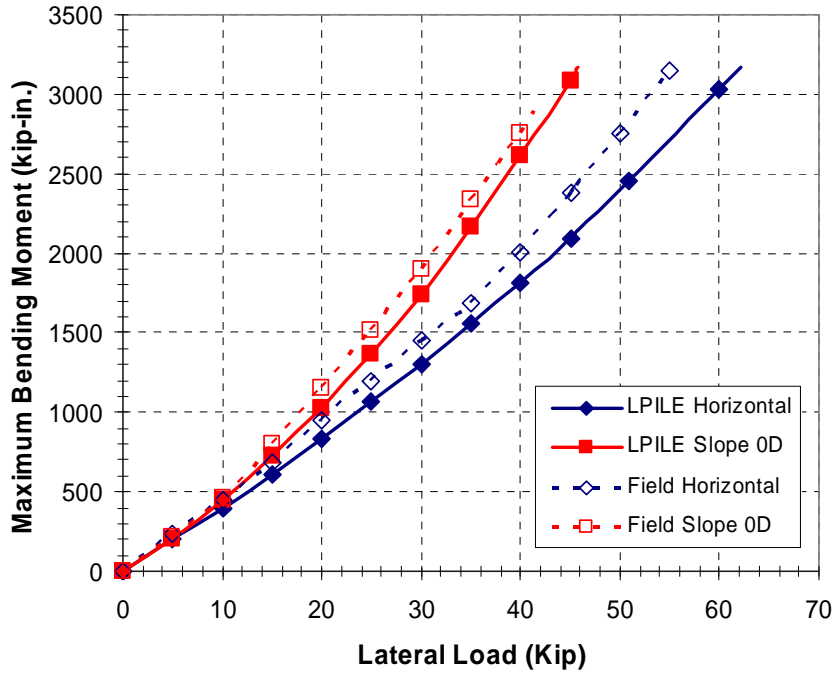
Figure 5.8 Comparison of Maximum Bending Moments.
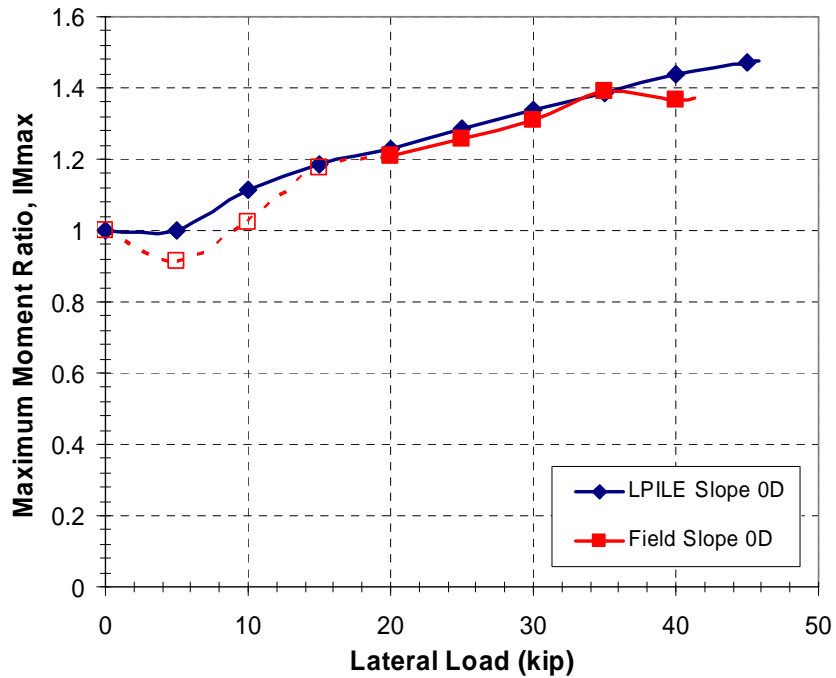
Figure 5.9 Maximum Moment Ratios.
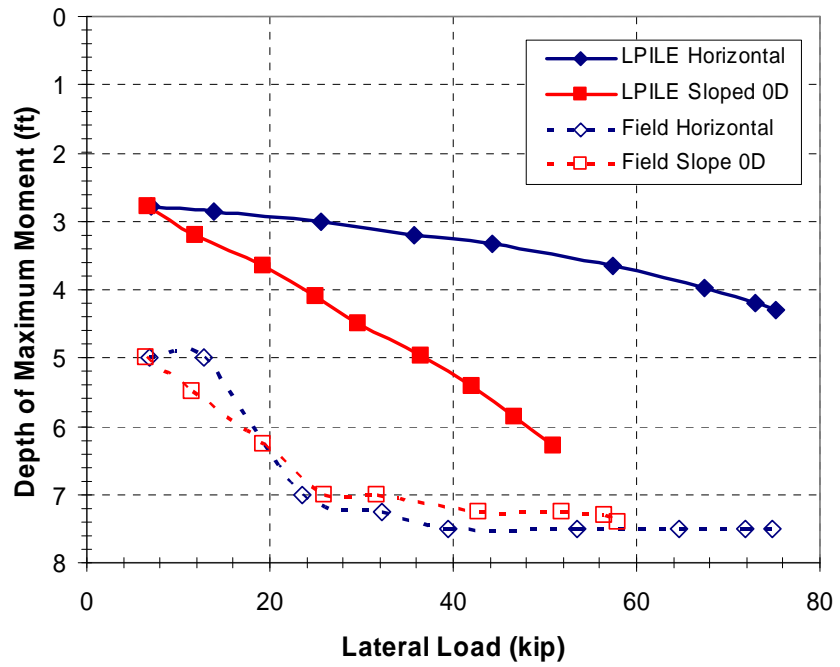
Figure 5.10 Comparison of Depth to Maximum Bending Moment from Field and LPILE.

CHAPTER 6 - MATHEMATICAL MODEL

6.1   INTRODUCTION

The theory behind the model is the assumption that at failure a wedge of soil forms in front of the pile. Resistance, then, is provided by friction along the planes of failure associated with the failure wedge and the normal force acting perpendicular to the bottom failure plane. Although many field observations, including those made in this study, have indicated that the assumption that a wedge of soil forms in front of the pile at failure is reasonable, other modes of failure do exist, which can govern the ultimate resistance. One such failure mode is the 'flow-around' mechanism discussed by Reese et al. (2000), where the pile moves through rather than with the soil. Such a failure mechanism generally governs the soil response at higher applied loads and results in lower capacities.

The failure wedge mathematical model, which computes the total ultimate lateral strength of the soil, does not account for the flow-around mode; however, as discussed in a subsequent section, modifications can be made to the mathematical model to allow for a comparison to be made between the two modes of failure at a given depth. The lower capacity then is taken as the ultimate capacity at that depth.

The mathematical models for both the wedge-type and flow-around failure modes are very simplified and idealistic and are, therefore, to be used with their limitations in mind. One of the primary limitations of the model is that it is derived for systems involving cohesionless soils only. Modifications to the model to account for contributions to the ultimate resistance from cohesion could make the model appropriate also for cohesive soils; however, due to time constraints such modifications are not included in this study. Because of the computational effort and the number of variables involved, the model is best suited for a computer program or spreadsheet.

6.2   ASSUMPTIONS

Because of the great number of variables and uncertainties present in the soil-pile interaction, some general assumptions are made in this model that greatly reduce the mathematical complexity of the model, yet are reasonable enough not to jeopardize the validity of the model. The following is a list of the major assumptions made regarding the variables, geometry, and mechanism involved in the model.
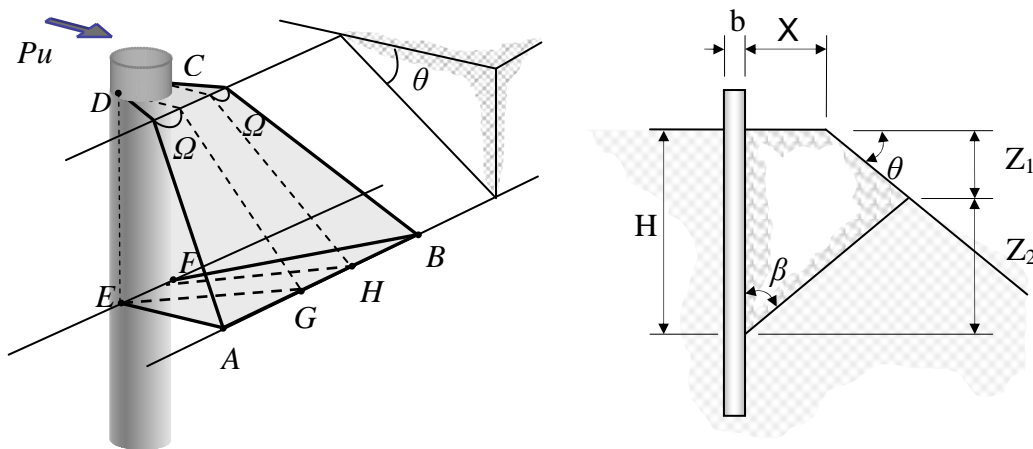
Figure 6.1 Illustration of Soil Wedge.

112

- The 'flow-around' failure mode is modeled by the method developed by Reese et al. (2000). Reese et al. use the same model for both horizontal and sloped profiles, with the caution that the model is based on two-dimensional behavior and, therefore, subject to uncertainty. For lack of a better model, however, the model developed by Reese et al. is used here to provide a comparison with the wedge-type failure mode.

- The wedge-type failure mode is modeled by a failure wedge forming in the general shape illustrated Figure 6.1. Such an assumption, to a large part, is based on the assumptions made by Gabr and Borden 1990 and the work of Reese (1962), which is supported by surface observations made in the field.

- The wedge depth, H, is taken as 9.5 pile diameters. This depth corresponds to the depth of significance discussed by Reese and van Impe (2001), who suggest values between 5 and 10 pile diameters. The model assumes that pile movement will be most significant within that depth, governing the overall depth of the wedge. The value is closer to the upper suggested limit due to field observations of the visible gap behind the pile extending down about 8 pile diameters and the maximum bending moments occurring at depths between 7 and 8 feet (Figure 4.16). Pile deflection vs. depth analyses from LPILE indicate pile lateral movement extending to 10.5 feet, corresponding to 9.8 pile diameters.

- The failure planes forming the wedge are assumed to be flat. This is an assumption also made by Gabr and Borden (1990) based on

113

recommendations made by Reese (1962). As discussed in Chapter 4, photographs taken during and after the field tests conducted in this study indicate that this assumption is somewhat incorrect for the case where the pile is located at the crest of the slope.

- The equation computes the ultimate lateral soil resistance and assumes that no contribution is made to the lateral resistance by either the pile or the interface between the pile and soil wedge. Thus the pile is assumed to be highly flexible. This is a conservative assumption also made by Gabr and Borden (1990).

- The failure wedge is assumed to be entirely contained in the slope. This also is a conservative assumption made by Gabr and Borden (1990). The effects of this assumption not being representative of the field conditions are briefly discussed towards the end of section 4.6.3.

- The soil behind the pile is assumed to make no contribution to the ultimate strength of the system. This assumption is made based on observations made in the field (see Chapter 4) and studies made by other researchers (see Chapter 2) of a gap forming behind the pile extending down at least 8 pile diameters.

- The soil is considered to be isotropic and homogenous, having no water table. This assumption is made to match the field conditions and to simplify the derivations.

- The soil in front of the pile and extending to the depth of significance is treated as a cohesionless medium. This assumption is made to match the

field conditions. Therefore, the model is suitable only for cohesionless soils.

- Failure wedge angle Ω is taken from field observations. Conservatively, an angle of $\phi/2$, as suggested by studies discussed in Chapter 2, could be assumed.

- Failure wedge angle β is taken as a constant with a value of $45^{\circ} + \phi/2$. This is a value widely suggested in literature.

- It is assumed that the full passive force is developed. This assumption is made in the form of the failure angle β, which governs the contribution to ultimate resistance from the normal force (see the section on derivation).

- Frictional resistance is assumed to come from only plane FEAB (see Figure 6.1). This is a reasonable assumption since, at failure, plane FEAB is the only plane of contact between the wedge and unaffected soil.

- The frictional coefficient is taken as a constant with a value equal to the tangent of ϕ, the internal angle of friction. This is a value widely suggested in literature.

- The pile is loaded in a free-head condition. This means that the pile has no applied moment and is not capped with adjacent piles. The model is, therefore, intended for single piles only.

6.3   DERIVATION

The ultimate resistance of the system is provided by the normal force acting perpendicular to the bottom of the failure wedge and by friction along the interface between the wedge and unaffected soil. Both of these components are dependent on the weight of the wedge. Hence, derivation of the weight of the wedge is of key importance and constitutes the majority of computations.

6.3.1   Weight Derivation

The wedge weight is the product of its density and volume. While density is easily obtained through geotechnical investigation, the volume calculation, due to its unusual shape, requires calculus. In calculating the volume, the wedge was thought of as the sum of infinite slices of trapezoidal shapes having thickness dz. This concept is illustrated in Figure 6.2. The incremental area was taken as a function of the depth, along with the constant variables discussed earlier. The volume, then, was calculated by taking the integral of the area function along the length of the pile equal to the depth of significance, H. Because of the shape of the wedge, however, the area function is not continuous with respect to depth. Therefore, the wedge has been divided into two sections. The first section extends from ground surface ($z = 0$) to where the wedge intersects the slope ($z = Z_1$) and the second section extends from where the first section ends ($z = Z_1$) to the depth of significance ($z = H$).
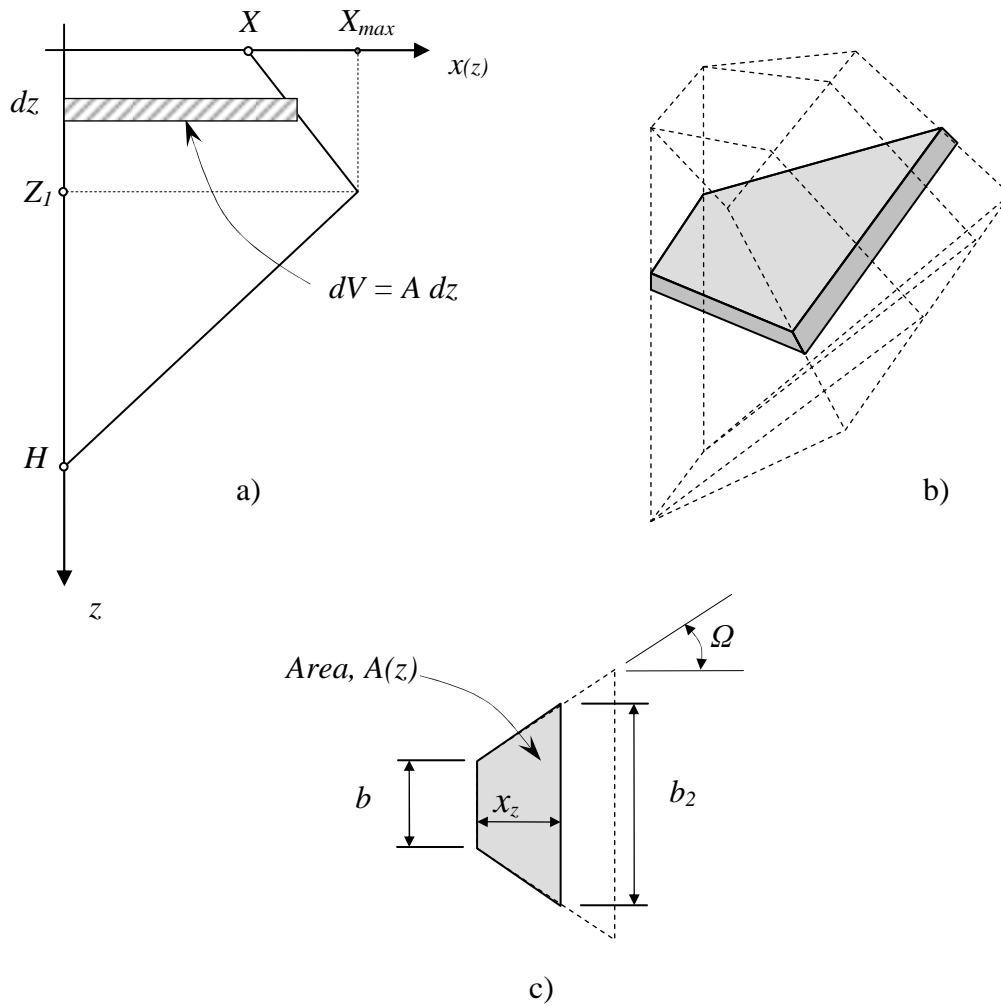
Figure 6.2 Volume and Area Derivation Illustrations.

The incremental area of the first section is expressed as:

$$A(z) = \frac{(b + b_2)x_z}{2} \tag{6-1}$$

where
$$x_z = X + z\tan(90 - \theta)$$
$$b_2 = b + 2x_z\tan\Omega$$

Thus,

$$A(z) = \frac{(b + b + 2x_z\tan\Omega)x_z}{2}$$
$$= [b + (X + z\tan(90 - \theta))\tan\Omega][X + z\tan(90 - \theta)]$$
$$= bX + X^2\tan\Omega + 2zX\tan(90 - \theta)\tan\Omega + zb\tan(90 - \theta) + z^2\tan^2(90 - \theta)\tan\Omega$$

Define the following:

$$J_1 = \tan\Omega$$
$$J_2 = \tan(90 - \theta)\tan\Omega$$
$$J_3 = \tan(90 - \theta)$$
$$J_4 = \tan^2(90 - \theta)\tan\Omega$$
$$Z_1 = \frac{H\tan\beta - X}{\tan(90 - \theta) + \tan\beta}$$

and the reduced formula for the area as a function of depth becomes:

$$A(z) = bX + X^2J_1 + 2zXJ_2 + zbJ_3 + z^2J_4$$

The volume of the first section is expressed as:

$$\tag{6-2}$$

$$= Z_1 bX + Z_1 X^2 J_1 + Z_1^2 XJ_2 + \frac{Z_1^2 bJ_3}{2} + \frac{Z_1^3 J_4}{3}$$

The incremental area of the second section is expressed as:

$$A(z) = \frac{(b + b_2) x_z}{2}$$

(6-3)

where

Thus,

$$A(z) = \frac{(b + b + 2x_z \tan \Omega) x_z}{2}$$
$$= [b + (H \tan\beta - z \tan\beta) \tan \Omega](H \tan\beta - z \tan\beta)$$
$$= bH \tan\beta + H^2 \tan^2\beta \tan\Omega - 2zH \tan^2\beta \tan\Omega - zb \tan\beta + z^2 \tan^2\beta \tan\Omega$$

Define the following:

$$J_5 = \tan\beta$$
$$J_6 = \tan^2\beta \tan\Omega$$
$$Z_2 = H - Z_1$$
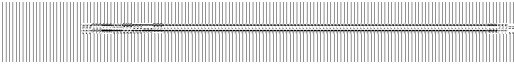
and the reduced formula for the area as a function of depth becomes:

$$A(z) = bHJ_5 + H^2 J_6 - 2zHJ_6 - zbJ_5 + z^2 J_6$$

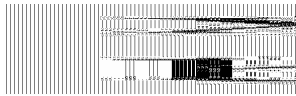The volume of the first section is expressed as:

(6-4)

$$= (Z_2H - \frac{H^2}{2} + \frac{Z_1^2}{2})bJ_5 + (Z_2H^2 + Z_1^2H - \frac{2H^3}{3} - \frac{Z_1^3}{3})J_6$$

The total volume of the wedge, therefore, will be the sum of the two volumes:

$$V_{TOT} = V_1 + V_2 \tag{6-5}$$

$$= Z_1bX + Z_1X^2J_1 + Z_1^2XJ_2 + \frac{Z_1^2bJ_3}{2} + \frac{Z_1^3J_4}{3}$$

$$+ (Z_2H - \frac{H^2}{2} + \frac{Z_1^2}{2})bJ_5 + (Z_2H^2 + Z_1^2H - \frac{2H^3}{3} - \frac{Z_1^3}{3})J_6$$

where
$$J_1 = \tan\Omega$$
$$J_2 = \tan(90 - \theta)\tan\Omega$$
$$J_3 = \tan(90 - \theta)$$
$$J_4 = \tan^2(90 - \theta)\tan\Omega$$
$$J_5 = \tan\beta$$
$$J_6 = \tan^2\beta\tan\Omega$$
$$Z_1 = \frac{H\tan\beta - X}{\tan(90 - \theta) + \tan\beta}$$
$$Z_2 = H - Z_1$$

The weight of the wedge, then, will be the product of the density, γ, and total volume:

$$W_{TOT} = \gamma V_{TOT} \tag{6-6}$$

6.3.2   Ultimate Soil Strength

The ultimate soil strength, P_{ult}, can be derived using the simple principles of statics. The loads acting on the wedge are shown in Figure 6.3 b), where W is the weight

of the wedge, N is the normal force, and T is the friction force developed along plane FEAB (see Figure 6.1). The forces in the x-direction and y-direction are summed and the unknowns are solved for by substitution of equations. The derivation is as follows:

x-direction:

$$= P_{ult} - N\cos\beta - N\tan\phi\sin\beta$$

y-direction:

$$= W - N\sin\beta + N\tan\phi\cos\beta$$

Solving for N:

$$N = \frac{W}{\sin\beta - \tan\phi\cos\beta}$$

Solving for P_{ult}:

$$P_{ult} = N\cos\beta + N\tan\phi\sin\beta$$

$$= \frac{W(\cos\beta + \tan\phi\sin\beta)}{(\sin\beta - \tan\phi\cos\beta)} \tag{6-7}$$

b)

a)
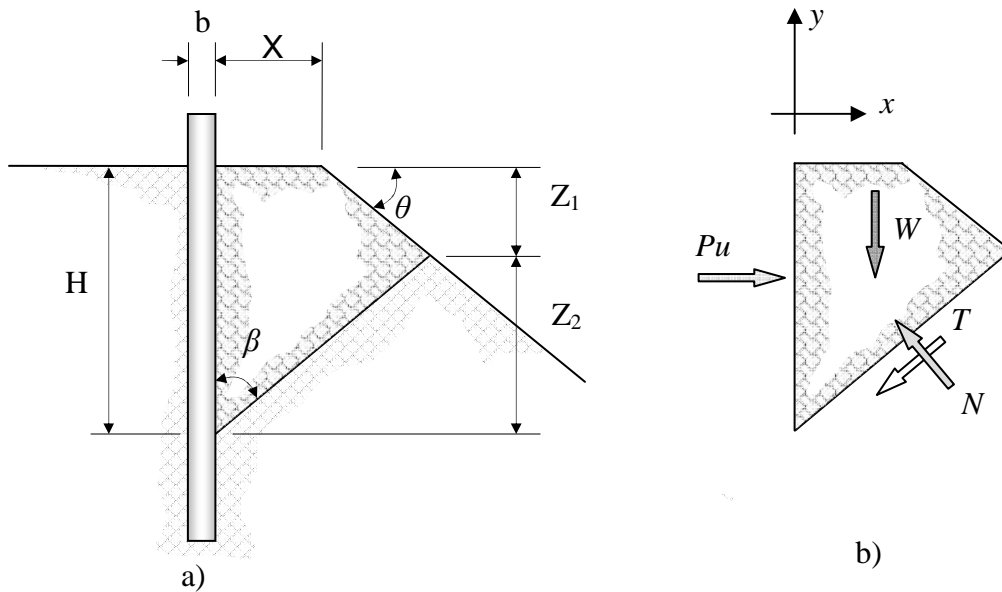
Figure 6.3 Ultimate Lateral Load Capacity Derivation Illustration.

6.3.3   Limit of Slope Effect

The theoretical distance of the pile from the crest, beyond which the effect of slope on the ultimate lateral strength may be neglected, will be where the wedge intersects not the slope but the flat surface between the slope crest and pile. This is illustrated in Figure 6.4. The distance, X_{lim}, was derived from geometry and is presented as a function of the depth of significance, H, and wedge angle β in Equation 6-8. For H values of 5 and 10 pile diameters (Reese and van Impe (2001) suggest 5 to 10 diameters for piles) and a β of 65° (β=45+ϕ), the equation suggests X_{lim} values of 11 and 21 pile diameters respectively. These values agree with values obtained by Boufia & Bouguerra (1995) and Mezazigh & Levacher (1998), who conducted small-scale model tests in centrifuges. The X_{lim} value from Equation 6-8 is, however, significantly higher than the

values suggested by Poulos (1976) and El Sawwaf (2006), who conducted non-centrifuge small-scale model tests.

$$X_{lim} = H \tan \beta \qquad\qquad\qquad (6\text{-}8)$$
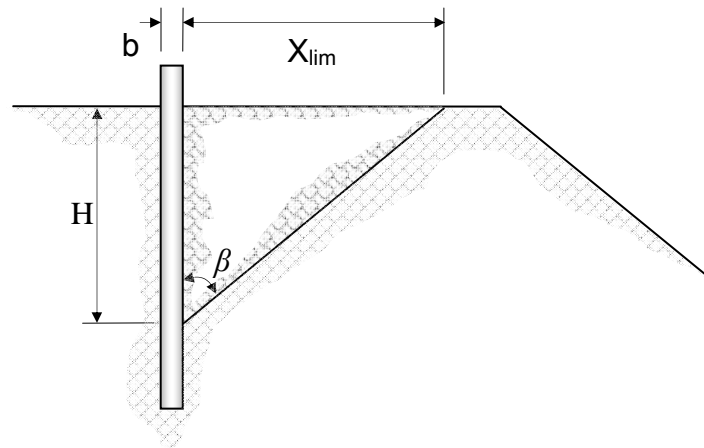
Figure 6.4 Illustration of Distance of Significance, X_{lim}.

6.3.4 Incremental Soil Resistance

To account for the flow-around failure mode, which governs at high applied loads, it is necessary to compute the lateral soil resistance at a given depth using both wedge-type and flow-around failure approaches and use the least as the ultimate resistance at that depth.

The ultimate resistance per unit length of pile in the wedge-type failure mode is obtained by differentiating the ultimate lateral strength, Equation 6-7, with respect to the depth H. This approach is used by Reese et al. (2000) in deriving the soil resistance per unit length of pile during the wedge-type failure in horizontal as well as sloped profiles.

123

The non-continuous geometry of the wedge requires two separate equations to account for all the depths in the domain. The differentiation by parts yields Equations 6-9 and 6-10 for the ultimate resistance of the soil per unit length of pile at a given depth, H:
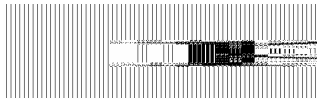
$$ \text{(6-9)} $$

where $0 < H \leq (X / \tan \beta)$

and
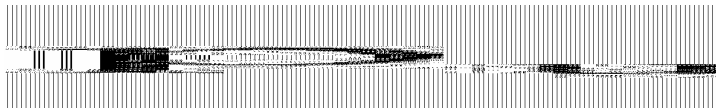
$$ \text{(6-10)} $$

where $H > (X / \tan \beta)$

The ultimate resistance per unit length of pile during the flow around failure mode (Reese et al., 2000) for both horizontal and sloped sandy profiles is given in Equation 6-11.

$$ \text{(6-11)} $$

where $H > 0$
       K_a = Active earth pressure coefficient
       K_0 = At-rest earth pressure coefficient

Equations 6-9 through 6-11 can be used to obtain approximate p-y curves for piles near the crest of a sandy slope. One such method for obtaining p-y curves is described by

Reese et al. (2000). The p-y curves, then, can be used to predict pile response under lateral loading.

6.4   RESULTS

Using a spreadsheet, a parametric study was conducted with Equation 6-7. The results of the study are presented in Figure 6.5 and Figure 6.6, which show the predicted effect of distance of the pile from slope crest on the ultimate lateral strength. To account for the changing value of the wedge angle, Ω, a quartic polynomial equation as a function of pile distance from slope crest was fitted to the two points obtained from the field test (see section 4.6.5) and a third point of $\Omega = \phi/2$ at the theoretical X_{lim}. The equation was incorporated into the spreadsheet, which was used to generate Figure 6.5, Figure 6.6, and Figure 6.8.

For piles located at the crest and three pile diameters from the crest of a 30º slope, Equation 6-7 predicted ultimate capacities of 59.5 kips and 69.2 kips respectively, which remarkably differ from the field results, 57.9 kips and 69.4 kips, by only 2.6 and 0.3 %, respectively. The input values used in the calculations are summarized in Table 6.1. The predicted load capacity of a pile in a horizontal profile, which could be taken as the peak value in the curve, was 170 kips. The discrepancy could be due to the 'flow-around' failure mode governing the ultimate resistance of the system, which is very likely given the fact that a failure wedge was not readily observable during the horizontal profile field test. The discrepancy could also be due to a more drastic reduction in Ω than anticipated. Without more data, however, it is reasonable only to assume that the mathematical model

is suitable for cases that involve slopes and piles within 3-5 pile diameters from the slope

crest.

Table 6.1 Input values for the sloped test results.

Pile Location, X/b:	0	3
Diameter, b (in.):	12.75	12.75
H/b ratio:	9.5	9.5
Angle β (deg.):	65	65
Angle Ω (deg.):	32	22.5
Slope angle, θ (deg.):	30	30
Soil unit weight, γ (pcf):	115	115
Internal friction, ɸ (deg.):	40	40

Results plotted in Figure 6.5 and Figure 6.6 show that the theoretical ultimate load

capacity curves peak to a maximum value, after which they rapidly decrease. These

points are plotted as "empty sets" as they do not accurately model the soil pile

interaction. The decrease in ultimate capacity after the peak is a result of negative

volume/weight calculated by the equation as the pile distance from the slope crest goes

past the limit discussed in the earlier section, which is problem is illustrated in Figure 6.7.

The inaccuracy can be easily corrected by conditional formatting of the equation in a

spreadsheet or other program to retain the capacity as the peak value for distances greater

than the limit calculated by Equation 6-8. Figure 6.5 shows ultimate capacities as a

function of pile distance from the crest for different internal friction angles. It can be

readily observed from Figure 6.5 that the soil's angle of friction has a significant effect

on the ultimate capacity of the soil. A decrease in the angle of friction of $10°$ causes a

reduction of about 50% in the ultimate load capacity. Although not as sensitive as to the

friction angle, the ultimate load capacity is also sensitive to the angle of the slope. This is

illustrated in Figure 6.6, which shows ultimate capacities as a function of pile proximity to slope crest for different slope angles. Here, a friction angle of 40º is used. These observations are consistent with the literature discussed in Chapter 2.

Figure 6.8 is a plot of the ultimate resistance ratios, Ψ, as a function of pile distance from the slope crest. Both the horizontal ultimate load from the field and theoretical horizontal load capacity, taken as the peak load of the curve, have been used to generate the resistance ratio curves in Figure 6.8. A comparison of ultimate resistance ratios for various pile distances from slope crest from this study and studies conducted in the past is presented in Figure 6.9. The equation from this study, used in the comparison, is based on the field rather than theoretical ultimate horizontal load capacity. It can be observed that a general agreement exists between the ratios suggested by the equation derived in this study and the ratios suggested by other studies.
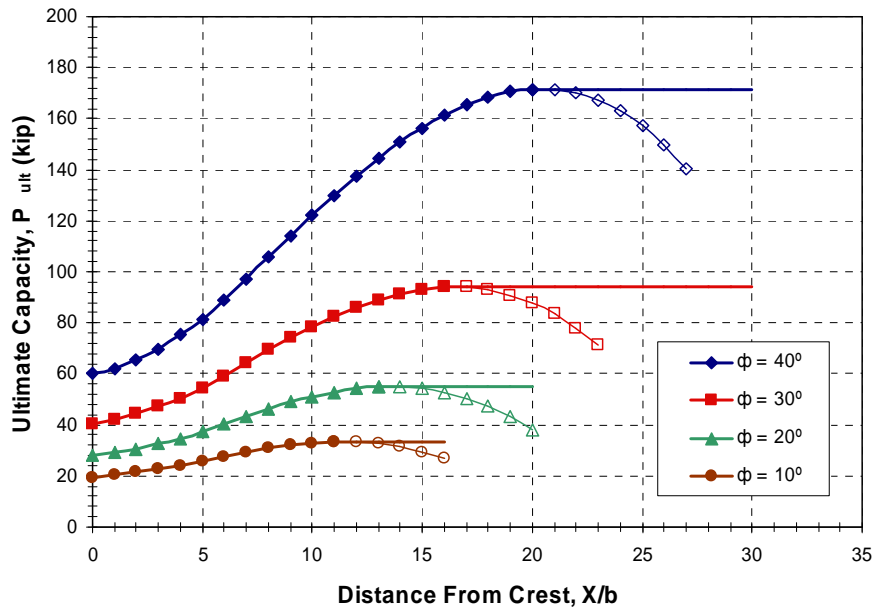

Figure 6.5 Ultimate Load Capacity for Different Friction Angles.
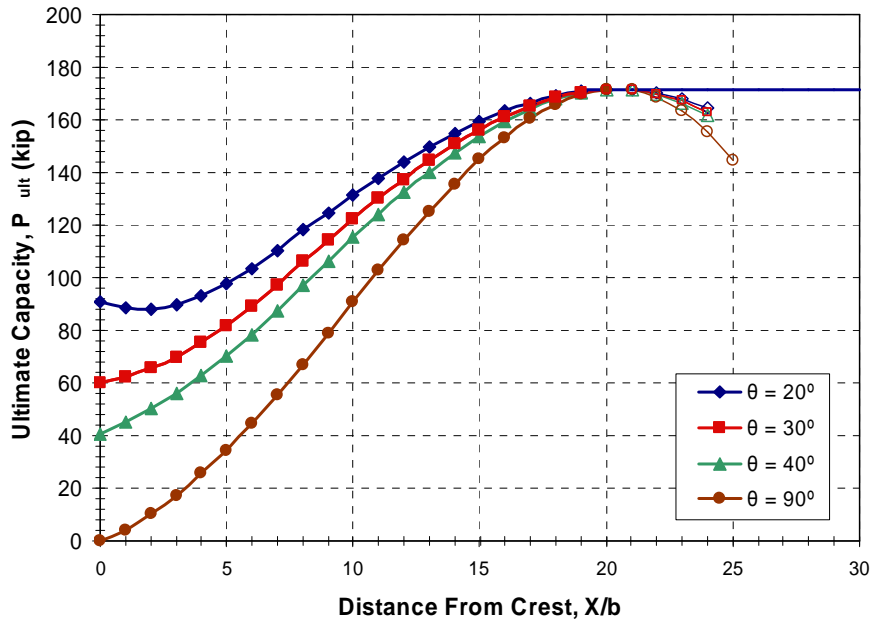
Figure 6.6 Ultimate Capacities for Different Slope Angles.
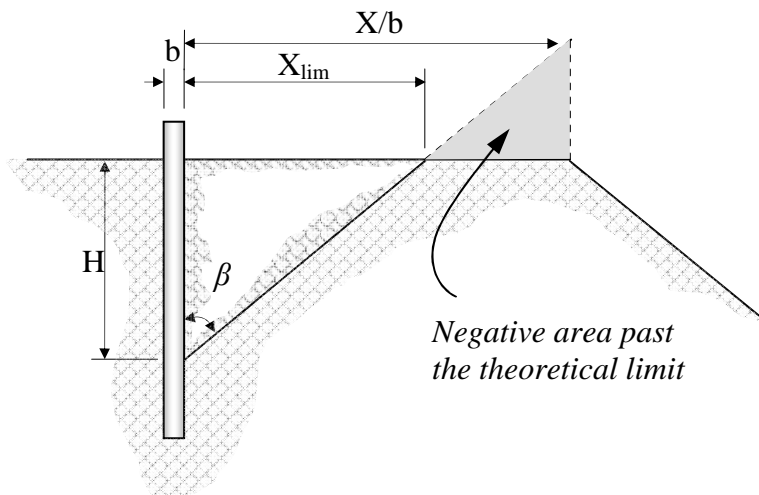
Figure 6.7 Illustration of Negative Theoretical Area.
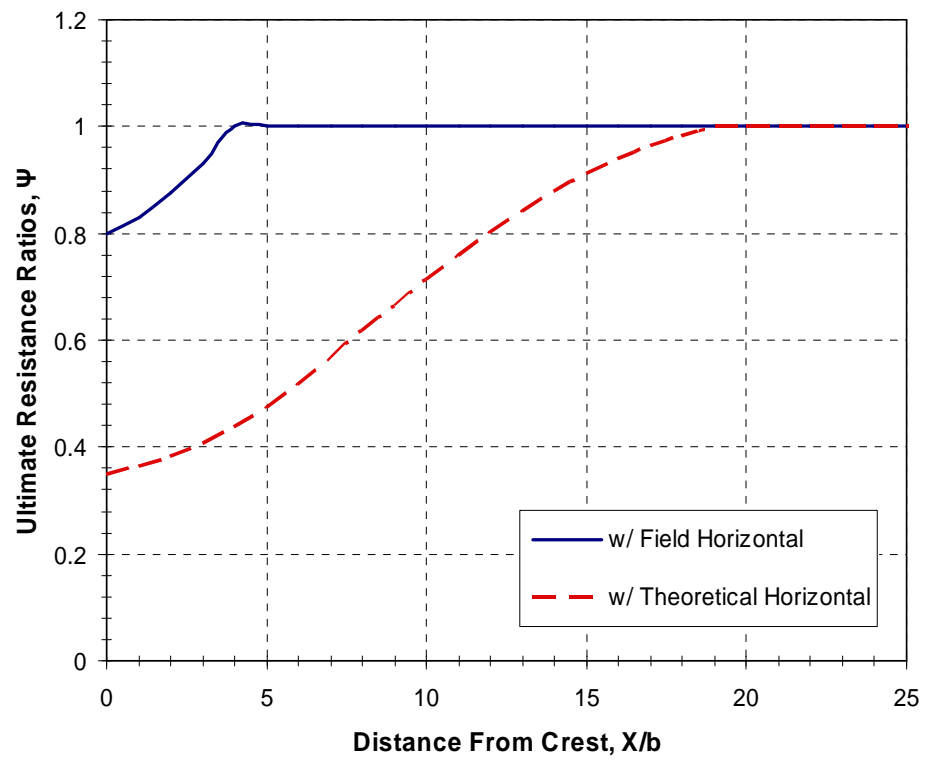
Figure 6.8 Ultimate Resistance Ratio Comparison.
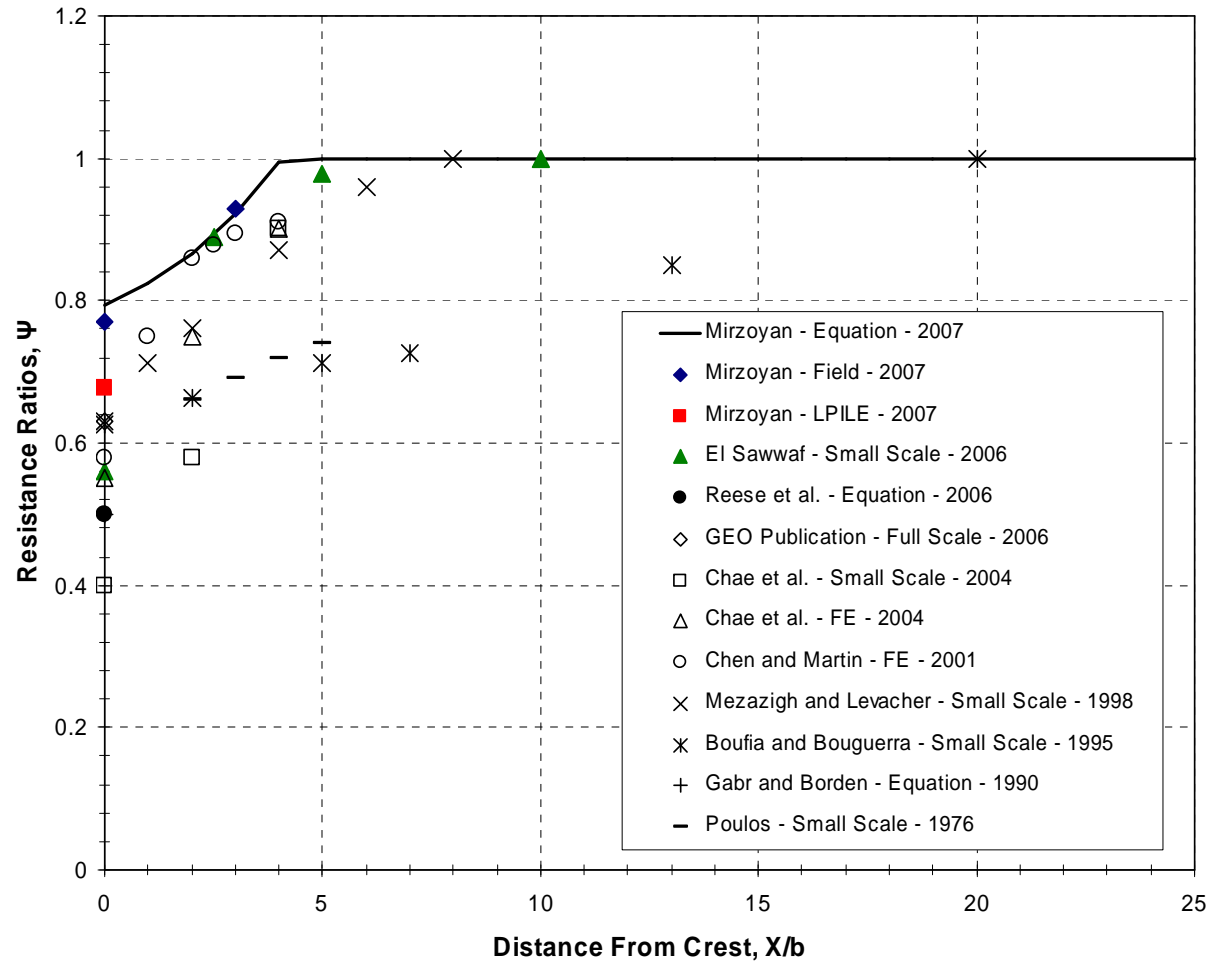
Figure 6.9 Comparison of Mathematical Model to Previous Studies.

Results of parametric tests using Equations 6-9 through 6-11 are presented in Figure 6.10, which shows the ultimate unit resistances as a function of depth for the three profiles tested. The figure shows resistances from both the flow-around and wedge-type failure criteria. As discussed earlier, the flow-around model does not depend on the soil geometry; hence, it is the same for all three profiles. The results indicate that in all three tests the resistance from flow-around failure is consistently higher for the depths considered and wedge-type failure mode governs the resistance; this, however, is not plausible since no failure wedge was observable in the field for test one. The discrepancy could be due to the consideration of active earth pressure in the flow-around failure model, which adds substantial resistance to the system. As discussed in previous chapters, a gap was observed in the field between the pile and unaffected soil behind the pile that remained open throughout the loading in all three tests. Such an observation
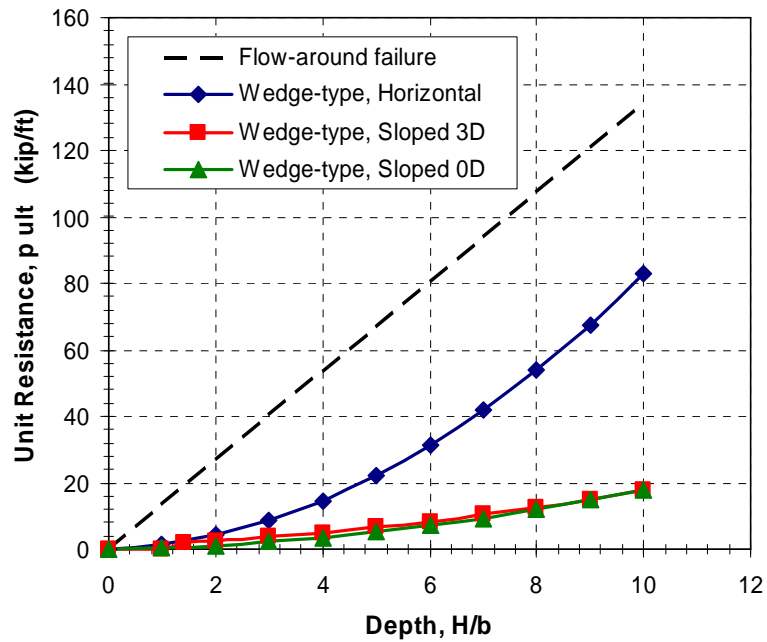
Figure 6.10 Ultimate Unit Resistances from Both Failure Modes.

131

indicates that the active pressure acting on the pile can be ruled out, and therefore, the flow-around failure model needs further refinement.

Figure 6.11 shows the failure modes with the adjusted flow-around failure model, which omits the contribution from active earth pressure. Figure 6.11 indicates that the flow-around failure mode governed the entire resistance in tests one and three and a majority of test two; this too, however, is not plausible since a failure wedge was readily observable in both tests two and three. Without more data to validate the flow-around model and the adjustment to account for no active pressure, it is difficult to determine which result most accurately represents resistance of the soil. The comparisons do, however, show general patterns that are in agreement with the field observations and past research.
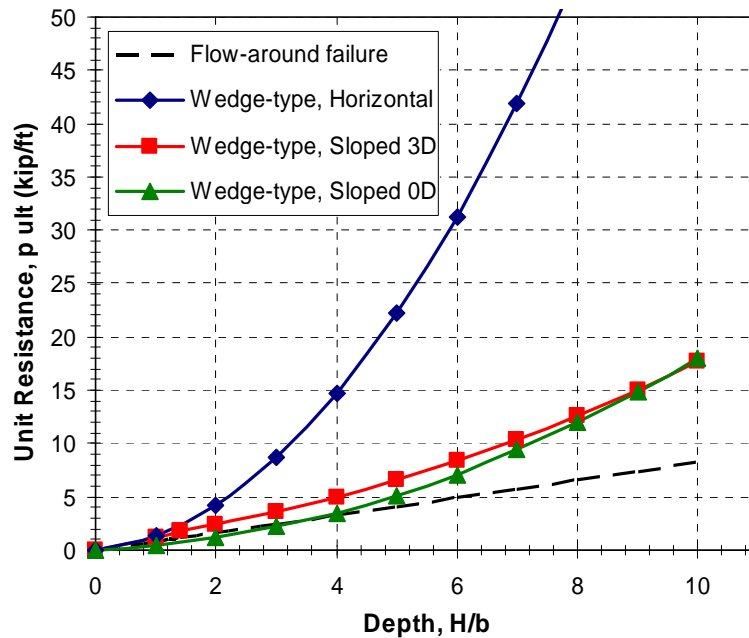
Figure 6.11 Ultimate Unit Resistances with Adjusted Flow-Around Model.

CHAPTER 7 - SUMMARY AND CONCLUSIONS

7.1   SUMMARY

To better understand the effects of soil slope and pile location relative to slope crest on the lateral response of a single pile, a set of three full scale tests were conducted between August 20th and September 20th of 2007. The tests were carried out in a soil profile consisting of an 8ft top layer of clean washed sand underlain by layers of silt, clay, and sand. The test site was located near the air traffic control tower of Salt Lake City International Airport. The variables in all three tests conducted were kept constant except for the profile geometry, which was the focus of the study. For the first test the pile was laterally loaded in a horizontal soil profile, this test served as a reference, to which results of subsequent tests were compared and contrasted. For the second test, a slope of approximately 30º from the horizontal was cut with the pile at the slope crest. And for the third test, a slope of 30º was cut such that the pile was three pile diameters from the slope crest. Slope angle and pile proximity to slope crest were chosen to simulate commonly found applications of laterally loaded piles near slope. Data was recorded and transferred to a data acquisition system and later analyzed and presented in this thesis. Of primary importance were effects of the slope on the ultimate lateral strength and maximum bending moment developed in the pile. Other points of interest

were the slope effect on soil failure patterns and location of maximum bending moment in pile. To obtain such results, various instruments were used with checks to guarantee reasonableness. The effect of slope on ultimate lateral strength was summarized in the form of Ψ, the ratio of ultimate lateral load capacity of a pile near a slope to the pile in a horizontal profile. And the effect of the slope on the maximum bending moment in the pile was summarized in the form of IM_{max}, the ratio of the maximum bending moment of a pile near a slope to the pile in a horizontal profile at a given applied load.

The single pile was also modeled in a finite difference based computer program, capable of modeling a pile in slope but was not able to account for pile proximity to slope. Therefore, only results of tests one and two were compared to the computer generated results. The program used was LPILE, developed by ENSOFT, Inc.

Finally, a mathematical model was developed based on the theory of the formation of a soil failure wedge providing resistance at the ultimate state. The mathematical model accounts for pile proximity to a slope crest. A set of parametric tests was carried out with the model and the results were compared to the field results.

7.2 CONCLUSIONS

7.2.1 Load and Deflection

- Piles located near a sloped profile experience a reduction in ultimate strength compared to piles located in horizontal soil profiles. For the case of a pile located at the slope crest, the reduction was approximately 23%, and for the case of a pile located three pile diameters from the slope crest,

134

the reduction was near 7%. Thus, pile proximity to slope has a significant effect on the amount of reduction in ultimate strength.

- The factors suggested by research done on small-scale models and mathematical models significantly overestimate the effect of slope on lateral load capacity of the pile-soil system.

- A deflection of approximately 0.5 in. was required for the shear zone to engage the slope surface and exhibit a reduction in soil resistance.

7.2.2 Bending Moments

- With respect to applied deflection, the slope appeared to have no significant effect on the maximum moment developed in the pile because, at the same deflection, piles near a slope also carried lower loads. With respect to applied lateral load, however, maximum bending moments in the piles in sloped profile were somewhat higher than in a horizontal profile. The pile located at the slope crest experienced an increase of approximately 40% and the pile located three pile diameters from the slope crest experienced an increase of approximately 30%. Thus, pile proximity to a slope increases the maximum bending moments developed in the pile at a given load due to a reduction in lateral restraint.

- The factors suggested by research done on small-scale models and mathematical models underestimate the effects of slope on maximum bending moments developed in piles.

- The locations of maximum and minimum bending moments in the pile were not affected by the presence of a slope.

7.2.3   Shear Failure Angle

- The shear failure angle, referred to as Ω, changed significantly with the slope and pile proximity to slope crest. The angle was broader for piles located at or near the slope crest. For the case of a pile located at the slope crest, Ω was observed to be approximately 75% of the angle of internal friction, ϕ. And for the case of a pile located three pile diameters from the slope crest, Ω was observed to be slightly greater than half of ϕ.

7.2.4   Gap Formation

- Although the sand used in the study was cohesionless clean sand, a gap formed behind the pile. This was primarily due to the partially saturated state of the soil. It suggests that active pressure behind the pile has no significant effect on the pile response under lateral loading in partially saturated sands.

7.2.5   Computer Modeling

- Friction angles much higher than typically used in engineering practice were required to obtain agreement between the measured and computed lateral load behavior for the steel pipe pile in dense sand within a

horizontal profile. These and previous results suggest that improved p-y

curve models may be necessary for sands at higher relative densities.

- Although a load vs. deflection curve match was obtained between the

  computer generated results from LPILE and measured results from the

  field in the case of a pile in horizontal profile using a friction angle of

  54.5°, no reasonable match was obtained for the case of a pile located at

  the slope crest. The computer program underestimated the lateral pile

  strength by approximately 20% for a given deflection. LPILE, therefore,

  can be used as a means of obtaining conservative lateral strengths of piles

  in sandy slopes.

- A very reasonable match, however, was obtain for the maximum bending

  moment vs. applied load curves in both the horizontal and sloped profile

  cases.

- LPILE consistently underestimated the depth to point of maximum

  bending moment in both the horizontal and sloped profile cases.

7.2.6   Mathematical Model

- With the given assumptions, ultimate lateral strength results from the

  mathematical model match reasonably well with the measured results

  form the field. The error between the model and field results was

  approximately 2.6% for the pile at slope crest and 0.2% for the pile three

  pile diameters from slope crest.

- The derived equation for ultimate resistance per unit length of pile can be used to obtain p-y curves that can then be used to predict the pile lateral response.

- The theoretical distance, beyond which the slope effect on ultimate lateral strength becomes negligible, was predicted by the model to be about 19 pile diameters using a wedge depth of 9.5 pile diameters.

- The ultimate lateral strength of a pile located at that distance from the slope crest, referred to as the theoretical horizontal ultimate strength, was predicted by the model to be double the strength of the pile in horizontal profile measured in the filed.   Unit resistance comparisons between the wedge-type and flow-around type failure modes indicate that in the horizontal case, the resistance would be governed by the flow-around mode, resulting in a lower ultimate strength.

REFERENCES

Ashour, M., Norris, G. (2000). "Modeling lateral soil-pile response based on soil pile interaction." *Journal of Geotechnical and Geoenvironmental Engineering,* ASCE,, 126(5), 420-428.

Ashour, M., Norris, G., and Pilling, P. (1998). "Lateral loading of a pile in layered soil using the strain wedge model.: *Journal of Geotechnical and Geoenvironmental Engineering,* ASCE, 124(4), 303-315.

Bhushan, K., Haley, S. C. and Fong, P. T. (1979). Lateral load tests on drilled piers in stiff clays. *Journal of the Geotechnical Engineering Division,* American Society of Civil Engineers, vol. 105, pp 969-985.

Bjerrum, L. (1972). "Embankments on soft ground," *Proceedings, Specialty Conference on Performance of Earth and Earth Supported Structures*, ASCE, Vol. 2, pp. 1-54.

Boufia, A., Bouguerra, A. (1995). Odelisation en centrifugeuse du comportement d'un pieu flexible charge horizontalement a proximite d'un talus." *Canadian Geotechnical Journal,* 32(2), 324-335.

Bowman. E. R. (1958). "Investigation of the lateral resistance to movement of a plate in cohesionless soil," thesis presented to the University of Texas, at Austin, Tex., in partial fulfillment of the requirements of the degree of master of Science.

Chae, K. S., Ugai, K., and Wakai, A. (2004). "Lateral resistance of short single piles and pile groups located near slopes." *International Journal of Geomechanics,* 4(2), 93-103.

Chen, C. Y. and Martin, G. R. 2001. "Effect of Embankment Slope on Lateral Response of Piles." *FLAC and Numerical Modeling in Geomechanics – 2001* (Proceedings of the 2nd International FLAC Conference, Lyon, France, October 2001). Billaux et al. (eds.). A.A. Belkema, Lisse, pp. 47-54.

Christensen, D. S. (2006). "Full scale static lateral load test of a 9 pile group in sand," Thesis (M.S.), Brigham Young University, Department of Civil and Environmental Engineering.

Davidson, H. L. (1982). "Laterally loaded drilled pier research." Final report prepared for Electrical Power Research Institute.

Duncan, J. M., Evans, L. T., Jr., and Ooi, P. S. K. (1994). "Lateral load analysis of single piles and drilled shafts.: *Journal of Geotechnical Engineering,* 120(6), 1018-1033.

El Sawwaf, M. (2006). "Lateral resistance of single pile located near geosynthetic reinforced slope." *Journal of Geotechnical and Geoenvironmental Engineering*, 132(10), 1336-1345.

Ensoft. 1999. *LPILE version 3.0 User's Manual.* Ensoft, Inc. Austin. Texas.

Frank R., Bangratz J. L., and Kutniak M. 1990. PILATE-LCPC: Programme de calcul d'un pieu isolé soumis a des efforts de flexion en tête et à des poussées latérals de sol. Laboratoire des Ponts et Chaussées, Paris, p 69.

Frank R., Shields D., and Domaschuk L. 1994. The effects of creep on laterally loaded piles. In The Proceedings of 13th International Conference on Soil Mechanics and Foundation Engineering (ICSMFE), New Delhi, India, pp. 501-504.

Gabr, M. A., Borden, R. H. (1990). Lateral Analysis of Piers Constructed on Slopes. *Journal of Geotechnical Engineering,* vol. 116 (12), pp 1831-1850.

GEO (2006). *Foundation Design and Construction (GEO Publication No. 1/2006).* Geotechnical Engineering Office, Hong Kong, 129 p.

Hetenyi, M. (1946). *Beams on elastic foundations,* University of Michigan Press, Ann Arbor, Michigan.

Matlock, H. (1970). "Correlations for design of laterally loaded piles in soft clay." *Proceedings, 2nd offshore Technology Conference,* Houston, Texas, 577-594.

McClelland, B., and Focht, J. A., Jr. (1958). "Soil modulus for laterally loaded piles." *Trans. Am. Soc. Civ. Eng., 123, 1049-1063.*

McCullough, N. J. and Dickenson, S. E. (2004). "The behavior of piles in sloping rock fill at marginal wharves." *Proceedings, Ports Conference 2004,* Houston, Texas, 86-96

Mezazigh, S., and Levacher, D. (1998). "Laterally loaded piles in sand: Slope effect on p-y reaction curves." *Canadian Geotechnical Journal,* 35, 433-441.

Peterson, K. T. (1996). "Static and dynamic lateral lead testing a full-scale pile group in clay," Thesis (M.S.), Brigham Young University, Department of Civil and Environmental Engineering.

Poulos, H. G. (1975). "Design of pile foundations" Research Report 21, *University of Sydney,* School of Engineering.

Poulos, H. G. (1976). "Behavior of laterally loaded piles near a cut or slope." *Australian Geomechanics Journal* 6(1), 6-12.

Poulos, H. G. and Davis, E. H. (1980). *Pile Foundation Analysis and Design.* John Wiley & Sons, New York, 397 p.

Prakash, S., Sharma, H. D. (1990). *Pile foundations in engineering practice,* Wiley-Interscience, New York, USA.

Randolph, M. F. (1981). "The response of flexible piles to lateral loading." *Geotechnique,* 31(2), 247-256.

Reese, L.C. (1962). "Ultimate resistance against a rigid cylinder moving laterally in a cohesionless soil." J. Soc. Pet. Engrs., 355-359.

Reese, L. C., Isenhower, W. M., Wang, S. T. (2006). *Analysis and design of shallow and deep foundations,* Wiley, New Jersey, USA.

Reese, L. C., and Matlock, H. (1956). "Non-dimensional solutions for laterally loaded piles with soil modulus assumed proportional to depth." *Proceedings, 8th Texas Conference on Soil Mechanics and Foundation Engineering, Austin, Texas, 1-23.*

Reese, L. C., van Impe, W. F. (2001). *Single piles and pile groups under lateral loading,* Balkema, Rotterdam, The Netherlands.

Reese, L. C., Wang, S. T., Isenhower, W.M., and Arrelaga, V. A., (2000). *Computer program LPILE Plus version 4.0 Technical Manual*, Ensoft, Inc., Austin, Texas.

Reese, L. C., and Welch, R. C. (1975). "Lateral loading of deep foundations in stiff clay." *Journal of Geotechnical and Geoenvironmental Engineering, 130(8), 878-882.*

Robertson, P. K. and Campanella, R. G., (1983). "Interpretation of cone penetration tests. Part I: Sand" *Canadian Geotechnical Journal*, 20, 718–733.

Rollins, K. M., Land, J.K., and Gerber, T.M. (2005). "Measured and computed lateral response of a pile group in sand." *Journal of Geotechnical and Geoenvironmental Engineering,* ASCE, Vol. 131, No. 1, pp.103-114.

Rollins, K. M., Johnson, S.R., Petersen, K.T., and Weaver, T.J. (2003a). "Static and dynamic lateral load behavior of pile groups based on full-scale testing," *13th*

International Conference on Offshore and Polar Drilling, International Society for Offshore and Polar Engineering, paper 2003-SAK-02, 8pp.

Rollins, K. M., Olsen, R.J., Egbett, J.J., Olsen, K.G., Jensen, D.H., and Garrett, B.H. (2003b). "Response, analysis, and design of pile groups subjected to static and dynamic lateral loads," Utah Department of Transportation Research and Development Division, Report No. UT-03.03.

Rollins, K. M., Peterson, K.T., and Weaver, T.J. (1998). "Lateral load behavior of full-scale pile group in clay," *Journal of Geotechnical Engineering,* ASCE, Vol. 124, No. 6, pp. 468-478.

Snyder, J. L. (2004). "Full-scale lateral-load tests of a 3x5 pile group in soft clays and silts," Thesis (M.S.), Brigham Young University, Department of Civil and Environmental Engineering.

Taylor, A. (2006). "Full-scale lateral-load test of a 1.2m diameter drilled shaft in sand," Thesis (M.S.), Brigham Young University, Department of Civil and Environmental Engineering.

Takeuchi, T., and Okada, A. (1986). "Prediction method for horizontal behavior of cast-in-place pile foundation dug by manpower on slope using shear elastic constants of ground." *Kisoko*, 14(6), 50-56 (in Japanese).

Tatsuoka, F., Zhou, S., Sato, T. and Shibuya, S. (1990): "Method of evaluating liquefaction potential and its application," *Seismic Hazards in the Soil Deposits in Urban Areas*. pp. 75-109 (in Japanese).

Tomlinson, M. J. (1994). *Pile design and construction practice,* 4th Edition., Viewpoint Publications, London, UK.

Wakai, A., Gose, S., and Ugai, K. (1999). "3-D elasto-plastic finite element analyses of pile foundations subjected to lateral loading." *Soils Found., 35(4), 1-7.* (1999)

Walsh, J. M. (2005). "Full scale lateral load test of a 3x5 pile group in sand," Thesis (M.S.), Brigham Young University, Department of Civil and Environmental Engineering.

Wang, S. T. and Reese, L. C. 1993. *COM624P – Laterally Loaded Pile Analysis Program for the Microcomputer. Version 2.0* U.S. Dept. of Transportation. Federal Highway Administration (FHWA). Publication No. FHWA-SA-91-048. August 1993.